Title
Dissecting the mechanism of cell fusion and secretion in Neurospora crassa

Author
Jun, Darae

Publication Date
2019

Peer reviewed|Thesis/dissertation

Dissecting the mechanism of cell fusion and secretion in *Neurospora crassa*

by

Darae Jun

A dissertation submitted in partial satisfaction of the

requirements for the degree of

Doctor of Philosophy

in

Microbiology

in the

Graduate Division

of the

University of California, Berkeley

Committee in charge:

Professor N. Louise Glass, Chair
Professor Randy Schekman
Professor Anastasios Melis

Spring 2019

Abstract

Dissecting the mechanism of cell fusion and secretion in *Neurospora crassa*

by

Darae Jun

Doctor of Philosophy in Microbiology

University of California, Berkeley

Professor N. Louise Glass, Chair

PART I

The saprotrophic fungus, *Neurospora crassa* has evolved to be exceptionally good at secreting large amounts of enzymes necessary to degrade exogenous complex carbohydrates. It is well established that *N. crassa* transcriptionally regulates the synthesis of these enzymes in order to utilize plant cell wall components as a carbon source. However, downstream regulation of the secretory pathway likely improves the efficiency of secretion and plant cell wall degradation. The mechanisms through which this occurs are still obscure. To elucidate these unknown mechanisms, we conducted a forward genetic screen to identify and characterize defective trafficking mutants that cannot translocate cellulases in the ER or that improperly retain cellulases in the ER instead of secreting them into the extracellular environment. We generated a mutant library using random mutagenesis of a strain with a GFP tagged endoglucanase (EG-2), to screen via microscopy for mutants with mislocalized EG-2. From the screen, we identified a particularly interesting mutant (10C2) that has EG-2-GFP mislocalization to the ER, a growth defect and temperature sensitivity. We used bulked segregant analysis to identify the putative causal mutation. The potential gene of interest encodes a scaffolding protein that is known to interact with multiple different proteins in various organisms, thus exhibiting diverse cellular functions in different organisms. However, its function in *N. crassa* has not been explored. Preliminary analysis suggested that this mutation causes a general secretion defect, as opposed to one specific to the cellulolytic response.

PART II

A large number of fusion genes have been identified in *Neurospora crassa*, however, functions of many of these genes are unknown. *ham-7* is one of the fusion genes, whose encoded HAM-7 protein has no conserved domains, is bound to the cell wall by a glycosylphosphatidylinositol (GPI)-anchor, and appears to be a homolog of a new family of polysaccharide monooxygenases (PMO). We made point mutations of the conserved histidines, which is one of the defining characteristics of a PMO, in *ham-7*. The point mutants have a disruption in the catalytic activity of HAM-7 and phenocopy *Δham-7*: flat growth, female sterility and inability to undergo chemotropic interaction and cell fusion. Previous studies indicated that *ham-7* may be playing a role in the cell wall integrity pathway, either involved in signaling or structure maintenance. *Δham-7* showed similar sensitivity as wild type cells induced by cell wall stress agents, which suggested that *ham-7* is more likely involved in signaling of cell fusion. We were not able to secrete HAM-7 by only truncating the GPI-anchor site, however, we were successful once we additionally removed three N-glycosylation cross-linkage sites. To understand the role of HAM-7 in the signaling pathway, we analyzed the differential expression levels of communication and fusion genes in *Δham-7*, *Δmak-1* and *Δmak-2* mutants. Our data indicated that *ham-7* functions downstream of *mak-1* and *mak-2*. Characterization of *ham-7* will provide a better understanding of the proteins involved in signaling and remodeling of the cell wall in *N. crassa.*

Table of Contents

List of Figures

Acknowledgements

First, I would like to dedicate my dissertation to my dad. He is not here to witness my milestones in life, but would be so proud to see me graduate with a doctorate degree.

I would like to thank Louise Glass who has been an instrumental person in making this project possible. First as a summer undergraduate student working in the lab, she showed interest and inspired me to further pursue science. She continued to show support and give guidance as I pursued my Ph.D. in her lab. She is a terrific mentor who is able to adjust her mentoring style to fit each individual. She has warmly encouraged and pushed me to strengthen my weaknesses. Louise has also been a great role model as a female scientist. Her connections to many prominent scientists has provided me the opportunity to have great collaborations, which were required to accomplish the work described in this dissertation. Overall, she also has keen eyes for great scientists. She also created a positive lab environment where all members could have informative discussions and enjoy the company of one another. I feel very fortunate to have been a member of this lab and I could not have asked for a better lab to do my graduate work.

A number of lab members have been incredibly important to my development as a scientist. They have helped me directly with techniques and lessons that have made this body of work possible. They have made tremendous contributions to my understanding of molecular biology, fungal biology, genetics and computational biology. Jason Liu, Lina Qin, Lori Huberman and Vincent Wu have guided through my secretion project; and Pedro Goncalves has guided me through my fusion project. Other lab mates who have contributed much advice and discussion include Jens Heller, Monika Fischer, David Kowbel, Sam Coradetti, Trevor Starr, Gabriel Rosenfield, Asen Daskalov, Yi Xiong, Timo Schuerg, Jiuhai Zhao, Wilfried Jonkers, Javier Palma-Guerrero. Jason, Lori, Lina, Pedro and Jens have been especially important mentors and role models during my time here at Berkeley. Gabriel has been an especially wonderful classmate, lab sibling and a friend that I had the privilege to go through graduate school and fun traveling adventures with. Also, the research presented regarding cell fusion would have not been possible without our collaborators− Elise Span, Tyler Detomasi and Professor Michael Marletta, with their expertise in biochemistry.

I would like to thank my family for their support and for bringing me food to make sure that I was properly nourished. My dad and mom are the reason I am where I am, and who I am. They have sacrificed so much to provide a better life for my siblings and I. They are the reason for my tenacity, work ethic and my survival instincts. Also, special thanks to my best friends− Adria Moss and Lauren Schmechel− for always being ready to comfort me with wine and chocolate from all the stress. Lastly, Xiao Ren who has been my biggest supporter and my sanity throughout graduate school and life. He has stayed by my side through the good times and the bad. He keeps me grounded; always pushing me to be a better person and encouraging me every step of the way when I was doubtful. All the people I have mentioned above have made a profound contribution to my academic and personal life, and there are simply no words that can adequately express my gratitude towards them.

Chapter 1. Introduction of *Neurospora crassa* as a model organism

1.1. Emergence of *N. crassa* as a model organism

Since the infestation of French bakeries in 1843, *Neurospora crassa* has been studied extensively as a model organism [1]. It is also known as "red bread mold" due to its color and initial discovery, however, it is a misnomer [2]. Although found on bread, its growth on bread is rare compared to other molds. Furthermore, *N. crassa* has a vibrant bright orange color as seen in Figure 1-1. The red color was observed from the carotenoid pigment development at the transition stage to conidiation, where the culture has been moved from dark to light. Thus, it is more accurate to describe it as an orange mold or filamentous fungus.

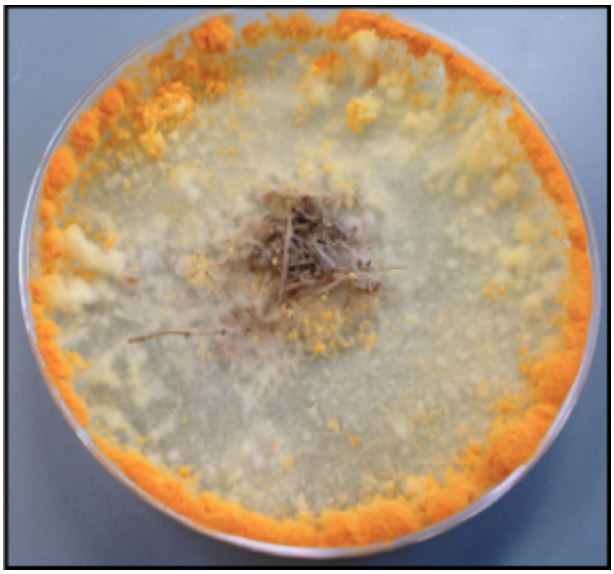

Figure 1-1. ***Neurospora crassa***

N. crassa is an ascomycete, the largest phylum in Fungi (Table 1-1). The defining feature of an ascomycete is the "ascus", which is a cylindrical sac that contains eight sexual spore-bearing cell or ascospores [1]. It has gained its fame as a model organism since Beadle and Tatum's discovery: "Each of these thousands of gene types has, in general, a unique specificity. This means that a given enzyme will usually have its final specificity set by one and only one gene" [3]. David Perkins further established *N. crassa* as a great system to perform eukaryotic genetic studies in the 1950s [1]. Aside from molecular regulation, *Neurospora* has provided valuable insights into metabolism that was fundamentally different than those of prokaryotes: "intragenic complementation, multi-domain proteins, the coordination of mitochondrial and nuclear gene activity, cellular compartmentation and substrate induction in biosynthetic pathways." In the 1960s and 1970s, *Saccharomyces cerevisiae* became a more tractable organism to study genetics and biochemistry as a single-celled eukaryote. *Neurospora* research was restored with the advancement of molecular techniques and is the leading organism to study photobiology and

circadian rhythms, the evolution of breeding systems, epigenetics and plant cell wall degradation.

Table 1-1. Scientific classification of *N. crassa*

Kingdom	Fungi
Phylum	Ascomycota
Subphylum	Pezizomycotina
Class	Sordariomycetes
Family	Sordariaceae
Genus	Neurospora
Species	crassa

1.1.1. Secret lifestyles of *N. crassa*

As a saprophytic fungus, *N. crassa* is normally found on burnt wood and dead plant matter in nature. However, a recent study suggests *N. crassa* to have a dynamic lifestyle, being able to switch from endophytic, pathogenic and saprophytic lifestyle [4]. This malleable lifestyle is likely triggered by the host and environmental changes. Because of its ability to efficiently degrade plant biomass, it is used as one of the model organisms to study ligno(hemi)cellulase secretion. Although the discovery of endophytic relationship of Scots pine (*Pinus sylvestris*) as the host plant for *N. crassa*, much is to be discovered about their lifestyles in nature and coevolution with its plant hosts [4].

1.1.2. The asexual life cycle of *N. crassa*

N. crassa spends most of its life cycle in the haploid state, being able to undergo both sexual and asexual reproduction [1]. Under the proper conditions for growth, asexual spores (conidia) will germinate, also known as germlings. The germlings has self and non-self recognition mechanism to discriminate against harming versus helping type; they can chemotropically grow towards germlings with genetic relatedness (only at certain loci) while veering away from those that are not genetically identical [5][6]. Once it has recognized a partner that is identical, the two germlings will fuse and grow as hyphae. Hyphal fusion will establish a mature colony. As carbon and nitrogen sources are used up, aerial hyphae will form and produce more macroconidia (Figure 1-2A).

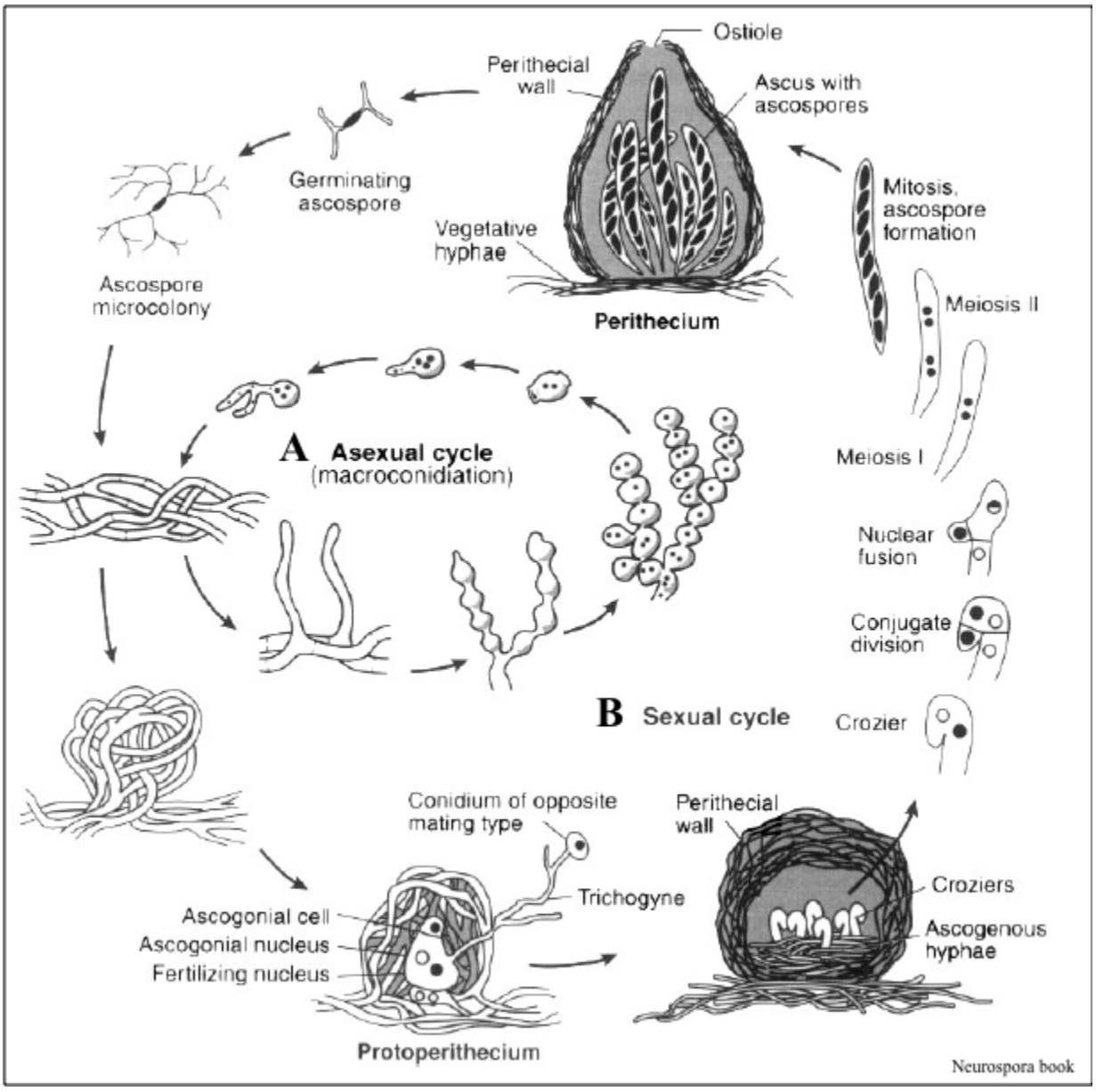

Figure 1-2. Life cycle of *N. crassa* [1]. a) Inner circle illustrates the asexual cycle, where macroconidia is formed from aerial hyphae and germinates into a new mycelium. b) Outer circle illustrates the sexual cycle, starting with a tricogyne from the protoperithecium is fertilized by a conidium of the opposite mating type, and asci containing ascospores are formed. The right side of the outer circle depicts nuclear fusion and meiosis in an individual ascus as it develops.

1.1.3. The sexual life cycle of *N. crassa*

Sexual reproduction in *N. crassa* requires interactions between strains with two alternative forms of the mating-type region, *mat A* or *mat a* (Figure 1-2B). Both mating types form male and female sexual structures, thus neither is exclusively gendered male or female [7]. Regardless of

the mating type, the parent strain that forms small knots of hyphae that are primordium fruiting body (protoperithecia) will be the female strain. To form protoperithecia, the female strain must be in carbon and nitrogen limited environment [8]. Protoperithecia will continue to develop into a dense, protective layer with outer hyphae (trichogynes) growing towards a pheromone emitted by the male strain of the opposite mating type. The trichogyne of the female strain will fuse with the conidium of the male strain. The male nucleus in transported down the trichogyne and into the ascogenous hyphae. In the ascogenous hyphae within the developing perithecium, opposite mating type nuclei undergo karyogamy, meiosis and a mitotic division to produce eight ascospores in each mature ascus. Mature perithecia form a beak, through which ascospores will be ejected out into the environment.

1.2. Filamentous fungi for lignocellulase secretion research

Because filamentous fungi are some of the most efficient lignocellulosic biomass degraders, they are commonly used for commercial enzyme production [9]. The challenge with engineering multicellular filamentous fungi for hypersecretion is that the secretory pathway has not been well characterized in these organisms and significant differences occur between these organisms and the much better characterized unicellular yeast, *Saccharomyces cerevisiae*. Some functions of the *S. cerevisiae* secretory pathway are paralleled in filamentous fungi, however, there are many differences due to morphological differences [10-13]. Although *S. cerevisiae* would be an ideal organism to study the cellulase secretion pathway, it does not naturally produce cellulases, nor does it secrete a large amount of protein as compared to industrial filamentous fungi [9]. Filamentous fungi have highly polarized growth, fast growth rate and ability to secrete large amounts of proteins. Yeast and metazoans lack a Spitzenkörper, a vesicle supply center located at the growing hyphal tip, that is found in filamentous fungi [14,15]. The hyphal tip is considered to be the principal region of protein secretion, thus the structure, and distribution of the organelles involved in the secretory pathway are dynamic in a growing hyphae [16].

Within the filamentous fungi, *Aspergillus* species and *Trichoderma reesei* have been the favored expression hosts for heterologous proteins of industrial applications [17]. In the 1940s, fermentation researchers screened *Aspergillus* species and identified *A. niger* as a high amylase producer [18]. Mutagenesis and screening selected strains with even more efficient amylase production. The corn industry utilizes amylase to convert starch to dextrin and glucose to produce various consumable products ranging from corn syrup to acidulants [19]. Moreover, glycoamylase study led to the discovery that transcription factors were the impeding factor of producing its target protein whose expression it controlled [20, 21]. Meanwhile, *T. reesei* was gaining the reputation as the indisputable champion in cellulase production, with publicly available strains able to secrete over 100 g/L of protein [22]. *T. reesei* was originally isolated as a contaminant on improperly stored canvas during WWII. It was subsequently mutagenized to produce mutant strains that secreted large amounts of cellulases under controlled fermentation conditions. Most of the work in *T. reesei* has been in the asexual phase, and only recently has sexual reproduction been explored. The industrial strain used to produce cellulases is female

sterile due to the mutation in *T. reesei* ortholog of the *N. crassa ham-5* (MAK-2 pathway scaffold) [23].

Around the time *T. reesei* was recognized as the model industrial strain to study cellulase production in the 1970s, *N. crassa* was identified as an equally potent cellulase producer [24]. Unlike *T. reesei*, the filamentous fungus *N. crassa* is a genetically and molecularly tractable organism and degrades plant cell wall material in its native habitat [25]. It has a well-documented sexual cycle and various tools to perform genetic association studies on wild alleles [26, 27]. Additionally, its 43 Mbp genome has been mapped and well annotated [28] and a nearly complete gene deletion strain collection is available [29]. These advantages make *N. crassa* an excellent model genetic system to study the cell biology of cellulase secretion.

1.2.1. Secretion of cellulases

The secretory pathway is essential for growth, survival, communication and homeostasis. In eukaryotes, the secretory pathway is important for transporting enzymes involved in cell wall synthesis and extracellular proteins, as well as proteins that are targeted for intracellular compartments. The traditional eukaryotic protein secretion begins with transcription of mRNA, translocation of the protein through the endoplasmic reticulum (ER) membrane to the Golgi apparatus for post-translational modification and sorting, and then directed to its final location [30]. As mentioned previously, *S. cerevisiae* is a good model organism to study the secretion pathway, however, it does not natively produce cellulases like *N. crassa*. Though filamentous fungi adhere to the canonical protein secretion pathway, much is unknown about post-transcriptional regulation of cellulase secretion. Studying the cellulase secretory pathway in *N. crassa* will provide a better understanding of the mechanism that allows filamentous fungi to produce such impressive quantities of secreted proteins.

1.2.2. ER stress responses

When unfolded proteins accumulate in the ER, ER stress responses are activated in order to restore ER homeostasis. There are multiple ER stress responses, but we will briefly discuss how critical HAC-1 and SREBP have a critical function contribute to the level of protein output from the cell. Unfolded protein response (UPR) is one of the stress responses regulated by HAC-1. Protein buildup in the ER activates IRE-1, which splices *hac-1* mRNA into a translatable form [31]. HAC-1 positively regulates genes responsible for enhancing ER folding capacity and more efficient protein trafficking [32, 33]. Although the ER stress response is evolutionarily conserved between metazoans and fungi, only the basic mechanism is conserved within the fungal Kingdom [34]. Up-regulation of UPR appears to be associated with ability to secrete large amount of proteins under lignocellulosic conditions in *T. reesei* [35], *A. nidulans* [36] and *N. crassa* [37, 38]. Cellulase secretion is reduced in *Δire-1* and *Δhac-1* mutants, but cellulase transcription is unaffected [37, 39].

The Sterol Regulatory Element Binding Protein (SREBP) pathway regulates sterol homeostasis, and is conserved from yeast to mammalian cells [40]. The mechanism in which ER stress induces SREBP activity in mammalian cells is not well understood [41]. Sterol-repleted cells retain the SREBP complex in the ER, but is transported to the Golgi by COPII in sterol-depleted cells [42]. Proteolytic cleavage releases the N-terminally bound SREBP from the Golgi membrane and subsequent transport into the nucleus results in activation the the transcription of cholesterol biosynthesis and lipid metabolism genes [42]. Deleting the transcription factor SREBP, *sah-2/sah2*, resulted in cellulase hypersecretion mutants in *N. crassa* and *T. reesei.* [43]. The *N. crassa* SREBP pathway positively regulates ergosterol biosynthesis and hypoxia adaptation, while negatively regulating protein secretion in the presence of lignocellulose [44]. Under high protein secretion conditions, the SREBP pathway negatively regulates extracellular oxygen-dependent enzymes, like PMOs, to limit the consumption of oxygen in the surrounding cells.

1.2.3. Endoplasmic reticulum import

Proteins designated for secretion are differentiated by the presence of N-terminal signal peptide (SP) [45-48]. SPs generally consist of three domains: a positive n-region, a hydrophobic h-region and a neutral, polar c-region that contains the SP cleavage site [49]. The extent of signal sequence conservation and length, and cleavage site varies by proteins [50]. The signal peptidase, an ER localized serine protease, recognizes and cleaves the SP off of the translocated protein [51]. Before the cleavage and degradation of SP, the peptide has to be translocated into the ER.

The two known protein translocation mechanisms into the ER are signal recognition particle (SRP)-dependent and SRP-independent pathway [52]. SRP-dependent pathway is co-translational translocation of the protein into the ER lumen, while SRP-independent pathway is translocation of unfolded translated peptides across the ER membrane [30]. In the SRP-dependent pathway, the SRP directs ribosomes engaged in mRNA translation of secreted proteins to the ER and is recruited to the surface of the ER by an SRP receptor [53]. Recently, it has been shown that SRP-independent mRNAs aggregate to the ER, which suggest that the SRP-dependent pathway is not the sole mechanism of mRNA transport to the ER [54]. Developing a comprehensive understanding of the SRP-independent pathway is important because nearly half of yeast secretome may be translocated through this pathway [55], and is likely similar for filamentous fungi. Although the SRP-dependent pathway has been well documented, little has been revealed about the SRP-independent pathway.

1.2.4. Delivery from the ER to the Golgi

Once the proteins are folded, glycosylated and monitored for quality control, they are delivered from the ER to the Golgi via vesicle transport [56, 57]. The COPII, vesicle coat protein, binds to ER membrane and deforms the membrane assist in vesicle budding process [58]. Concurrently, ER cargo adaptors incorporate secreted proteins with sorting signals into the budding vesicle,

and transport them to the Golgi compartments. Secreted proteins continue on in the secretory pathway, while ER cargo proteins are recycled back to the ER by COPI. The transportation of proteins in the ER are determined by the specificity of cargo adaptors: p24 is for GPI-anchored and soluble secreted proteins, Emp46/47 is for glycoproteins, and Erv14 is for multispanning transmembrane proteins [59]. Erv41/Erv46 is a retrograde cargo adaptor to retrieve escaped ER-proteins from the Golgi. ER cargo adaptors are important in facilitating efficient ER exit of cellulases, including major cellulases CBH-1 and CBH-2 (cellobiohydrolase); p24 was required for CBH-1 and ERV-29 for CBH-2 in *N. crassa*.

1.2.5. Post-translational modification

Protein folding and post-translational modification occur after the protein has been translocated into the ER. Hsp70 is the chaperone protein that is responsible for protein folding, degradation, translocation and interactions [60]. Disulfide isomerases form, rearrange and reduce disulfide bonds of the translocated protein [61]. The disulfide bridges provide stability of the proteins, and in the case for cellulases, provides thermal stability.

Most secreted proteins are glycosylated by the addition of glycans and other organic molecules [62]. Glycosylation is important for protein stability, proper folding and localization. The glycosylation process is somewhat different in filamentous fungi than in the yeast *S. cerevisiae*. Filamentous fungi have a conserved N-glycosylation pathway, where they form complex, hybrid and high-mannose N-glycans [63]. There is a large sequence divergence in filamentous fungal N-glycan and O-glycan synthesis genes from *S. cerevisiae.* Glycan chains are added to the nascent protein in the ER and then delivered to the Golgi for further modification [64]. Additional glycosylation in the Golgi results in higher molecular weight in mature proteins than the immature proteins in the ER. From the Golgi, proteins are packaged into transport vesicles for delivery to downstream compartments, which include the vacuolar system or the Spitzenkörper [64, 65]. It is also common to bypass the Spitzenkörper and the proteins are directly delivered to the plasma membrane (PM) [66]. Then, proteins must go through the cell wall to be secreted out into the external environment [67].

Chapter 2. Investigating the mechanism of enzyme translocation through the secretory pathway of *Neurospora crassa*

2.1. Introduction

As scavengers of lignocellulosic biomass in the environment and the most efficient lignocellulosic biomass degraders, filamentous fungi have evolved to be exceptionally good at secreting large amounts of proteins [9]. Whole genome approach of mutagenesis screens advanced the discovery of hypersecreting mutants from various *Aspergillus* species and *Trichoderma reesei*. Conducting multiple rounds of mutagenesis and screening in these species generated an extremely efficient hypersecreting strains that are used in industry and research [19]. Development of reverse genetics provided a gene-centric method to study the actions of specific genes to study protein secretion. Many stages of protein secretion can be manipulated for more effective and efficient protein production, which is why forward and reverse genetic approaches is a great approach to identify and characterize secretion mutants.

Previously, a *N. crassa* strain with deletions in three major β-glucosidase genes (Δ3βG) and with a GFP tagged endoglucanase (*eg-2-gfp*) under its native promoter was used as the platform for mutagenesis to identify hyper and hypo-secretion mutants [68]. The Δ3BG strain induces the expression and secretion of cellulases in the presence of cellobiose, a glucose dimer and product of cellulose degradation [69]. Mutagenesis was performed using methylnitronitrosoguanidine (NTG), which adds alkyl group to guanine and thymine to generate mutations resulting in mutants with single nucleotide polymorphisms (SNPs). The advantage of using this mutant library over the deletion collection is not needing to individually insert *eg-2-gfp* into each deletion strain to study the phenotype of a range of mutants.

This mutagenesis library was enriched for mutants with a higher level of induction as measured by the GFP output. Fluorescent activated cell sorting (FACS) was used as the primary screen to identify mutants with the highest cellulase production, the top 0.1%. An unmutagenized population was first analyzed, and the threshold for sorting was placed above the highest values. Individual conidial spores were sorted into each well of 96-well plates (Figure 2-1). Sorting of the hits that were more fluorescent than the control population meant that the isolated mutants were increased in EG-2-GFP accumulation in the cell wall.

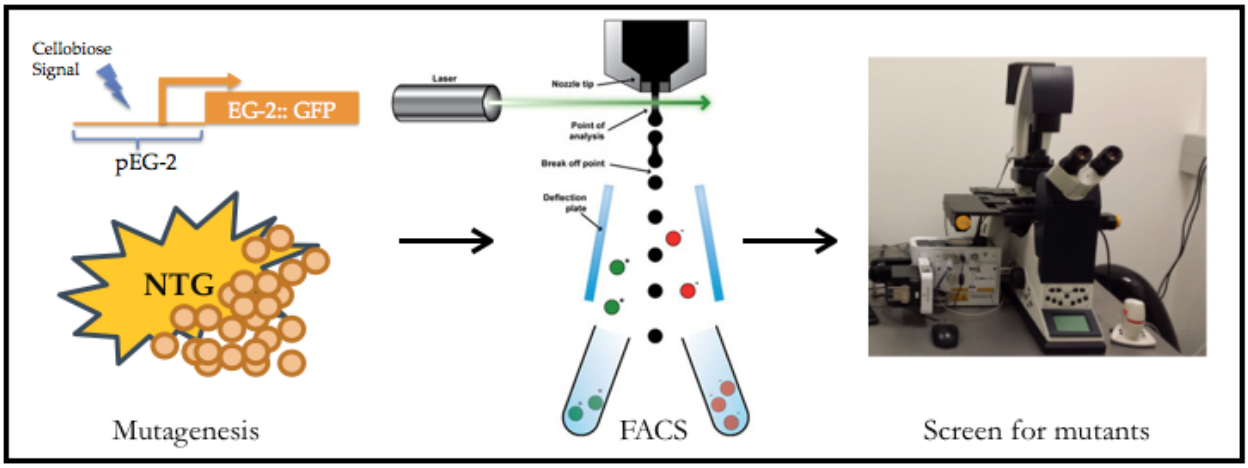

Figure 2-1. Creation of NTG mutant library. We used Δ3βG (EG-2-GFP under its native promoter) as the parental strain for NTG mutagenesis. Cellobiose was used to induce cellulase production in potential mutants, followed by FACS to screen for mutants with top 0.1% fluorescence. Secondary screens for EG-2-GFP intracellular mislocalization mutants were done via microscopy.

One caveat of the primary screening is that FACS could not sort out the difference between hypersecreters with GFP in the cell wall versus hyposecreters with intracellularly localized GFP. Thus, sorting of hits increased in EG-2-GFP accumulation also enriched for mutants that were accumulating EG-2-GFP intracellularly. Mutants with intracellular EG-2-GFP were first identified through functional overexpression on CMC agar, where the supernatant of cellulase induced mutants were spotted on CMC plates to assay for enzyme activity. Higher concentration of secreted enzymes resulted in larger radius of CMC-degradation on the plate, which can be visualized by the increased halo clearance. However, CMC plates had spots with no halo clearance, suggesting that the hyposecretion mutants bypassed FACS screening. We used the confocal microscope as a secondary screen to identify the hyposecreters for this study. In this chapter, we used a forward genetics approach to screen through mutants that contained modified alleles that displayed defective cellulase trafficking phenotype to discover genes involved in protein trafficking.

2.2 Materials & Methods

2.2.1 Culture methods and maintenance

The culture methods, standard media and detailed set of protocols for *N. crassa* is accessible at http://www.fgsc.net/Neurospora/NeurosporaProtocolGuide.htm. Vogel's minimal medium (VMM) is used as the standard media to culture *N. crassa*. For initial growth, Δ3βG strain was grown for 6-10 days on 1.5% agar and 2% sucrose VMM slant, and the conidial suspension was filtered with cheesecloth to remove the mycelium. To induce cellulase secretion in the Δ3βG strain, it was grown in VMM + 2% cellobiose.

2.2.2. Mutagenesis and fluorescence-activated cell sorting (FACS) analysis

NTG mutagenesis and screen was performed on *Δ3βG; eg-2-gfp* as described by [68]. *Δ3βG; eg-2-gfp* is a WT strain with three out of the seven major beta-glucosidase genes knocked out (Znameroski, Coradetti *et al.* 2012) and an endoglucanase with a native promoter and a C-terminally tagged GFP (EG-2-GFP) at the native locus. We used the hemocytometer to count and inoculate 1 x 10^8 Δ3βG conidial cells into two 50 mL conical tubes, bringing up to 25 mL with autoclaved 1x PBS (pH 7.0). We added 50 µL of NTG to the conidial suspension, and rotated the tube for two hours. Following the mutagenesis, we washed the cells three times with 50 mL of 1X Vogel's salts + 0.1% sodium thiosulfate and removed the supernatant; we repeated the wash step with 50 mL of 2% cellobiose and removed the supernatant. The suspension was added into a 250 mL flask with 100 mL of 2% cellobiose + 1x Vogel's salts, followed by 14 hr incubation in 25° C, shaking at 220 RPM. The cultures were centrifuged on a tabletop centrifuge at 1000 RPM and resuspended in 5 mL of VMM at 4°C. The conidial suspension was filtered using a 20 µm filter and diluted to 1 x 10^7 conidia/mL. WT and the mutagenized strains were analyzed via fluorescence-activated cell sorting (FACS) to identify highly fluorescent cells. Forward scatter (FSC) and side scatter (SSC) of Δ3βG were used as a proxy for size and viability. We sorted for conidia with <1% of highest GFP fluorescence, and inoculated each cell into an individual well of the 96-well plates.

2.2.3. Screening for hyposecreting mutants from the NTG mutagenesis library

Full expression of cellulases in *Δ3βG; eg-2-gfp* were induced with cellobiose to look at the intracellular localization of EG-2-GFP of all the mutants generated from the NTG mutagenesis. The mutants were inoculated for 16 hours and imaged in glass bottomed 96-well plates using a confocal microscope (Leica/Yokogawa Spinning Disk confocal Microscope). We selected mutants that had intracellular EG-2-GFP localization, and backcrossed to *Δ3βG; eg-2-gfp* to get homokaryotic strains. Homokaryons were backcrossed again to *Δ3βG; eg-2-gfp* for genomic pooling and bulk segregant analysis.

2.2.4. Genomic pooling and bulk segregant analysis (BSA)

Bulked segregant analysis was performed, as described by Heller *et al.* [6], with minor modifications. 36 progeny were pooled from the second backcross of 10C2 and *Δ3βG; eg-2-gfp*, with half of the progeny displaying WT phenotype and the other half 10C2 phenotype. 10C2 had three phenotype that co-segregated with the mutation: temperature sensitivity, growth defect and intracellular localization of EG-2-GFP. We used DNeasy Blood & Tissue kit (Qiagen Inc.) to extract and pool the genomic DNA. The samples were submitted to for library-prepping (TruSeq DNA LT kit, Illumina) and sequenced on HiSeq2000, 100 paired-end reads (Vincent J. Coates Genomics Sequencing Laboratory, Berkeley). Low-quality reads in the paired-end reads with a minimum mean depth of genome coverage of 71 were filtered out using fastx toolkit (http://hannonlab.cshl.edu/fastx_toolkit/index.html) and depth-of-coverage programs from Genome Analysis Toolkit (GATK) v2.3-9, respectively [70]. The filtered reads were mapped to the reference *N. crassa* OR74 genome v12 using Bowtie2.0 [71], and realigned for indels using

realigner-target-creator and indel-realigner programs from GATK [70]. The program calculated the percentage of allele frequency of each nucleotide compared to the parental sequenced; the allele frequency percentages were plotted on a line graph to identify region(s) of 100% segregation between the two pools of progeny.

2.2.5. Forced heterokaryons and complementation

For forced heterokaryon assays, strains bearing different auxotrophic markers would be co-inoculated detect complementation [72]. We modified the protocol found in Xiang *et al.* to form heterokaryons with a deletion/*his-3* auxotrophic (*Δ/his*-) strain and a temperature sensitive, 10C2. We used *his-3* and temperature sensitivity to test for complementation of the causal mutation. 3 x 10^6 conidia/mL of *Δ/his*- was mixed with 3 x 10^5 conidia/mL of 10C2 in a 150 µl spore suspension. The mixture was spread on VMM + FIGS agar plates, which allowed tight colonial growth. Due to the complementation of auxotrophic marker and temperature sensitivity, only prototrophic heterokaryons should be able to grow on VMM+FIGS at 37° C.

2.2.6. Germling fusion assay

Strains were grown on slants for 4-6 days and harvested into 1 mL sterile water. We used cheesecloth to filter the mycelium from the conidial suspension. The suspension was adjusted to have a final concentration of 1 X 10^7 conidia/mL. 300 µL of the conidial suspension was taken and gently spread throughout a VMM plate. The plates were left to dry for 30 minutes, and incubated in the dark 30°C incubator for three to five hours. To image the germlings, 1 cm^2 agar squares were cut out and observed with a Zeiss Axioskop 2, equipped with a Q Imaging Retiga-2000R camera (Surrey). The germlings were visualized with 40X/1.30 Plan-Neofluar oil immersion objective, and iVision Mac4.5 software was used for the imaging to assess for cell fusion competency.

2.2.7. Strain construction and transformation

gBlock fragment with the point mutation in the NES region of NCU01409 was created by IDT DNA. 177th amino acid was changed from leucine (CTT) to phenylalanine (TTT). NCU01409 ^{Leu177Phe} was cloned into pMF272 vector with *tef-1* promoter, V5 tag and *ccg-1* terminator. For *N. crassa* transformation, 7-10 day old conidia were harvested and washed with 1M sorbitol [29]. Counted the concentration of conidia using a hemocytometer and diluted to a final concentration of 5 X 10^9 conidia/mL. The conidial cells and plasmids were combined into a 1mm gap cuvette and electroporated with the setting of 1.5 kV, 25 uF and 600 ohms. Immediately, 1M sorbitol was added to the electroporated cells and plated on proper transformation plates with FIGS for colonial growth. *his-3* transformants could be heterokaryons, thus the progeny were backcrossed to *his-3* parental strain to select for prototrophic progeny.

2.3. Results

2.3.1. Screening and identifying homokaryotic progeny that display an EG-2 mis-localization phenotype

The forward genetic screen was conducted in order to identify cellulase hyposecreting mutants that did not localize EG-2-GFP to the cell periphery, which is likely caused by defective secretion and intracellular accumulation of cellulases. Using the mutant library, we screened through more than 1000 individual mutants that showed increased GFP fluorescence via FACs, but reduced cellulase activity. These mutant were exposed to cellobiose to induce cellulase production (and EG-2-GFP) and were subsequently visualized in 96 well plates, with glass bottoms, using a confocal microscope to assess intracellular EG-2-GFP fluorescence. After screening through these mutants, we narrowed the 1000 mutants down to six interesting EG-2-GFP mis-localization mutants (Figure 2-2).

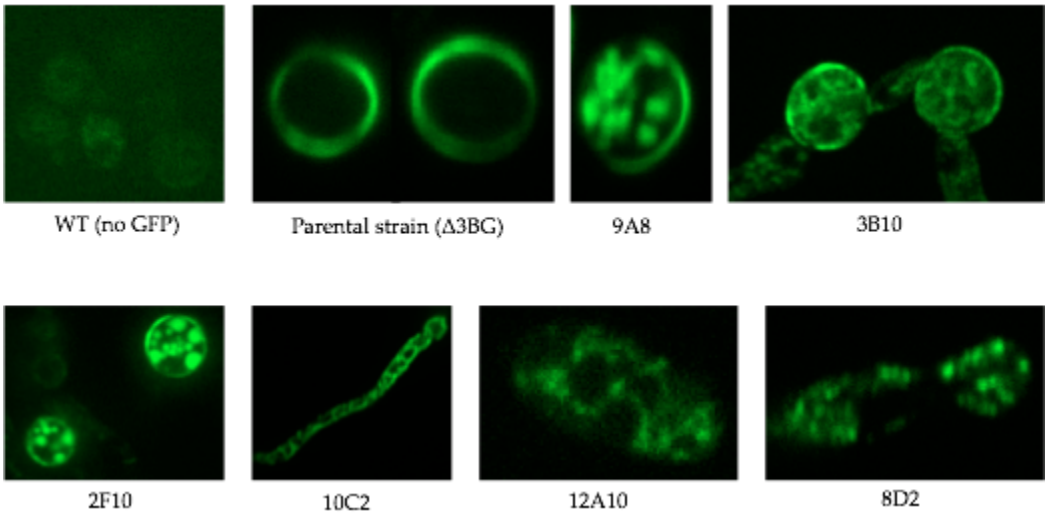

Figure 2-2. Microscopy of EG-2-GFP in NTG mutants. In Δ3βG cells, induction of cellulolytic response results in EG-2-GFP accumulation in the cell periphery, while the identified mutants have intracellular mislocalization.

It was possible that the six selected mutant strains of *N. crassa* are heterokaryons, where both the WT and mutant nuclei are in the same cell. Thus, we isolated homokaryotic strains from mutants that show intracellular EG-2-GFP by back crossing these strains to the parental Δ3βG strain and isolating individual ascospores. Since the locus of the mutation was unknown, the progeny could not be genotyped, but were rather screened by the EG-2-GFP mislocalization phenotype. 10C2 phenotype segregated with the WT phenotype 1:1, which implies a single mutation is the cause of the defect rather than multiple mutations.

10C2 grew very poorly and was characterized by very low conidiation. However, 10C2 grew even more poorly in the initial 30° C incubation. Although incubating 10C2 at room temperature

(25°C; RT) did not increase aerial hyphae or conidial production, lowering the temperature did allow 10C2 to grow faster. To test for temperature sensitivity, we incubated the freshly inoculated slants of 10C2 in RT and at 37° C (Figure 2-3C). Discovering temperature sensitivity provided a third phenotype to help with the co-segregation analysis. We were able to track 10C2 progeny with growth defect, EG-2-GFP mislocalization and temperature sensitivity, while Δ3βG had WT-like phenotype and cell wall EG-2-GFP localization (Figure 2-3A,B).

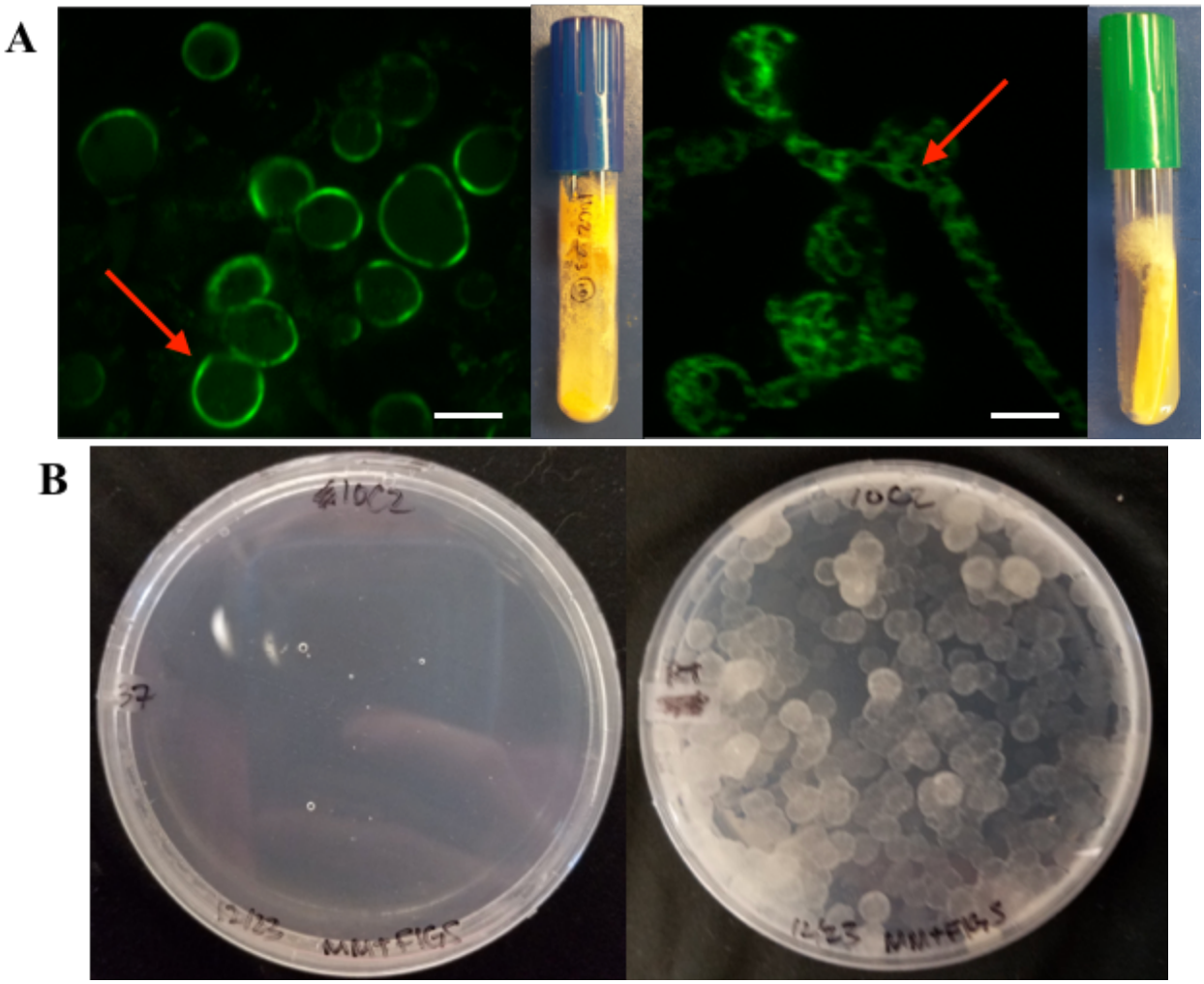

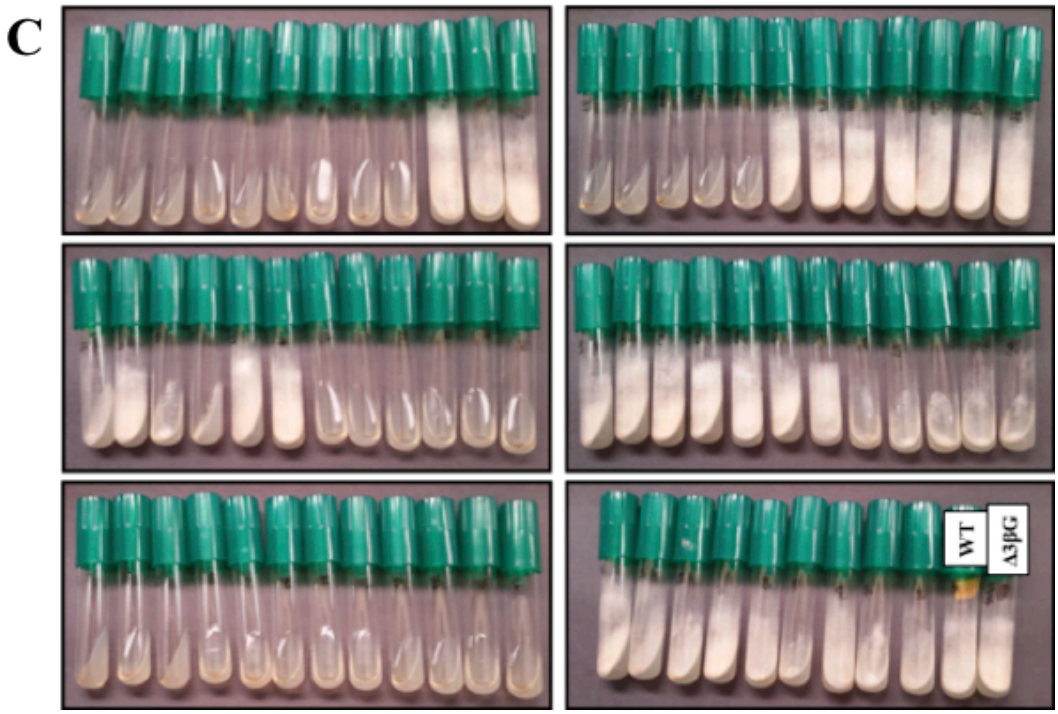

Figure 2-3. Phenotypic characterization of 10C2 mutant. a) Induction of cellulolytic response results in EG-2-GFP accumulation in the cell periphery Δ3βG germlings, while in 10C2 germlings, EG-2-GFP accumulates in nuclear envelope (NE)/ER. Scale bar- 5 μm b) 10C2 mutant is temperature sensitive, not being able to grow at 37° C as seen by the plates and the slants. c) Segregation of temperature sensitivity phenotype in progeny of the 10C2 x Δ3βG cross. WT and Δ3βG strains are in the far right bottom figure.

2.3.2. Mapping of the causal mutation

After validating the phenotypic defects are due to a single locus (external of the *eg-2-gfp*) in homokaryotic 10C2, we conducted bulk segregant analysis (BSA) to identify the mutation resulting in mislocalization of EG-2-GFP. BSA is a method of mapping the causal mutation(s) for a particular trait by segregation of phenotype, pooling genomic DNA of progeny and Illumina sequencing the genomic pools [73]. BSA compares the SNP frequency of the pooled DNA from two or more segregating populations by phenotype, where parental SNP frequency at non-causal loci are equally represented (50%) due to random homologous recombination events and at causal loci, SNP frequency will indicate a lack of recombination surrounding the causal SNP [74]. First, we backcrossed the homokaryons to the parents to individually phenotype 36 mutants and 36 WT strains. The temperature sensitivity and EG-2-GFP mislocalization of 10C2 mutant were linked, which allowed for quicker selectivity of progeny (Figure 2-3C). We isolated genomic DNA from individuals, and normalized their DNA into a control pool, and a mutant pool [73, 75]. 36 progenies are sufficient to get a clear resolution; beyond this number, the resolution of SNPs does not improve significantly enough to increase the genomic pool size [75].

Linkage group V (LGV) in Figure 2-4 shows the two populations have SNP frequencies that deviate from 50% in the region of interest due to independent segregation and recombination, assuming parental and mutant alleles at unlinked regions of the genome are equally represented [76]. The regions that showed 100% segregation, underlined by black bars in Figure 2-4, between the parental strain and the mutant progeny covered a total of 1 Mb region in LGV.

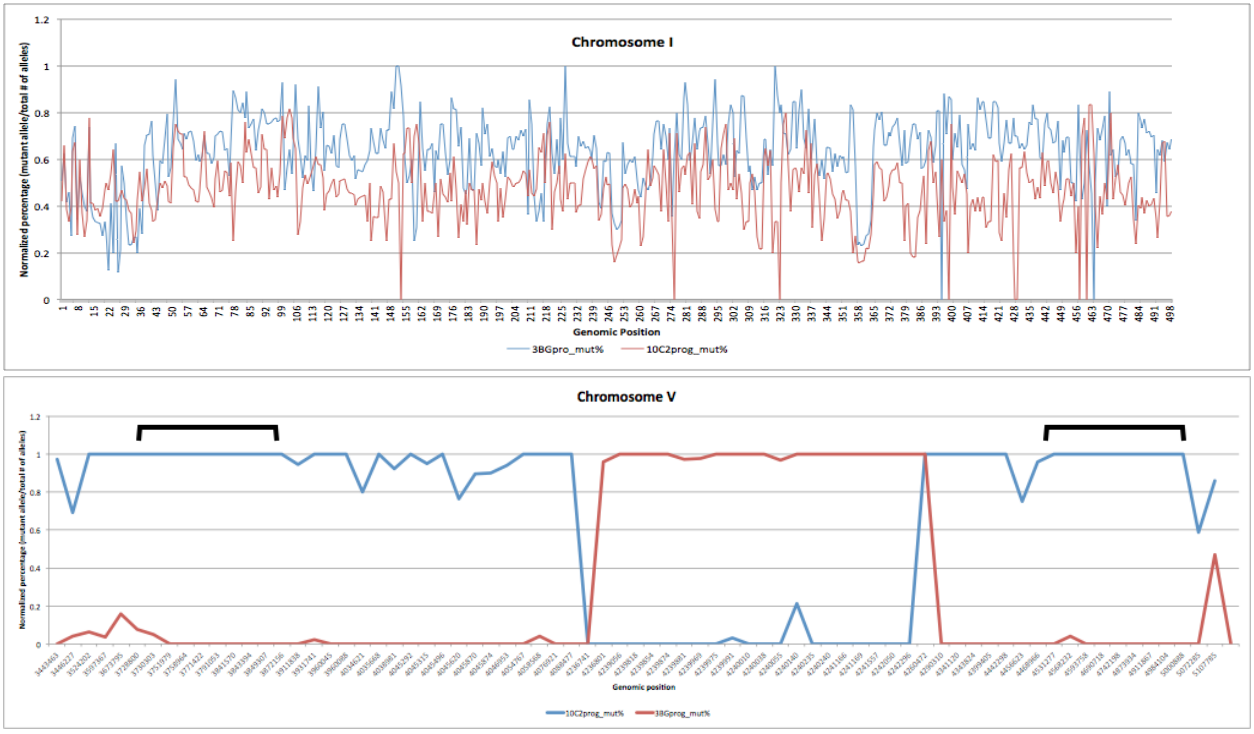

Figure 2-4. Mapping the causal mutation. Pooled genomic DNA of segregants of 10C2-like progeny (blue line) and Δ3βG-like progeny (red line) were sequenced and SNPs were compared to the reference genome (*N. crassa* OR74). Parental SNP frequency at non-causal loci fluctuates around 50% due to random homologous recombination events, as seen in the LGI (chromosome I) graph on the top. The causal SNP will have a 100% allele segregation, which is seen in the LGV (chromosome V) graph with black bars.

2.3.3. Identification of the causal mutation

Nine out of 73 SNPs in LGV had a non-synonymous change in an ORF that resulted in missense mutations. The rest of the SNPs were in intergenic regions and/or had a synonymous change. Table 2-1 lists the nine potential genes that may cause the 10C2 mutant phenotype. *sec39* and *bbp-1* are essential in *S. cerevisiae* and only available as heterokaryons in the *N. crassa* knockout library; and a mitochondrial hydrolase (NCU04110) deletion strain was not available. The six remaining homokaryotic deletion strains were crossed with a histidine auxotrophic strain (*his-3*) for a forced heterokaryon assay. Rather than using two auxotrophic strains, we formed

heterokaryons between the deletion mutants containing the *his-3* mutation and the 10C2 temperature-sensitive strain and incubating on minimal medium lacking histidine at restrictive temperature (37°C). The *his-3* strain will not grow in media without the supplementation of histidine, and 10C2 strain will not grown in non-permissive temperature, 37°C. Thus, prototropic heterokaryons can only be detected in selective conditions (VMM at 37°) if the *his-3* strain can complement the causal mutation in 10C2. If 10C2 fuses with a strain carrying the deletion of the gene responsible for the mutant phenotype, we would expect no growth in VMM + FIGS plate incubated at non-permissive temperature, 37°C. If a deletion strain does not carry a deletion of the causal gene, then a forced heterokaryon with 10C2 should allow growth at 37°C. In these forced heterokaryon tests, strains carrying deletions of NCU01285, NCU01381, *cwr-2*, NCU04147 or NCU06706 formed viable colonies, while a strain carrying a deletion of NCU01409 was not able to form colonies with 10C2 at 37°C (Figure 2-5). However, the ΔNCU01409; *his-3* + 10C2 heterokaryons were able to grow at RT and displayed mis-localization of EG-2-GFP.

Table 2-1. Genes with missense mutation in the LGV region of 100% segregation

Genes	Het vs Hom (*N. crassa*)	Viability in null mutant (*S. cerevisiae*)	Temp. sensitivity (*S. cerevisiae*)
TMD/major facilitator superfamily	homokaryon	viable (low homology)	no
sec39	heterokaryon	inviable	yes
NCU01381	homokaryon	viable	No
cwr-2	homokaryon	viable	no
RanBP	homokaryon	viable (low homology)	no
mitochondrial hydrolase	not in the knockout library	viable	no
bbp-1	heterokaryon	inviable	yes
Ser/Thr protein phosphatase	homokaryon	viable	no
killer toxin sensitivity	homokaryon	viable	no

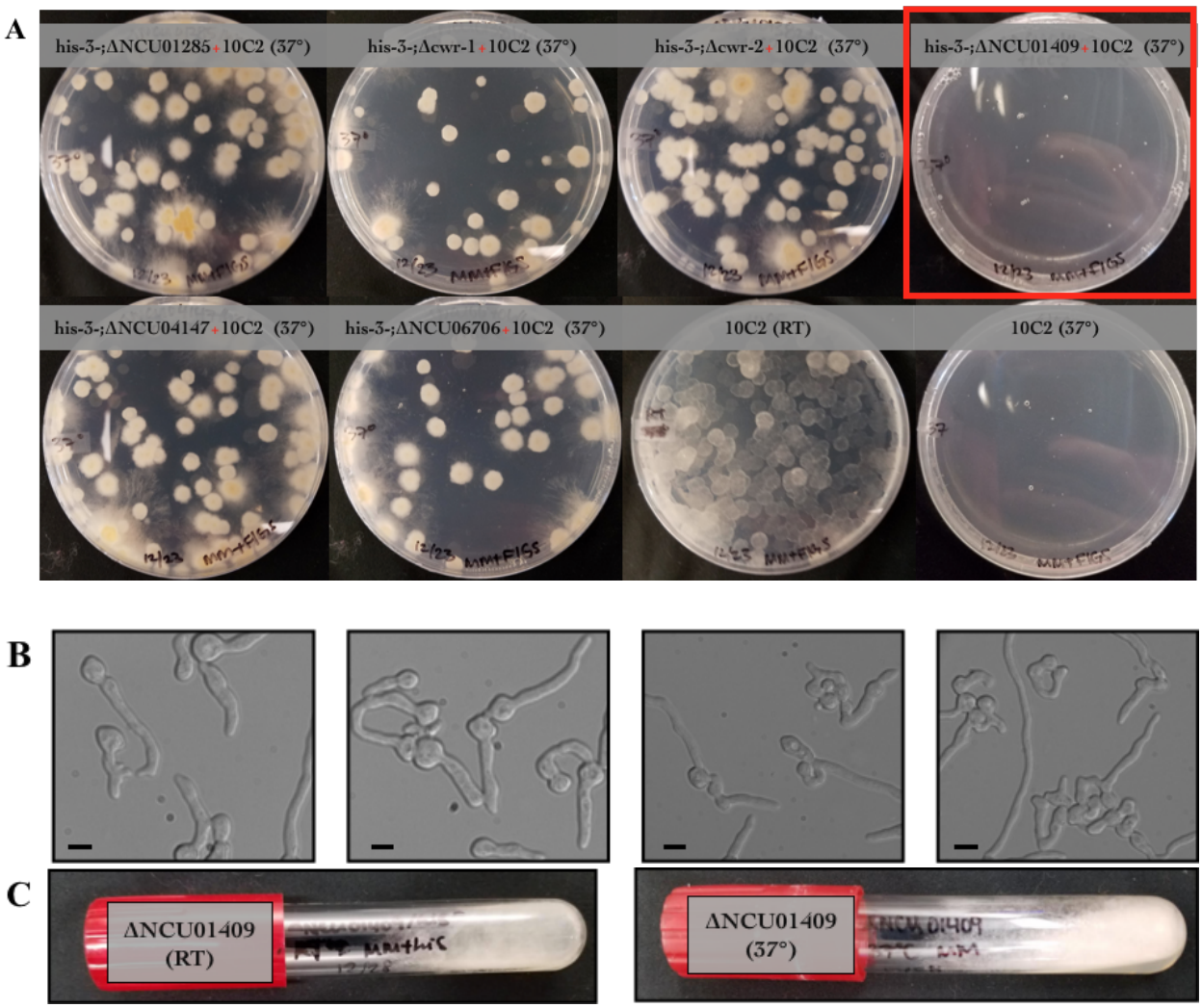

Figure 2-5. Forced heterokaryon assay. a) Heterokaryons were forced between histidine auxotrophic strains lacking the indicated genes and the 10C2 mutant. If deletions were not causal, 10C2 should complement the histidine auxotrophy of the Δ/*his-3* strain, while the Δ/*his-3* strain should complement the temperature sensitivity of 10C2. When heterokaryons were forced between 10C2 and strains WT with a deletion strain containing the causative mutation, the heterokaryon was unable to grow at 37°. b) Abundance of cell fusion between ΔNCU01409 germlings show that lack of growth in the forced heterokaryon assay was not due to fusion defect. Scale bar- 5 μm c) A strain carrying a deletion of NCU01409 did not show a temperature sensitivity phenotype.

We wanted to verify that ΔNCU01409; *his-3* + 10C2 heterokaryons did not grow in 37°C due to fusion defect via germling fusion assay. The abundance of cell fusion between ΔNCU01409 germlings show that lack of growth in the forced heterokaryon assay was not due to fusion defect (Figure 2-5B). With NCU01409 as the likely causal mutant, we looked at ΔNCU01409 phenotype (Figure 2-5C). Unlike the 10C2 mutant, the deletion strain was not temperature

sensitive. One possibility is that the specific point mutation in 10C2 causes the temperature sensitive mutant phenotype. To better understand this possibility, we proceeded to analyze NCU01409. NCU01409 encodes a Ran-binding protein microtubule-organizing center (RanBPM), which belongs to the RAS superfamily and is essential for the translocation of RNA and proteins through the nuclear pore complex [77]. Although RanBPM is conserved in various eukaryotic organisms, such as human, rhesus macaque, mouse, and frog [78], it exhibits different cellular functions due to its interaction with a broad spectrum of proteins. 45 binding partners were known in 2012 [79], and the list is continuously increasing. Different RanBPM-protein interactions impact various roles in cellular processes, ranging from protein stability, regulator of transcription activity, cell cycle to neurological functions.

N. crassa RanBPM share 38% identity with human and mouse RanBPM. Human and mouse RanBPM is a nucleocytoplasmic protein, and possesses two motifs that confer nuclear localization: 1) first 25 amino acid sequences are PQ rich and 2) non-canonical nuclear localization signal located near the C-terminus [80]. *N. crassa* does not have the poly-PQ N-terminal region, however, it contains all the domains that are conserved in other mammalian RanBPMs: immediately upstream of the spore lysis A and ryanodine receptor (IUS-SPRY), lissencephaly type-1 homology (LisH), carboxy-terminal to the LisH (CTLH) and CT11-RanBPM (CRA) (Figure 2-6). The IUS-SPRY domain is associated with protein-protein interactions, the LisH/CTLH domain is associated with functions related to cell migration, microtubule dynamics, chromosome segregation and other cellular processes [82], and the CRA domain is a α-helical structure with an unknown function [83]. RanBPM has motifs that allow them to localize in the nucleus, however, they also have localizations has nuclear export signal (NES), IUS-SPRY and LisH/CTLH domains that promote cytoplasmic localization [80].

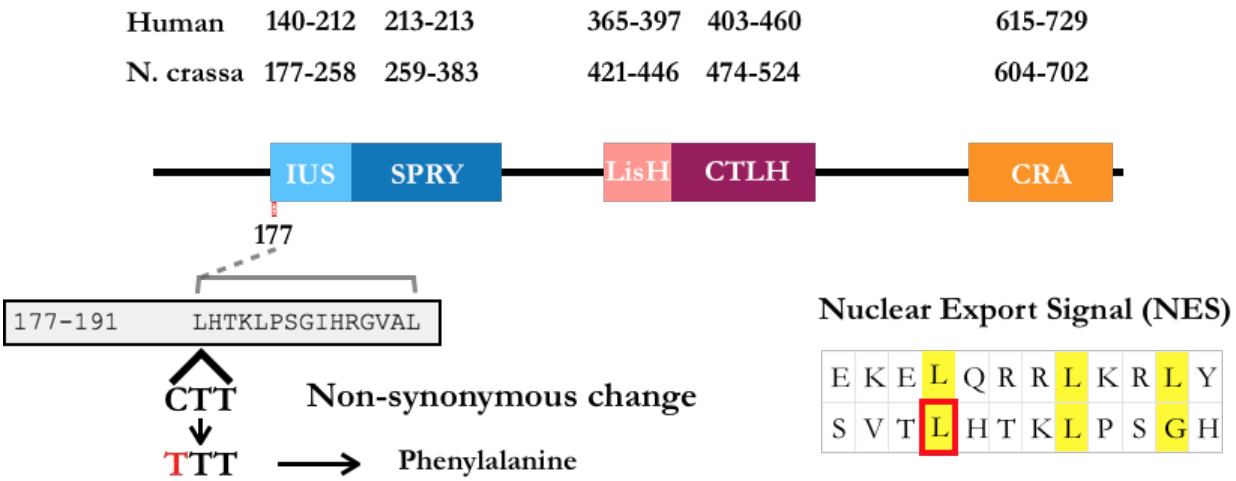

Figure 2-6. Leucine to phenylalanine mutation in the nuclear export signal (NES). A missense mutation changed the 177th amino acid from leucine to phenylalanine in the 10C2 mutant, which is predicted to be in a nuclear export

signal (LocNES, online NES predictor). The NES is found at the amino acid sequence 177-191. Alignment of the *N. crassa* and human NES shows that the causal SNP is in the first leucine sequence of the NES sequence. In other organisms, NES binds to an export receptor (CRM1) and assists in nucleocytoplasmic transport.

The non-synonymous mutation in RanBPM changed the 177th amino acid from leucine to phenylalanine. Further analysis of RanBPM sequences revealed that this mutation is embedded in the nuclear export signal (NES, found at the amino acid sequence 177-191) as shown in Figure 2-7. Due to the contradicting temperature sensitive phenotype of the point mutation in 10C2 and ΔNCU01409, it is critical to validate that Leu177Phe is the causal mutation. 10C2 was an extremely sick strain with highly reduced conidiation, therefore collecting enough conidia for complementation via transformation is challenging. We opted for recreating the NCU01409^{Leu177Phe} point mutation, however, we have not been successful at cloning and troubleshooting. In order to firmly conclude that Leu177Phe change is the causal mutation, we will still need to demonstrate that Leu177Phe mutation results in temperature sensitivity, intracellular EG-2-GFP localization and poor growth.

2.4. Discussion

The initial design of the mutagenesis library was tailored identify cellulase hypersecreting strains. Among hypersecreters, we also identified EG-2-GFP hyposecreting strains. Studying hyposecreters could lead to discovering genes that are regulating cellulase secretion. Branching off of the original project, we did not have the right criteria to specifically identify cellulase secretion defective mutants. To specifically enrich for intracellular EG-2-GFP mutants, we reconstructed the NTG library with a modification. We spheroplasted cells after mutagenesis to eliminate the mutants that localize EG-2-GFP to the cell wall. The rationale for spheroplasting was to eliminate the hypersecreting strains, consequently the fluorescence will be only detected from intracellular EG-2-GFP. However, this approach did not work because those with high background fluorescence became the top 1% fluorescent cells. This could be due to some of the spherolasted cells dying and some strains may have had degradation of EG-2-GFP. Hence, we followed through with screening the original NTG library.

Although we did not identify genes involved specifically involved in the regulation of cellulase secretion, we identified a mutation that induced a general secretion defect. The Leu177Phe mutation in the NES region of NCU01409 trapped EG-2-GFP in the NE/ER. A co-localization assay with different secretory pathway markers will discriminate whether the mis-localization of EG-2-GFP is in the NE or the ER. Along with the co-localization assay, it would be interesting to observe the localization pattern of other secreted proteins. This would provide a clearer view of whether NCU01409 is involved in regulating cellulases and other proteins through the secretory pathway.

To further confirm that this missense mutation is the cause of growth defect, we need to show introducing the Leu177Phe mutation in the RanBPM will simulate the 10C2 phenotype. Various methods were attempted for cloning NCU01409^{Leu177Phe}, but were not successful. Amplification of NCU01409 from the genomic DNA worked, however, the gene would never get incorporated into the desired vector. As simple of a procedure of cloning the gene into TOPO-blunt end vector did not work. To recreate NCU01409^{Leu177Phe} for validation as the causal mutation, different vectors using gene synthesis method may result in successful cloning.

It is unusual that the full NCU01409 deletion does not confer the same phenotypic defect as the point mutation in 10C2 strain. This may be due to the mutated in the predicted NES region of RanBPM, which is also nested in the beginning of IUS-SPRY domain. The NES binds to an export receptor (CRM1) and assists in nucleocytoplasmic transport in other organisms. Most of the NES characterized, up-to-date, consists of a non-conserved motif made up of hydrophobic residues and conserved leucines [83]. It is shown that the nuclear export of RanBPM is impaired when the conserved leucines in this hydrophobic groove are mutated. Additionally, IUS-SPRY domain is involved in protein-protein interactions, thus it is possible that EG-2-GFP mislocalization is the result of the change in the affinity of NES binding to CRM1. Change in the binding affinity potentially impairs the efficient release of CRM1-NES export complexes from the nuclear pore complex.

Although the function of RanBPM is diverse, there is conservation of the domains, which is seen by the low homology in RanBPM in *S. cerevisiae*. To date, there are about 45 different types of proteins that are associated with RanBPM, which results in a variety of multimeric complexes. However, not much is understood about the mechanism of partner recognition. So far, it is known that the IUS-SPRY domain recognizes a motif that has a considerable sequence variability that allows for multiple binding proteins [84]. This domain mediates protein–protein interactions, and the interacting partners and the molecular determinants of the binding specificity remain unknown. RanBPM regulates various signaling pathways, including kinases, transcription factors, membrane receptors, adhesion molecules, structural proteins, cell cycle regulators and others [79]. The diverse cellular roles advocate development of RanBPM as drug therapeutics for various diseases. Aside from examining the function of the RanBPM domains, a comprehensive investigation is required on the post-translational modification to understand its regulatory mechanism. If the missense in the NES is truly the causal mutation, it will be interesting to see how this amino acid substitution in RanBPM is involved in targeting and secretion of cellulases and other cellular proteins.

Chapter 3. Defining the role of HAM-7 in signaling and regulation of chemotropic interactions during cell fusion

3.1. Introduction

3.1.1. Communication and cell fusion

Cell-to-cell communication and cell fusion are critical for sexual development, vegetative growth and conidial anastomosis tubes (CATs) [85-90]. Colony and network establishments of *N. crassa*. Some of the advantages of hyphal fusion within colonies are the capability to share and translocate resources, to enhance colony cooperation, to heal and exchange genetic material [91]. Hyphal fusion can be broken down into three physiological stages: "pre-contact, post-contact and post-fusion" [92]. Pre-contact phase is when the cells show chemotropic growth towards other cells that have genetic identity at allorecognition loci. When two cells come in contact, they will either continue to extend or adhere and arrest their growth. Upon adhesion, cell walls will be broken down and membranes remodeled, followed by cytoplasmic mixing. Fusion between cells that have different allelic specificity at allorecognition loci can be aborted during chemotropic interactions, during cell adhesion, or trigger post-fusion programmed cell death, depending on the allorecognition locus [93]. Fusing with non-genetically identical cells increases the likelihood of acquiring deleterious infectious elements, parasitism or resource plundering [87].

A number of fusion mutants have been identified, and they have two common phenotypes: 1) flat growth and 2) female sterility [94-97]. The fusion genes can be separated into four categories: transcription factors, signal transduction pathway components, proteins involved in vesicular trafficking, and cell wall remodeling proteins [94]. There have been advancements in defining functions genes during fusion events in all of the listed categories except for the identification of signals, receptors and cell wall remodeling proteins. Strains containing mutation is any of five genes are affected in membrane fusion [98], but the signal and the receptor are yet to be identified in *N. crassa*.

3.1.2. The Cell Wall Integrity (CWI) pathway

The fungal cell wall is a highly dynamic structure that is important for growth, morphogenesis and protecting the cell from external stresses. The cell wall integrity (CWI) pathway is the responsible signaling pathway for the maintenance of the cellular integrity for hyphal growth, colony morphology, and sexual development. Mitogen-Activated Protein Kinase (MAPK) is an essential signaling complex, conserved across the Fungal Kingdom. The *S. cerevisiae* CWI pathway is activated by five different wall sensors: Wsc1, Wsc2, Wsc3, Mid2 and Mtl1 [99]. These membrane-spanning sensors share several common features: have an N-terminal signal peptide, contain at least one predicted transmembrane domain, short cytoplasmic tails and heavily O-mannosylated extracellular region (rich in serines and threonines). These sensors are functional isozymes, where they differ in the specificities and regulate different processes, thus triggered by different environmental cues. Only two genes have been identified as potential sensors in *N. crassa*, *wsc-1* and *ham-7,* and it seems plausible to have multiple cell wall sensors [100]. *wsc-1* encodes a transmembrane protein with extensive homology to the yeast Wsc family of sensor proteins. In *N. crassa*, WSC-1 (and its homolog WSC-2) activates the cell wall integrity MAK-1 MAP kinase pathway [100].

The *N. crassa* CWI MAPK signaling cascade is composed of *mik-1* (MAPK kinase kinase), *mek-1* (MAPK kinase) and *mak-1* (MAPK). Varieties of external stimuli (heat and oxidative stress, hypo-osmotic shock, pheromone-induced morphogenesis, etc) that cause cell wall stress trigger the MAPK cascade, sequentially phosphorylating the MAPK pathway [101, 102]. The cell wall integrity pathway monitors cell wall stress, which involve cell wall sensors, protein kinase C, plasma membrane-associated small GTPase Rho1 and MAPK signaling cascade [100]. Deletion mutants display morphological defects, such as reduced growth rates, aerial hyphae and (or nearly abolished) conidial production defects, and an inability to form female reproductive structures [103-106]. Mutants show sensitivity to cell wall stress agents with a defective CWI signaling pathway.

Although a scaffold protein is not essential for functionality of MAPK pathways, it functions as a regulator or a buffer for the signaling pathways. Although there is no ortholog of Spa2p (*S. cerevisiae* scaffold protein that interacts with CWI MAPKK and MAPK) in *N. crassa, soft (so)/ham-1* has been identified a scaffold protein that interacts with MIK-1 and MEK-1 [107-109]. SOFT alternately localizes to the tip of the cell periphery and disperses to the cytoplasm during chemotropic interactions [110]. The SOFT complexes will form puncta at the tip and disassemble at eight-minute intervals, as long as the chemotropic growth in communicating germlings or hyphae occurs. P-MAK-1 also has a dynamic localization during chemotropism. MAK-1 is phosphorylated in the cytoplasm during tropic growth, while cell-to-cell contact recognition recruits the kinase to the cell cortex [108]. After the germlings come in contact with their communicating partners, MAK-1 and SOFT will accumulate at the fusion site. The *S. macrospora soft* ortholog (PRO1) interacts with PKC1 (an upstream activator of the CWI pathway) [111].

3.1.4. MAK-2 pathway

Functional overlaps indicate cross talk between CWI pathway, SOFT and the MAK-2 pathway. Previous data showed that the MAK-2 MAPK pathway participates in early communication between fusion partners and for making conidia and hyphae fusion competent [87,105,112,113]. The MAK-2 pathway is composed of NRC-1 (MAPKKK), MEK-2 (MAPKK) and MAK-2 (MAPK). MAK-2 pathway is orthologous to the ERK 1/2 pathway in mammals and the pheromone response pathway in *S. cerevisiae*; they are known to be involved in variety of processes such as cell movement, differentiation, proliferation and apoptosis [114,115]. MAK-2 pathway functions are associated with sexual reproduction, conidiation, hyphal fusion and vegetative growth [106,116-119]. HAM-5 is the scaffold protein that binds NRC-1, MEK-2, MAK-2 and STE-50 into a complex in *N. crassa* [102][BR]; HAM-5 and Ste5p in *S. cerevisiae* are functional homologs, but are unrelated to each other in sequence or ancestry [121-124]. For full phosphorylation of MAK-1, *mik-1, mek-2* and *nrc-1* are required; these genes are also important for phosphorylation of MAK-2, but to a lesser degree [102,107,125,126]. Similar to the SOFT complex, the MAK-2/MEK-2/NRC-1/HAM-5 complex assembles and disassembles at the tip of the cell in eight minute intervals during the chemotropic growth. Cells that are genetically identical and undergoing chemotropic with GFP/RFP-tagged versions of any of the MAK-2 pathway constituents and show assembly of the MAK-2/MEK-2/NRC-1/HAM-5 complex at one tip, while the GFP/RFP-tagged SOFT complex assembles at the tip of the partner germling. Oscillation of the MAK-2 complex at cell tips is completely out of phase with the SOFT complex during chemotropic interactions [110,121,127].

PP-1 is a C2H2-Zn^{2+} transcription factor, which is homologous to the pheromone response pathway transcription factor, Ste12p in *S. cerevisiae* [102,128]. Microarray and RNA-seq analyses indicate PP-1 as the downstream transcription factor target of MAK-2 [102,129] Also Monika. MAK-2 activates or de-represses PP-1; activation of PP-1 triggers *adv-1* transcription, which results in transcription of cell fusion genes, which are regulated by ADV-1 [129]. Concurrently, MAK-1 operates upstream of ADV-1 independently of PP-1. *mak-1* is necessary for full phosphorylation of MAK-2 [125,130-132].

3.1.5. The STRIPAK complex

Along with MAPK cascades, the striatin interacting phosphatase and kinase (STRIPAK) complex is highly conserved in mammalian cells [133]. In mammalian cells, the STRIPAK complex regulates cytoskeletal organization, cell migration and cell morphology, while it is important for sexual development, growth and cell fusion in fungal cells [134]. *N. crassa* STRIPAK complex contains heterotrimeric protein phosphatase 2A (PP2A), serine/threonine phosphatase (PPG-1), hyphal anastomosis-2, -3 and -4 (HAM-2, HAM-3 and HAM-4), and general STRIPAK scaffold (MOB-3). HAM-2 and HAM-4 are membrane anchors, and HAM-3 is the striatin, a phosphatase regulator. Studies indicate that these proteins are interacts with the CWI and the MAK-2 pathways. A weak protein-protein interaction between MAK-2 and PPG-1, PP2A-A, HAM-3 and MOB-3 were identified through an affinity-purification mass spectrometry experiment [121]. MAP kinases regulate other proteins through phosphorylation, and MAK-2 phosphorylates several of the communication and cell fusion proteins, including components of the MAK-2 and CWI pathways [127]. MAK-2 is also required for HAM-3, HAM-4, PP2A-A and MOB-3 are all phosphorylation; mob-3 and ham-3 are essential for full phosphorylation of MAK-1.

3.1.6. Hyphal anastomosis-7 (*ham-7*)

Oscillation of the SOFT and MAK-2 complexes at the cell cortex are activated for chemotropic growth and cell fusion [110]. When the two cells come in contact with one another, directed growth terminates and adhesion occurs. Then, the cell walls are digested and remodeled, followed by cytoplasmic mixing during fusion. Thus far, many fusion mutants have been identified by their flat phenotype, female sterility and defective cell fusion [94]. In most cell fusion mutants, MAK-1, MAK-2 or STRIPAK signaling pathway components are affected [102,131,135-137]. The next two chapters will be focused on the characterization of *hyphal anastomosis-7* (*ham-7*). The *Δham-7* mutant was identified in a screen to find fusion mutants in *N. crassa* [94]. It is particularly interesting because of its deletion phenotype, but also due to the possibility that it may be a possible candidate for receptor signaling and regulation of the cell-cell fusion.

HAM-7 is a 230 amino acid protein with an N-terminal signal peptide and a C-terminal glycosylphosphatidylinositol (GPI)-anchor (Figure 3-1A), which is also true for its paralog NCU02884. The *Δham-7* mutant has a flat phenotype and is unable to undergo chemotropic interactions and cell fusion, while ΔNCU02884 maintained WT phenotype with growth, cell fusion and ability to form protoperithecia. From the known cell fusion genes, HAM-7 is the only protein to be extracellularly located [94]. MAK-1 phosphorylation activity was significantly reduced in the *Δham-7* and *Δwsc-1* mutants, which suggests that they act upstream of *mak-1* [100]. However, *Δwsc-1* and CWI deletion mutants show sensitivity to cell wall stress drugs, while *Δham-7* did not. Furthermore, *Δwsc-1* is capable of CAT fusion and producing

protoperithecia, while *Δham-7* and CWI deletion mutants are not. These data suggest that *ham-7* functions in a different readouts of the MAK-1 pathway; *wsc-1* regulates cell wall stress, while *ham-7* regulates cell fusion. Although characterized as a fusion mutant, bioinformatic analysis and genetic evidence indicate that *ham-7* is a polysaccharide monooxygenase (PMO, which will be further discussed in Chapter 4).

3.1.7. HAM-7 function in other Ascomycete species

No ortholog of *ham-7* is present in *S. cerevisiae*, while *Epichloë festucae* (*symB*), *Podospora anserina* (IDC2) and *Aspergillus flavus* (*hamG*) orthologs that are involved in hyphal fusion (Figure 3-1B). *ham-7* has 65% identity with *symB*, while it has 68% identity similarity to IDC2. 54% similarity to *hamG*. Deletion of *ham-7* orthologs has similar phenotypic defect; additionally deletion of *adv-1* orthologs result in fusion defect and down-regulation of the cell fusion genes, including *ham-7* orthologs [138,168]. Alignment of these five proteins show conserved histidine brace, axial tyrosine and four cysteines in all the orthologs.

E. festucae is an Ascomycete fungus that forms a mutualistic symbiosis with *Lolium* grasses. *ΔSymB* results in hyphal fusion defect, hyper-conidiation and disrupted host interaction. SymB-eGFP localizes at the cell periphery, as seen with IDC2 and HAM-7. *P. anserina* is a dung-colonizing Ascomycete fungus. IDC2 and IDC3 are involved in cell non-autonomous signaling of fruiting body development in *P. anserina* [141]. These genes were discovered during a screening of Impaired for the Development of Crippled growth mutants. Similar to *Δham-7* mutant, the ΔIDC2 mutant has poor growth, lacks aerial hyphae, anastomosis and is unable to undergo sexual reproduction. IDC2 is also predicted to be bound to the membrane with a GPI-anchor. One study mutated each cysteine to serine and observed that these residues are essential for the function of IDC2. Though the exact role of the cysteine residues are unknown, it has been speculated that they increase protein stability with the disulfide bridges.

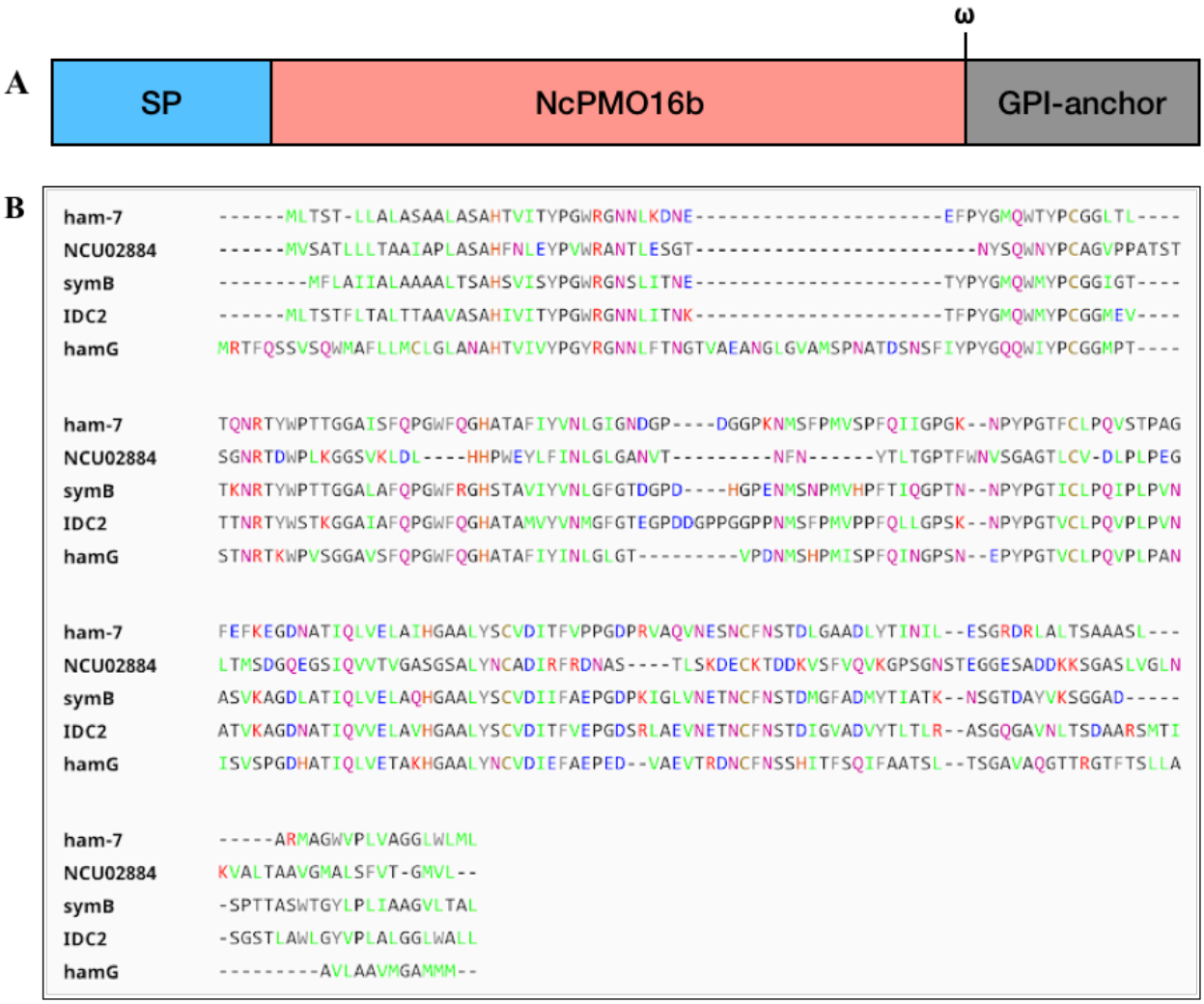

Figure 3-1. Alignment of HAM-7 homolog. histidine brace in red box, four cysteines in blue blox and axial tyrosine found in most fungal PMO9 family in black box).

Chapter 4. Defining the role of HAM-7 as a new member of the polysaccharide monooxygenases (PMOs) family in *N. crassa*

4.1. Introduction

Polysaccharide monooxygenases (PMOs) are copper containing oxygenases that degrade recalcitrant polysaccharides via oxidative mechanism alongside hydrolases and other electron transfer components [151]. PMO polysaccharide oxidation is accompanied by reduction of molecular oxygen to water. Initially PMOs were thought to have a sole function as hydrolases, hence PMO9 and PMO10 were known as GH61 and CBM33, respectively. Based on the sequence similarity and binding substrate, they have been classified into different families as seen in Table 4-1 [142-149]. However, recent discoveries reclassified them as auxiliary activity (AA) enzymes due to their ability to significantly boost the activity of canonical enzymes by providing easier access to their active polysaccharides [151]. It should also be noted that several names have been assigned to these PMOs and one main confusion is between the usage of PMO vs lytic PMO (LPMO). "Lytic" could misguide the function of the enzymes as performing the elimination reaction from the unstable intermediates [150]. The *ham-7* locus encodes a protein predicted to be bound to the cell wall by a glycosylphosphatidylinositol (GPI)-anchor, and protein alignment of HAM-7 indicated that it encodes a PMO. In *N. crassa, ham-7* mutants fail to undergo chemotropic interaction and somatic cell fusion. In collaboration with the Marletta Laboratory, we show that HAM-7 plays a role in signaling processes and chemotropic interactions. The goal is to purify and characterize HAM-7 for a better understanding of the proteins involved in in cell fusion of *N. crassa.*

Table 4-1. Classification of PMO families based on amino acid sequence similarities and binding substrates.

AA/PMO family	Sources	Substrate
9 (formerly GH61)	Fungi	Cellulose
10 (formerly CBM33)	Bacteria	Chitin/Cellulose
11	Virus	Chitin
13	Fungi	Starch
14	Fungi	Xylan
15	Fungi	Chitin
16	Fungi	Cellulose
17	Fungi	Unknown

4.2. Materials and methods

4.2.1. Peroxide formation assay

Horseradish peroxidase (HRP) coupled assay was used to detect the catalytic properties associated with oxygenase activity of NCU02884. Amplex Red is used as the substrate for the photometric detection of peroxide in NCU02884 reactions over time. Assays contained 100 µL of 100 mM HEPES (7.0), 0.5 µM NCU02884, 0.5 U/mL HRP, 50 µM Amplex Red, and 50 µM ascorbate. Reactions were carried out in flat-bottom, untreated 96-well plates (Corning), and detection at 573 nm was performed with a SpectraMax 340 plate reader (Molecular Devices) and analyzed with SoftMax Pro software.

4.2.2. Strain construction and transformation

To test for the importance of the conserved histidine residues in HAM-7, *Ptef-1-ham-7*, *Ptef-1-ham-7*^{H18A} and *Ptef-1-ham-7*^{H76A} were inserted at the *his-3* locus in the *Δham-7; his-3* auxotrophic strain. *Ptef-1* is a constitutively active promoter. *Xba*I-*ham-7*-*Nru*I was amplified from the genomic DNA and ligated into pMF272 vector via T4 ligase. PFU ultra II was used to make the point mutation from CAC (histidine) to GCT (alanine) at 18th and 76th amino acid in *ham-7*.

The predicted GPI-anchor (SAAASLARMAGWVPLVAGGLWLML) was truncated to release HAM-7 (HAM-7TR) from the cell wall. Failure to secrete HAM-7TR prompted mutation of three predicted N-glycosylation sites that are predicted to crosslink HAM-7 to the cell wall. Prediction of glycosites in eukaryotic glycoproteins (GlycoEP) web server predicted five and seven N-glycosylation sites in HAM-7 and NCU02884, respectively. After aligning the two proteins, there were three N-glycosylation sites that were unique to HAM-7. Amino acids 122, 156 and 163 were mutated from asparagine (N) to glutamine (Q) in the gBlocks Gene Fragments (IDT) to create *Ptef-1-ham-7TR*^{N122QN157QN163Q} vector. These constructs were tagged with either GFP or V5 tag in the pMF272 vectors and transformed into *N. crassa his-3* locus via electroporation method described previously [29]. *Ptef-1-ham-7TR*^{N122QN157QN163Q} transformants were backcrossed with *his-3* to ensure homokaryotic strains. Ascospores were harvested and germinated on MM to select for *Ptef-1-ham-7TR*^{N122QN157QN163Q} progeny. The genomic DNA of strains that grew on MM were extracted and sequenced for verification.

The same construction strategy was employed for the overexpression of NCU02884 in the *ΔNCU02884Δham-7* strain. *Xba*I-NCU02884-*Nru*I was amplified from the genomic DNA and ligated into pMF272 vector via T4 ligase. *Ptef-1*-NCU02884 was inserted into the *his-3* locus of *ΔNCU02884Δham-7/his-3-*. Transformants were backcrossed with *his-3* to ensure homokaryotic strains, and desired strain was selected on MM. The selected progeny were genotyped for the double deletions and the overexpression of NCU02884 at the *his-3* locus.

4.2.3. Race tube assay

Race tubes were prepared using 25 mL plastic pipettes filled with 13 mL VMM agar (modified from FGSC protocol). Once the VVM media solidified, the pipette tips were broken off. Strains were grown and filtered as mentioned in previous chapters. Each race tube was inoculated with 1 x 10^6 conidia at the edge of the media at the open end of the race tube. If using mycelia, size 2 plug was used to remove a circular piece of mycelia from an agar plate to the race tube. The agar with mycelia was placed on the edge of the media on the open end of the race tube. The opening was sealed with breathable sealing tape (Thermo Scientific). The race tubes were placed under constant light at 25°C and growth was measured at 24 hr intervals.

4.2.4. Western blot on supernatant and cell lysate

In 250 mL flasks, 1 x 10^8 conidia were suspended into 100 mL of liquid VMM. The flasks were grown under constant light at 25°C, shaking at 220 rpm. The flasks were shaken for 24 hrs, then the supernatant was collected for SDS-PAGE gel and Western blot analyses. Protein concentration was measured via Bradford assay, using BSA as the standard; the absorbance was measured at 595 nm using a spectrometer. After normalizing for protein concentrations, samples were denatured with beta-mercaptoethanol at 70°C for 10 min. The samples were run on Nu-PAGE 4-12% Bis-Tris gel (Invitrogen) and subjected to the standard Western blot protocol. 10% BSA was used for overnight blocking and 3% BSA for antibody incubation. GFP (Roche) and V5 (Invitrogen) mouse monoclonal primary antibodies and goat anti-mouse secondary antibody were used.

Western blot on cell lysates

Mycelia were obtained from the same flasks used to collect the supernatant, mentioned above; the mycelial biomass was filtered through a Büchner funnel on nitrocellulose membrane and frozen immediately in liquid nitrogen. Harvested cells were immediately transferred to a mortar and fast frozen by pouring liquid nitrogen on to the cells. The cells were ground with a pestle until they formed a fine powder (sample was kept frozen with liquid nitrogen as needed during grinding). 500 -1000 µL (volume dependent on the amount of cells) of protein extraction buffer [100mM Tris/HCL pH 7.4, 1% SDS with 1X protease cocktail (Calbiochem/Novabiochem/Novagen)] was added to the ground cells and the solutions was spun at 4°C for 30 minutes (6000 RPM).

For germlings, suspensions of 1 x 10^6 conidia/mL were prepared and inoculated into 175 mL of liquid VMM. 35 mL of the dilution was plated on five 150 X 15mm petri dishes, and the plates were incubated at 34°C without agitation for 4 hrs. Cells were first scraped off the petri dishes with cell spreader and then filtered by the same method as above. The biomass were collected into 2 mL screw cap tubes with silica beads and immediately frozen in liquid nitrogen. Accumulation of hyphal biomass was easy, so we were able to grind the frozen biomass via mortar. More biomass is likely to be lost in the process of grinding, thus we opted for bead

beating for the germling biomass. After 30 seconds of bead beating, 333 µL of a different protein extraction buffer was used [103] and centrifuged as described above.

The aqueous portion of the germling and mycelial samples was collected protein concentration was determined using Bradford assay. 100 mL of the supernatant was concentrated down to 500 µL via Amicon™ Ultra-15 Centrifugal Filters 10 MWCO (Fisher Scientific). Interestingly, bead beating resulted in higher total protein concentration, yet had fainter bands in the Ponceau staining and Western blot. The total protein extracted from the lysate was normalized to the sample with the lowest concentration for a Western blot. Germling and hyphal protein samples from cell lysis were subjected to the same Western blot method as described above.

4.3. Results

4.3.1. HAM-7 as a putative PMO

Through structural and phylogenetic analysis, the Marletta laboratory identified 20 PMOs in *N. crassa.* These PMOs have been classified into different families based on sequence similarity and binding substrate (Table 4-2). Clustering indicate two new families of PMO with unknown binding substrates; NCU02884 and HAM-7 clusters into PMO17, while NCU02613 clusters by itself into PMO18 (Table 4-1). NCU02884 is a paralog of HAM-7 with similar protein characteristics: roughly 220 amino acids long, has a signal peptide and a GPI-anchor site, and has the conserved histidine brace and tyrosine residue. Homology model in Figure 4-1A shows NCU02884 and HAM-7 share common structural properties, with the sequence identity of 28% and similarity of 56.5% [127].

Table 4-2. List of predicted or characterized PMOs in *N. crassa*

PMO family	Binding substrate	Gene ID
PMO9	Cellulose	NCU00836
		NCU02344
		NCU03328
		NCU07974
		NCU08760
		NCU01867
		NCU02916
		NCU01050

		NCU02240
		NCU07898
		NCU03000
		NCU07520
		NCU07760
		NCU05969
PMO11	Chitin	NCU01380
		NCU00822
		NCU05932
		NCU05404
PMO13	Hemicellulose	NCU08746
PMO17	Unknown	NCU02884
		NCU00881
PMO18	Unknown	NCU02613

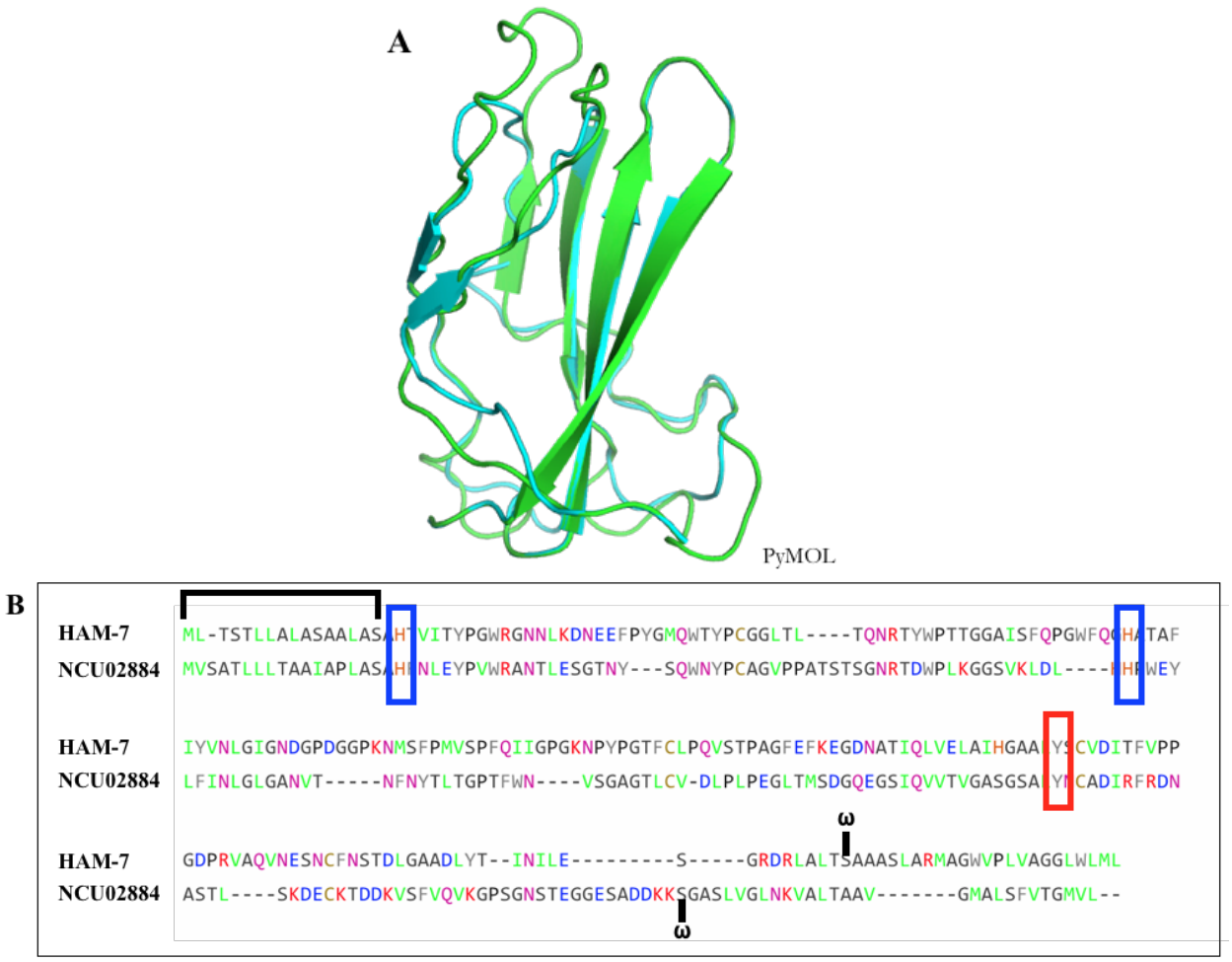

Figure 4-1. Alignment of HAM-7 and NCU02884. a) Using PyMOL to create a homology model of the HAM-7 and NCU02884. Sequence identity is 28% and similarity is 56.5% (HHpred server). b) A pairwise sequence alignment marked with black bracket for the signal peptide (SP), boxes for the conserved histidine brace (blue) axial tyrosine residue (red), and ω for the GPI-anchor attachment site.

Although NCU02884 and HAM-7 have enough similarity to create a homology model (Figure 3-1), it is hard to make a homology model for different families due to very low sequence homology. Nevertheless, the available structures of PMOs from the known families reveal a conserved β-sandwich, with disulfide bond(s) for stability, and a type II Cu center on a flat protein surface [151]. Two histidine residues in a motif termed the histidine brace coordinate the monocopper center, which has become the defining characteristic of PMOs. The first histidine starts the mature peptide after the signal peptide cleavage and has the N_{ε}-methylation; the second histidine is the PMO active site [151]. The N_{ε}-methylation of the first histidine is found in fungal PMOs, but not in bacterial PMOs.

Both NCU02884 and *ham-7* have a signal peptide, a conserved histidine brace and axial tyrosine residue, and ω site (Figure 4-1B). ω site is where the GPI transamidase cleaves the C-terminal

signal resulting in attachment of the preformed GPI-anchor to the target protein [152]. The GPI-anchor tethers the protein extracellularly to the cell membrane, and the axial tyrosine is involved in hydrogen bonding at the active site in the fungal PMO9 family. Additionally, these two proteins have the typical length of a PMO, which is roughly 220 amino acids.

4.3.2. Overexpression of NCU02884 in *Δham-7*ΔNCU02884

While it is possible to have redundancy in function between NCU02884 and *ham-7*, however, *Δham-7* and ΔNCU02884 mutants have a severe phenotypic difference. ΔNCU02884 mutants have a WT phenotype with growth, cell fusion and ability to form protoperithecia (Figure 4-2). We looked at the expression of NCU02884 in WT germlings, which showed essentially no expression (<1FPKM). In different growth conditions, there is a little bit higher expression but still 10-100 fold lower in comparison to *ham-7* expression. We reasoned that lack of fusion defect may be due to having a low expression, and it might be possible that NCU02884 has a redundant function. If these two proteins are similar in function, overexpression of NCU02884 in *Δham-7*ΔNCU02884 (OE NCU02884) should be able to rescue *Δham-7* defects.

OE NCU02884 had an intermediate growth on a slant, but was not able to rescue the *Δham-7* defect; OE NCU02884 phenocopied *Δham-7*, except that the strain appeared to have more and fluffier aerial hyphae (Figure 4-2A). Although there was no quantification of the growth rate or aerial hyphal growth, visually it was more comparable to *Δham-7* than WT. OE NCU02884 was slow to establish colonies from conidial inoculation, while it had comparable growth from hyphal inoculation on a VMM plate (data not shown). There are no other known PMOs that cause such a striking growth defect as *Δham-7* when deleted. Inability to complement the *Δham-7* defects suggest that there is no genetic redundancy.

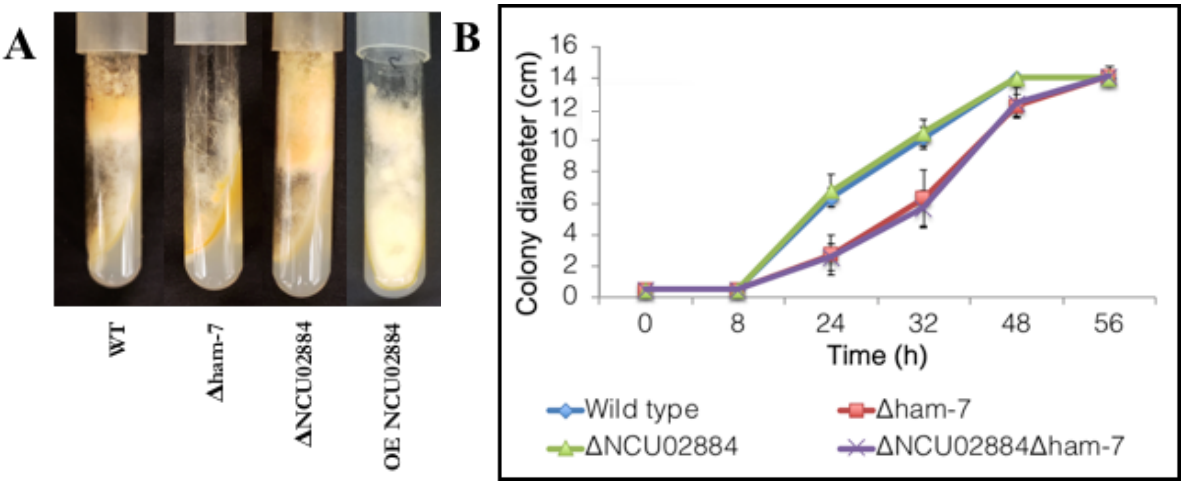

Figure 4-2. Phenotypic difference in ΔNCU02884 and *Δham-7*. a) ΔNCU02884 mutant has WT-like growth, *Δham-7* mutant has the typical fusion mutant phenotype, and OE NCU02884 has an intermediate growth that is more comparable to *Δham-7*. OE NCU02884 has a little bit more and fluffier (cloud-

like) aerial hyphae than *Δham-7*, however, the aerial hyphal growth has not been quantified to claim significant difference; the rest of the phenotype reflect that of *Δham-7*. b) There is a significant difference in the growth rate between ΔNCU02884 and *Δham-7*. The ΔNCU02884; *Δham-7* double deletion strain has *Δham-7* growth-like growth properties and cell fusion defect and does not display an additive or synergistic phenotypic defects.

4.3.3. Verification of HAM-7 as a putative PMO

To verify the bioinformatic analyses on HAM-7 as a PMO, we made individual mutations of the conserved histidine sites. We transformed *ham-7*^{H18A} and *ham-7*^{H76A} into the *his-3* locus of *Δham-7; his-3* mutant strain, and included targeting a WT version of HAM-7 to the *his-3* locus (*Δham-7; his-3::Ptef-1-ham-7,* refer to as *OE ham-7*) as a control. As the histidine brace is essential for PMO activity, mutation in the histidine residue would render HAM-7 unfunctional. If HAM-7 is a PMO, *Δham-7; his-3:: ham-7*^{H18A} and *Δham-7; his-3:: ham-7*^{H76A} (refer to as H18A and H76A, respectively) should duplicate the *Δham-7* phenotype. The strain containing the H18A and H76A mutations phenocopied the *Δham-7* growth and cell fusion defects, while the *OE ham-7* restored WT growth rate and cell fusion (Figure 4-1). Although some fusion mutants can have partially reduced germling fusion, strains bearing the *Δham-7,* H18A and H76A mutations have complete abolishment of germling fusion; H18A and H76A were unable to form protoperithecia, while *OE ham-7* were able to restore germling fusion and form protoperithecia (Figure 4-3). *Δham-7* aerial hyphal extends half of WT, 11 mm ± 1.3 and 18.2 mm ± 2.6, respectively [AT]. The same aerial hyphal growth was observed in H18A and H76A (Figure 4-3). H18A and H76 duplicates averaged 9.5 mm of arial hyphal extension, and 25.4 mm for *OE ham-7*.

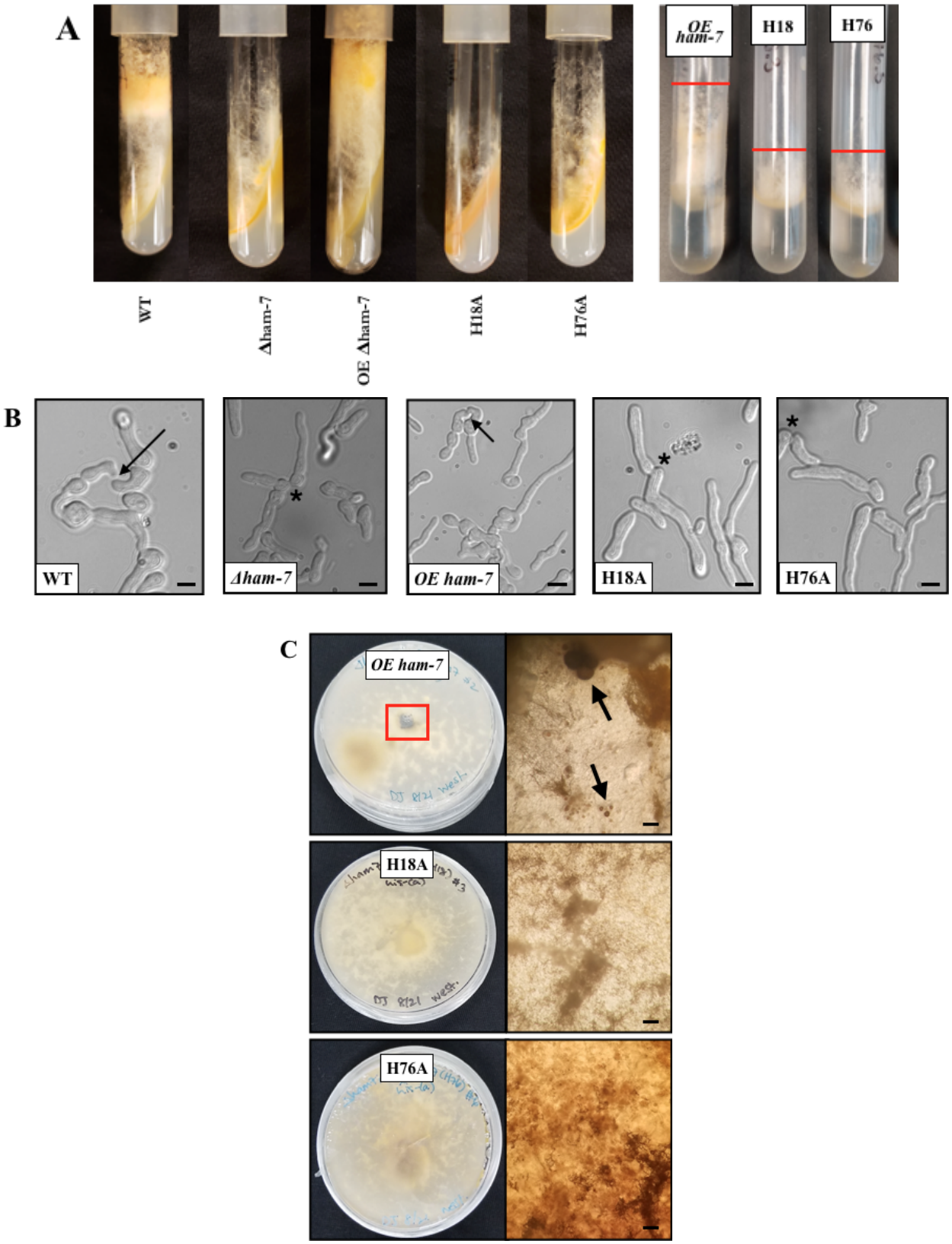

Figure 4-3. Mutation in the conserved histidine brace results in loss of PMO function. *OE ham-7* has restoration of WT phenotype, while H18A and H76A

maintains *Δham-7* phenotype: a) aerial hyphae (red line: tip of the aerial hyphae extension) b) germling fusion (scale bar: 5 μm, black arrow: fusion, asterisks: contact point, but no fusion) and c) formation of protoperithecia (scale bar: 100 μm, left panel: red box, right panel: black arrow). The right panel is an image from the dissecting microscope of the plate shown on the left panel.

Plates and race tubes inoculated with *Δham-7,* H18A and H76A mutant conidia showed significantly slower growth rate (Figure 4-3A) than WT strains. This observation is consistent with the study showing strains lacking the ability to fuse has slower colony establishment than strains that are able to fuse [153,154]. However, the growth rate of colony establishment is not correlated with linear growth rate of hyphal colony [153]; slower establishment does not result in slower hyphal growth. Race tube experiments, inoculated with mature mycelium, shows no significant difference in the growth rate (Figure 4-3B). Along with brief microscopic observation (data not shown), it appears that H18A and H76A have delayed germination but a comparable hyphal growth to WT.

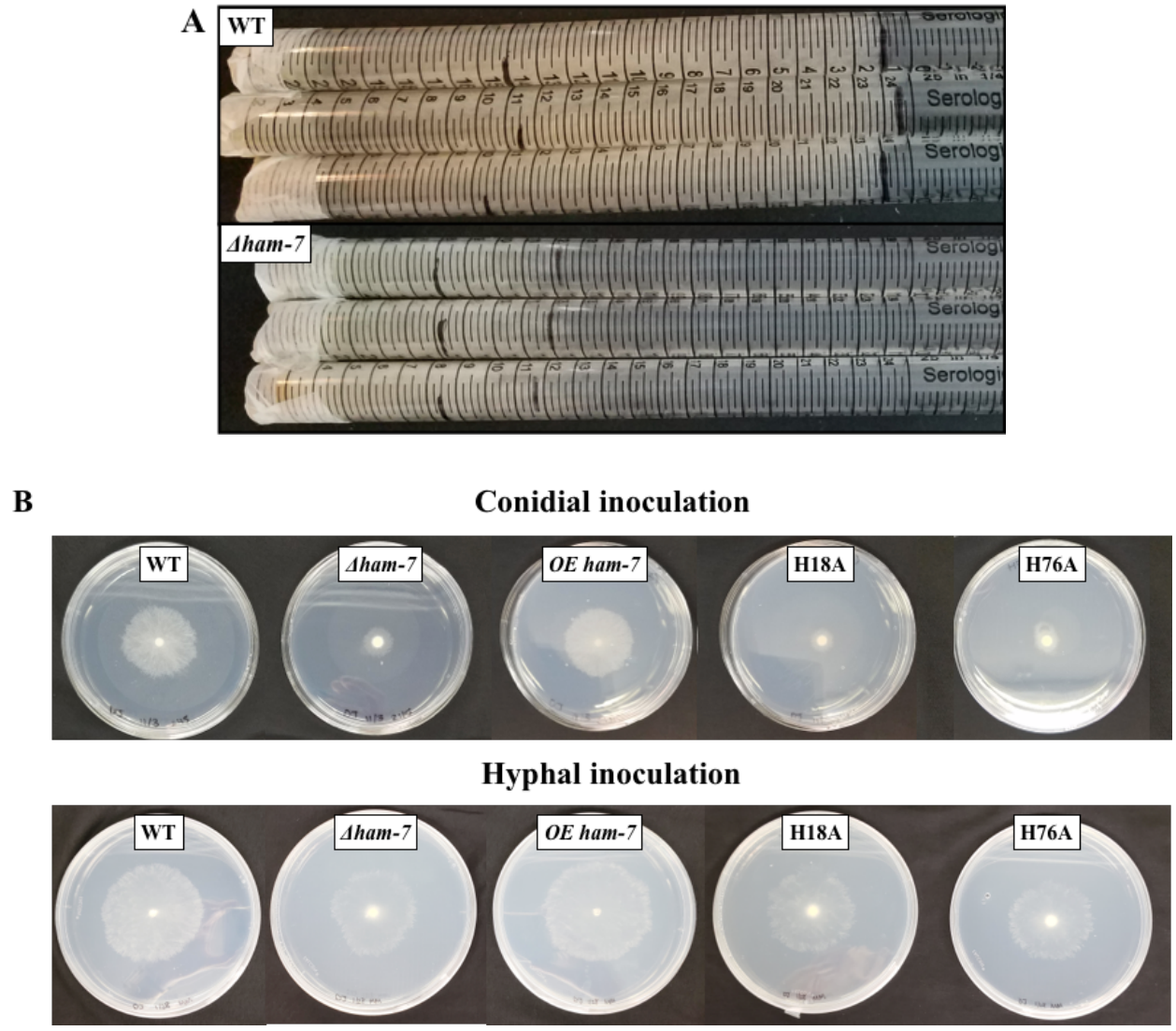

Figure 4-4. *Δham-7* has slower colony establishment. a) **Figure 4-4. *Δham-7* has slower colony establishment.** a) Race tubes, inoculated with conidia, show *Δham-7* a has slower growth than WT. b) The *OE ham-7* restores WT-like growth, while H18A and H76A maintain *Δham-7* growth when inoculated with conidia. However, there is not such drastic differences between the WT and the mutants (as seen in conidial inoculations) when VMM plates were inoculated with mature hyphae from these same strains. Cultures were grown for 24 hrs.

4.3.3. Truncation of the GPI-anchor of HAM-7 for secretion

Previously, the Marletta lab overexpressed HIS-tagged NCU02884 with a truncated GPI-anchor (NCU02884TR-HIS6X). NCU02884TR-HIS6X was able to be secreted out of the cell and was isolated from the secretome via HIS-tag purification. We predicted the protein molecular weight (MW) using a predictor tool (https://www.bioinformatics.org/sms/prot_mw.html), and compared

to the protein MW measured on a gel. Purified NCU02884TR-HIS6X on the SDS-PAGE gel is 12 kDa greater than the predicted MW (23 kDa), suggesting that it is glycosylated (Figure 4-5). From intracellular fractions, HA-HAM-7 is 18 kDa heavier than the predicted MW at 24.5 kDa [BJ].

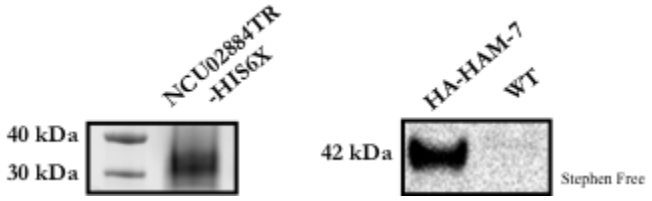

Figure 4-5. Molecular weight of NCU02884TR-HIS6X and HA-HAM-7. Western blots show purified NCU02884TR-HIS6X, on a SDS-PAGE gel, has a 12 kDa greater MW, and intracellular HA-HAM-7 (N-terminally HA-tagged, full length HAM-7) has an 18 kDa greater MW than the predicted weight (21.5 kDa and 25.5 kDa, respectively) [BJ].

Initial substrate binding assay results showed that secreted NCU02884TR bound to β-1,3-glucan, however, a glycosyl hydrolase contaminated the sample. Hypotheses based on previous discovery of β-1,3-glucan as the binding substrate led the hypothesis that HAM-7 and NCU02884 were modifying the fungal cell wall. HAM-7 is more essential than NCU02884, thus we focused on identifying the binding substrate of HAM-7 to better understand its function.

Unlike NCU02884-TR, HAM-7TR (truncation of the GPI-anchor) did not result in the secretion of HAM-7 to the outside of the cell. We tagged HAM-7TR with GFP (HAM-7TR-GFP) and confirmed that it is still bound at the cell wall (Figure 4-6). Although HAM-7TR-GFP is bound to the cell wall, it still showed a similar growth defect as the *Δham-7* mutant and was unable to undergo germling fusion. We suspected that a difference in the binding of NCU02884 and HAM-7 to the cell wall based occurred based on the significance of the protein to the cell. The *Δham-7* mutant has a morphological defect, while the ΔNCU02884 mutant does not; *ham-7* has higher expression, while NCU02884 has near 0 expression in WT cells. These data suggest that if these two proteins have redundant function, HAM-7 has a more important cellular function, while NCU02884 is a disposable paralog.

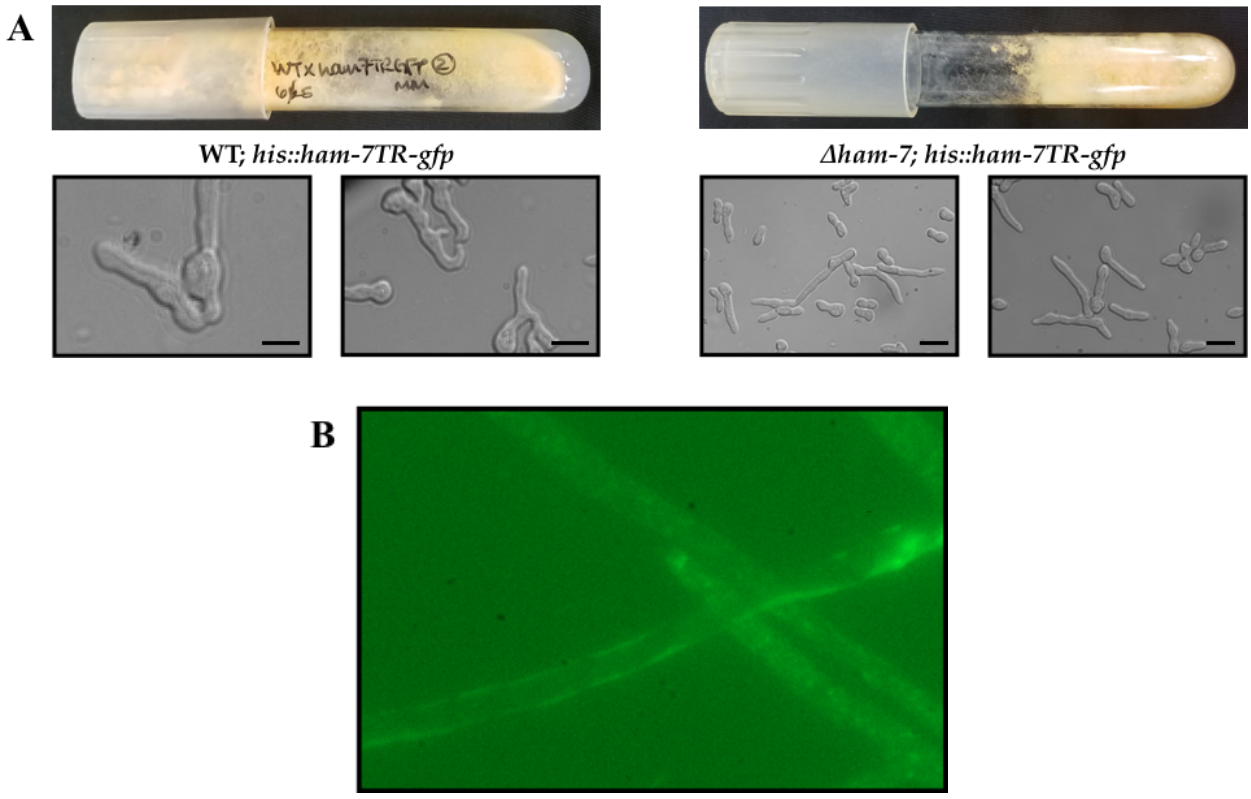

Figure 4-6. HAM-7TR-GFP localizes in the cell wall. HAM-7TR-GFP has a growth defect and loses ability to form protoperithecia, but truncation of GPI-anchor is not enough to secrete HAM-7 out of the cell. Scale bar: 10 μm

4.3.4. Additional mutation in N-glycosylation sites in HAM-7 for secretion

N. crassa requires N-linked oligosaccharides to incorporate cell wall proteins into the cell wall matrix [155]. HAM-7 is likely more glycosylated than NCU02884, as seen by the larger difference in the actual versus predicted molecular weight in those proteins (Figure 4-6); thus, we inferred that HAM-7TR was still bound to the cell wall from the crosslinking. Fungi has evolved multiple ways to crosslink glycoproteins to the cell wall to provide redundancy in function and strengthen the cell wall [125]. Most of the cell wall structural proteins are crosslinked to the cell wall, and have signal peptides and a GPI-anchor signal. Galactomannan oligosaccharide, which is required for the covalent incorporation of cell wall proteins, attaches to the N-linked oligosaccharides of *N. crassa* [155]. Mutants lacking galactomannan synthesis secreted their cell wall proteins, which shows N-glycosylation is another mechanism to ensure proteins crosslinking to the cell wall. To bypass the crosslinking of the protein, we assessed which N-glycosylation to mutate. Five possible N-glycosylation sites were predicted in HAM-7 by GlycoEP, a web server that is optimized to predict glycosylation sites using eukaryotic glycosite dataset. Figure 4-7 shows the alignment of HAM-7 and NCU02884 and five N-glycosylation sites in HAM-7. Out of the five, we selected three asparagine (N) residues unique to HAM-7 and mutated these to glutamine residues (Q). N-glycosylation sites are usually mutated to glutamine because it has the most conserved amino acid substitution and differs by a

single methylene group [156]. Two different tags were used for *ham-7*$^{N122Q\ N157Q\ N163Q}$ *TR,* GFP and V5. GFP was for cellar visualization by microscopy, and V5 was used in case the GFP tag was too large and disrupted the function of the tagged protein.

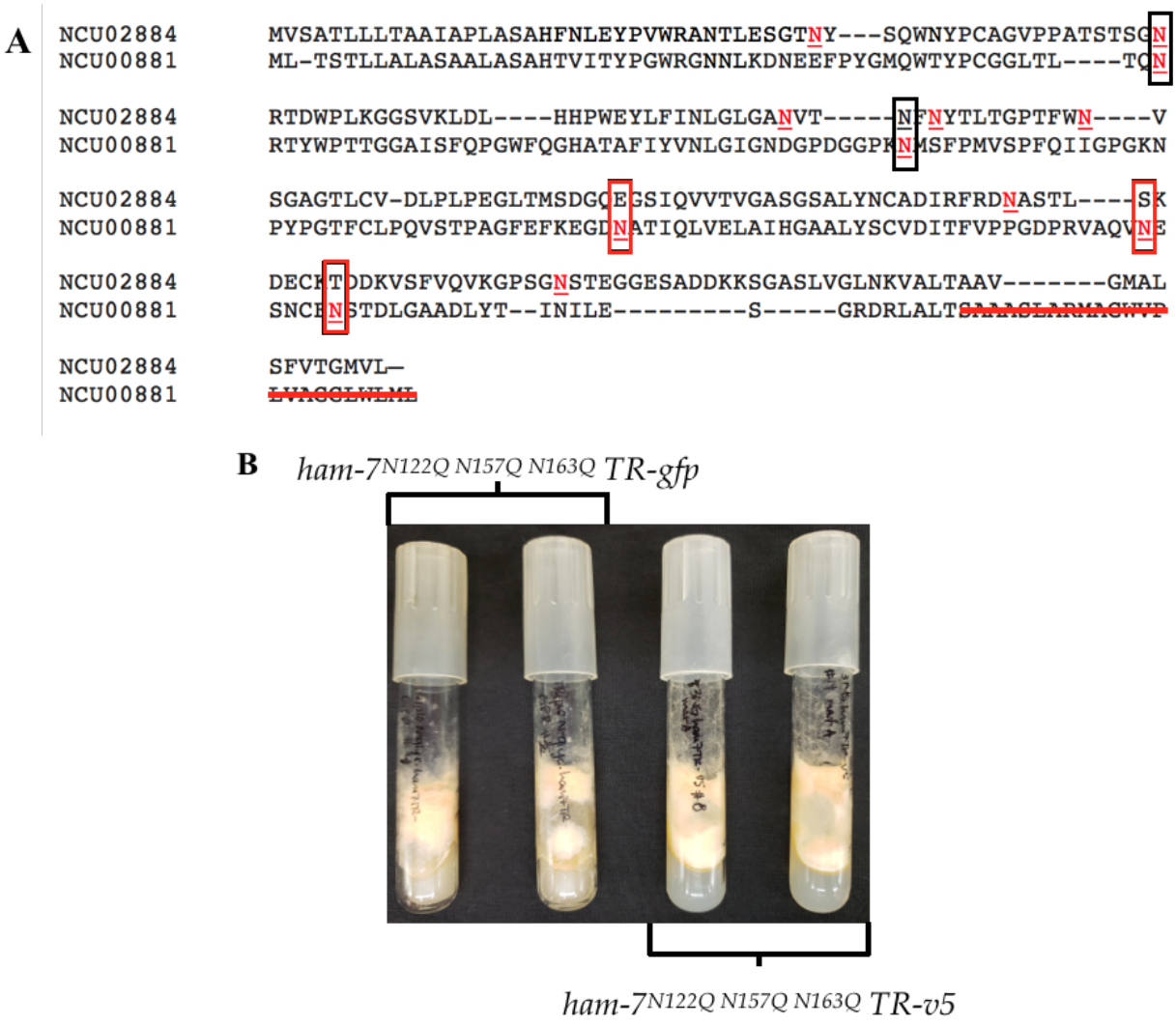

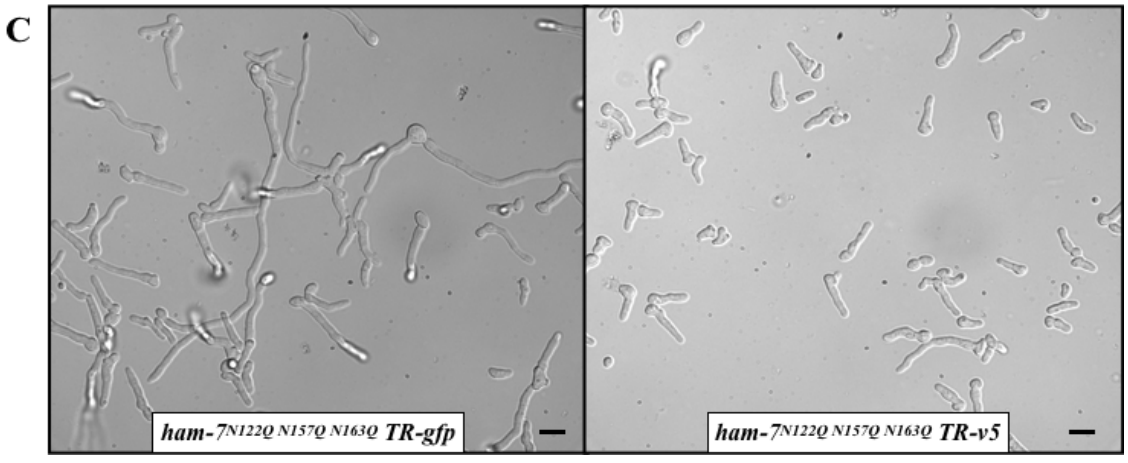

Figure 4-7. Removal of HAM-7 unique N-glycosylation sites. a) Boxes highlight predicted N-glycosylation sites in HAM-7. Black box: N-glycosylation sites that are also present in NCU02884. Red box: N-glycosylation sites that are unique to HAM-7. To secrete HAM-7, we removed the GPI-anchor and mutate the three asparagines to glutamines. b) *ham-7*$^{N122Q\ N157Q\ N163Q}$ *TR-gfp/v5* have intermediate growth phenotype, but has closer resemblance to *Δham-7*. c) *ham-7*$^{N122Q\ N157Q\ N163Q}$ *TR-gfp/v5* strains lack germling fusion. Scale bar: 10 μm

ham-7$^{N122Q\ N157Q\ N163Q}$ *TR-gfp/v5* had intermediate growth phenotype; the strains were not as sick as the *Δham-7* mutant (Figure 4-7). However, these mutants were not able to undergo germling fusion. Interestingly though, there was no GFP fluorescence in *ham-7*$^{N122Q\ N157Q\ N163Q}$*TR-gfp* progeny observed in the cell wall, in contrast to what was seen in HAM-7TR-GFP strains.

The lack of intracellular GFP fluorescence could indicate two things: HAM-7$^{N122Q\ N157Q\ N163Q}$ TR-GFP is not produced or it is being secreted. To differentiate these two possibility, we harvested germlings and mycelia at 24 hrs and lysed them to verify the presence of HAM-7$^{N122Q\ N157Q\ N163Q}$ TR-GFP/V5 inside the cell. Cells were lysed via different methods due to the differences in final fungal biomass. Nothing was conclusive from the faint bands seen on the Western blot on germling samples, but a strong band at a size predicted to be HAM-7$^{N122Q\ N157Q\ N163Q}$ TR-GFP was observed in the hyphal samples. EG-2-GFP was not observed because Δ3βG; EG-2-GFP was grown in VMM rather than cellobiose, which induces endoglucanase production. The molecular weight for EG-2-GFP is 69 kDa, DOC-1-V5 is 93 kDa, HAM-7 is 41 kDa, GPI-anchor is 2.5 kDa, GFP is 27 kDa, V5 is 1.5 kDa and N-glycosylation is 2.5 kDa. The predicted molecular weight of HAM-7$^{N122Q\ N157Q\ N163Q}$ TR-GFP is calculated to be 58 kDa:

41 kDa (HAM-7) - 2.5 kDa (GPI-anchor) + 27 kDa (GFP tag) - 7.5 kDa (removal of 3 N-glycosylation)

The predicted molecular weight for the HAM-7$^{N122Q\ N157Q\ N163Q}$ TR-V5 is 32.5 kDa:

41 kDa (HAM-7) - 2.5 kDa (GPI-anchor) + 1.5 kDa (V5 tag) - 7.5 kDa (removal of 3 N-glycosylation)

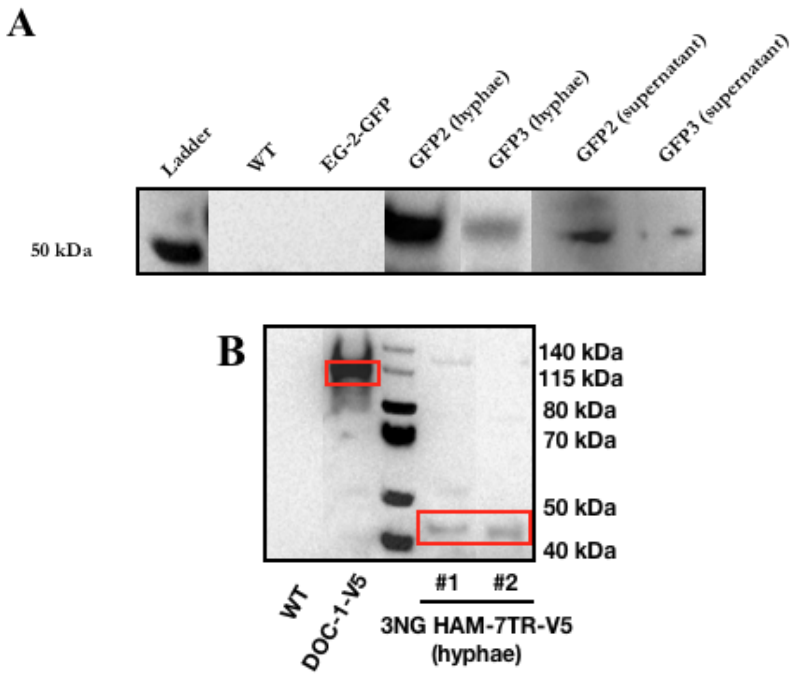

Figure 4-8. Detection of HAM-7$^{N122Q\ N157Q\ N163Q}$ TR- GFP/V5 in cell lysate and supernatant via Western blot. HAM-7$^{N122Q\ N157Q\ N163Q}$ TR- GFP b) HAM-7$^{N122Q\ N157Q\ N163Q}$ TR-V5 was present in the hyphae, but was not detectable in the supernatant (data not shown).

To test if HAM-7$^{N122Q\ N157Q\ N163Q}$ TR- GFP/V5 was secreted, we probed the supernatant with anti-GFP and anti-V5 antibodies. HAM-7$^{N122Q\ N157Q\ N163Q}$ TR- GFP #2 has a faint band where we predict the molecular weight of the protein to be. We detected the right length band for HAM-7$^{N122Q\ N157Q\ N163Q}$ TR-GFP again in sample #1 and #2, where we doubled the media and time to allow more protein accumulation. However, HAM-7$^{N122Q\ N157Q\ N163Q}$ TR-V5 did not have detectable bands.

4.4. Conclusion

As a secreted extracellular protein, HAM-7 has a N-terminal signal peptide and a C-terminal GPI-anchor site. Increasing the modifications to the protein will increase the likelihood of interrupting proper folding and functionality.To identify the binding substrate of HAM-7, the purified protein must remain functional. We attempted multiple approaches to secrete HAM-7 that we have not described in this chapter. Ultimately, we were able to release the full HAM-7 protein into the supernatant by removing three out of the five N-glycosylation sites and the GPI-anchor, but the integrity of the protein for biochemical assays is yet to be determined.

Even though we were able to see bands for HAM-7$^{N122Q\ N157Q\ N163Q}$ TR-GFP in the supernatant, they were still faint bands. Consistent with HAM-7$^{N122Q\ N157Q\ N163Q}$ TR-V5, we saw bands in the cell lysate, but not in the supernatant. These data suggest there was not enough protein

accumulation in the supernatant for purification. Theoretically, using a constitutively active promoter (*Ptef-1*) should eliminate the issue of having little protein production. Despite using *Ptef-1*, HAM-7$^{N122Q\ N157Q\ N163Q}$ TR-GFP is found in low levels in the supernatant. This could be due to protein degradation due to improper folding of the protein. We are currently confirming the secretion of HAM-7$^{N122Q\ N157Q\ N163Q}$ TR-GFP by running the protein gel samples through the mass-spectrometry (MS). If HAM-7 is identified in the MS data, we will scale-up protein production and test the PMO activity of HAM-7$^{N122Q\ N157Q\ N163Q}$ TR. Western blots and MS do not tell the functionality of the proteins whether it is disrupted by the tag or the protein modification. Horseradish peroxidase coupled assay can measure the reactivity of PMOs; in the absence of a polysaccharide substrate, PMOs reduce O_2 and produce H_2O_2 [BP]. After testing the functionality of the PMO, future plans will be to identify the binding substrate via electrospray-ionization-mass spectrometry and to create a crystal structure of the new PMO family.

As an alternative to expression in *N. crassa*, we have been developing methods to heterologously express HIS6X tagged HAM-7$^{N122Q\ N157Q\ N163Q}$ TR in *Pichia pastoris*. A major advantage of *P. pastoris* over bacterial expression systems is that the yeast has the potential to perform many of the post-translational modifications typically associated with higher eukaryotes, such as processing of signal sequences (both pre and prepro type), protein folding, disulfide bridge formation, certain types of lipid addition, and O- and N-linked glycosylation [157].

Other HAM-7 orthologs are likely to be in the PMO17 family based on the alignment, conservation of core PMO characteristics and similar phenotypic defects in the deletion mutants. They have a signal peptide and extracellularly bound to the cell wall by a GPI-anchor, along with conserved histidine brace, tyrosine and four cysteine residues. With high sequence similarity, it would explain the intermediate phenotype seen in *P. anserina* when expressing GFP tagged *E. festucae* IDC2 (EfIDC2-GFP) [141]. The GFP tag was fused right after the signal peptide cleavage site and threonine 198 (a region of non-conservation) of EfIDC2. We speculate the intermediate phenotype was the result of GFP interfering with the active site of the first conserved histidine, while fusing the GFP after threonine 198 caused an improper folding of IDC2. Regardless, they pursued to analyze the localization of EfIDC2-GFP and observed that it localizes to the cell wall. Although EfIDC2-GFP was likely a nonfunctional protein, due to the GPI-anchor and the crosslinking, EfIDC2-GFP localized to the cell wall. Protein modification does not interrupt the ability of HAM-7 ortholog from binding to the cell wall.

Data presented in this chapter suggest that HAM-7 is part of a new PMO family, PMO17. The N-terminal signal peptide directs the PMOs to be secreted, where they boost the efficiency of cellulases to degrade recalcitrant polysaccharides while lowering the enzyme loading [143]. PMO17 is particularly interesting because HAM-7 and NCU02884 are the only PMOs to-date that are known to have a GPI-anchor. Moreover, HAM-7 is the only PMO that plays a role in signaling and morphogenesis in fungi. Deletion of other PMOs does not generate growth or cell

fusion defective phenotype, including its homolog NCU02884. There is much to be explored about the function of PMOs. Ultimate goal is to investigate the role of the PMOs in cell signaling, chemotropic interactions and regulation of cell wall deconstruction during cell fusion, using *N. crassa* as a model system. Unraveling the role of PMO17 will shift our perspective on the function and involvement of these enzymes in biological processes, such as cell fusion.

PERMISSION TO USE DATA

Many thanks to collaborators Elise Span and Tyler Detomasi in the Marletta laboratory for allowing use of the *N. crassa* biochemistry data, and Stephen Free for his advice.

Chapter 5. Involvement of *ham-7* in the cell wall integrity pathway

5.1. Introduction

Previous studies identified *wsc-1* (orthologous to yeast Wsc family) and *ham-7* as cell wall sensors, working upstream to regulate the activities of the CWI pathway [100]. The phosphorylation of MAK-1 is significantly reduced *Δwsc-1* and *Δham-7* mutants. As predicted cell wall sensors, *Δham-7* and *Δwsc-1* mutants do not fully phenocopy each other or *Δmak-1* mutant phenotypes [132,158,159]. While a *Δwsc-1* mutant has reduced growth rate, conidiation defects and sensitivity to cell wall stress agents, it can undergo hyphal anastomosis and forms protoperithecia. The *Δham-7* mutant lacks cell fusion, has defects in protoperithecium development, exhibits flat growth (no tight compact growth like *Δwsc-1*), but has WT-like resistance to stress agents [100]. The *Δmak-1* mutant phenocopies both the *Δwsc-1* and *Δham-7* mutant phenotypes. This phenotypic discrepancy between the *Δwsc-1* and *Δham-7* mutants led to the speculation that the two genes are functioning differently in regulating the CWI pathway.

While MAK-1 phosphorylation data suggest that *ham-7* could be a cell wall sensor and function upstream of the CWI MAPK pathway [100], further verification was needed to confirm this hypothesis. Changes in circadian rhythm and cell wall stress can cause a change in phosphorylation of MAK-1, and there may be more activation cues that have not been discovered. Without having a clearer understanding of the different modes of MAK-1 activation, it is hard to make conclusions on phosphorylation data that might result in pleiotropic effects. Due to the lack of understanding of different modes of MAK-1 activation, quantification of phosphorylation activity is not a reliable method to determine whether *ham-7* is upstream of *mak-1* in the CWI pathway. To further explore the role of *ham-7* in the communication and fusion mechanism, we conducted RNA-sequencing in germlings to compare the expression patterns of *Δham-7, Δmak-1* and *Δmak-2* mutants. The comprehensive RNA-seq analysis supports the hypothesis that HAM-7 does not function upstream of the CWI pathway, but rather downstream of *mak-1*.

5.2. Materials and methods

5.2.1. Cell wall stress assay

To prepare the plates for the cell wall stress assay, 45 mL VMM + FIGS + drug were added on to 150 x 15mm petri dishes. Conidial suspension of 1 x 10^6 spores/mL was prepared as the most concentrated dilution, and a series of 1:5 dilution was spotted on the plates, 5 µL per spot. Different concentrations of the drugs and lytic enzymes were tested to find the optimal concentration to test the sensitivity of the strains. The range of concentrations tested for Calcofluor white was 0.01-0.1µg/mL, Caspofungin was 1-1.5 µg/mL and Congo Red was 0.05-0.14 mg/mL, and lysing enzyme went as high as 75 mg/mL (had no effect). The paradoxical effect has been demonstrated in Caspofungin, where high drug concentrations derepressed or activated resistance mechanisms, which allowed growth on media with caspofungin above the minimum inhibitory concentration [160].

5.2.2. RNA isolation

WT *mat A*, WT *mat a*, *Δham-7, Δmak-1* and *Δmak-2* strains had three biological replicates. Both of the mating types for the WT control were submitted because *Δham-7* and *Δmak-1* were *mat A* and *Δmak-2* was *mat a*. In order to obtain enough conidia for the RNA extraction, several 150 x 15 mm VMM plates were inoculated with *Δham-7, Δmak-1* and *Δmak-2* strains. 1 x 10^8 conidia

was suspended into 100 mL of liquid VMM, and were grown under constant light at 25°C. The flasks were shaken at 220 RPM for 4.5 hours to reach the germination stage and left still for an additional 2.5 hours to induce germling chemotropic interactions and cell fusion. Due to slower conidial germination of *Δham-7, Δmak-1*, and *Δmak-2* strains (visualized under the microscope), these strains were shaken for 4.5 hours instead of the normal 2.5 hours for germination to reach WT levels. The germlings were filtered using nitrocellulose membranes (0.45 μm), added into 2 mL screw-cap tubes with glass beads and flash frozen in liquid nitrogen. RNA extraction was conducted using the TRIzol-based protocol found in Leeder *et al.* 2013 [130]. RNA samples were cleaned using Qiagen RNeasy kit and DNaseI, and tested for the expression of the deleted gene in *Δham-7, Δmak-1*, and *Δmak-2* strains via qRT-PCR. After the confirmation of the deletion strains, the RNA samples were submitted to QB3-Berkeley Vincent J. Coates Genomics Sequencing Laboratory for the bioanalyzer, mRNA library preparation and sequenced for 50-bp single reads on the HiSeq4000.

5.2.3. qRT-PCR

RNA samples for qRT-PCR reactions were prepared following the manufacturer protocols for the Bioline SensiFast™ SYBR® no-ROX One-Step kit and Bio-Rad CFX Connect™ Real-Time PCR Detection System. Each sample had technical duplicates of the biological triplicates in a 96-well plate, each reaction consisting of 20 μL. Expression data was normalized to both actin and wild-type following the 2^{-DDCt} method [161].

5.2.4. RNA-sequencing and transcript abundance

HiSat2 v2.0.5 [162] was used to align the RNA sequences to *N. crassa* OR74A genomic transcripts (v12) [163]. After the alignment, Cufflinks v2.2.1 was used to measure transcript abundance (fragments per kilobase of transcript per million mapped reads, FPKM) and quantify differential gene expression [164].

First, all the genes that had p-value <0.05 and were significantly different (up-/down-regulated) in the *Δmak-1* and *Δmak-2* strains were compiled. Then, genes that were differentially regulated between WT *mat A* and *mat a* strains were removed from lists. The shortened list of genes was input in Venny 2.1 (http://bioinfogp.cnb.csic.es/tools/venny/index.html) to find overlapping genes.

The gene IDs from the different compiled lists were analyzed with gene ontology (GO) enrichment [165] in FungiDB (https://fungidb.org/fungidb/), and subjected to the preset parameters provided (evidence: computed & curated, limit to GO Slim terms: no, and P-value: 0.05) to assess related biological processes. The GO terms were enriched using reduce and visualize gene ontology (REVIGO), where the parameter was set as small (0.5) for "allowed similarity". After the enrichment, the cluster representatives may be submitted to four different visualization procedures: scatterplots, a graph-based visualization, tree maps, and tag clouds [166].

Cluster 3.0 software suite (bonsai.hgc.jp/~mdehoon/software/cluster/software.htm) was used for hierarchical clustering. Hierarchical clustering was performed using the using the average linkage method with uncentered correlation as the similarity metric. Before clustering, FPKMs from each strain/condition were averaged, log-transformed, and centered on the geometric mean

across conditions. After the clustering, the heatmap was visualized using TreeMap v. 2019.1.0 (https://www.treemap.com/download/all/).

5.3. Results

5.3.1. Phosphorylation of MAK-1 and MAK-2

Deleting the *mik-1*, *mek-1* and *mak-1* CWI pathway kinases, results in reduced vegetative growth, cell fusion defects, an inability to produce protoperithecia and extremely low macro- and microconidiation [132,87,159]. The *Δwsc-1 and Δham-7* mutants do not have the same phenotypic defects, and only partially phenocopy *Δmik-1*, *Δmek-1* and *Δmak-1* mutant phenotypes [100]. Significantly reduced phosphorylation of MAK-1 (P-MAK-1) in *Δwsc-1 and Δham-7* introduced the hypothesis that these genes are cell wall sensors and function upstream of the CWI pathway. The WSC family of proteins is known to function as cell wall sensors for the CWI and stress response pathway in *S. cerevisiae* and *Aspergillus* species, however, there is no other evidence that indicates *ham-7* works upstream of *mak-1*.

We sought to verify the MAK-1 activity results in the *Δham-7* mutant by replicating the Western blot on P-MAK-1 in *Δham-7* germlings. However, we observed inconsistent levels of MAK-1 and MAK-2 phosphorylation to the previously published data. However, even biological replicates of WT showed variation in MAK-1 and MAK-2 phosphorylation (data not shown). Rhythmic phosphorylation of MAK-1 and MAK-2 indicates that the MAP kinases are clock-regulated in *N. crassa* [167]. In addition, Fleißner et al., showed dynamic phosphorylation activity of MAK-1 and MAK-2 through an 8.5 hour time period in germlings [108]. Their data suggests that there are two components to the cell fusion reaction: initiation and maintenance of the tropic interactions of the fusing cells and mediation of cell-cell recognition upon contact. They hypothesized that lower MAK-1 activity in the cytoplasm induces directed growth, while accelerated expansive MAK-1 activation induces recruitment to the cell cortex for cell-cell contact recognition. Due to the lack of understanding of different modes of MAK-1 activation, it is difficult to assess what is causing the inconsistency of MAK-1 activity. These results make it difficult to make definitive statements regarding whether *ham-7* is upstream of *mak-1* in the CWI pathway through phosphorylation activity. The variability in phosphorylation of the MAP kinases deemed quantification of P-MAK-1 not a good method of determining whether *ham-7* functions upstream of *mak-1*.

In the *Podospora anserina* ortholog, IDC2, the deletion strain also did not show reduced MAK-1 activity via Western blot [141]. Furthermore, in *Epichloë festucae*, Western blot analysis of MpkA (ortholog of MAK-1) and MpkB (ortholog of MAK-2) phosphorylation and localization of MpkA-eGFP and MpkB-eGFP showed no difference between WT and *ΔsymB* (*ham-7* ortholog) mutants [168]. The inconsistency of P-MAK-1 in *N. crassa* and HAM-7 orthologs questions the function of *ham-7* as an upstream regulator of *mak-1*.

5.3.2. The role of HAM-7 in the cell wall integrity (CWI) pathway

The phenotypic differences in *Δwsc-1* and *Δham-7* demonstrates that they are working in different cellular pathways: cell fusion or cell wall stress. The inconsistency in the activity of the MAK-1 prompted us to repeat the cell wall stress assay in the *Δham-7* mutant relative to WT. To examine if *Δham-7* was causing a structural defect in the cell wall, we tested the sensitivity to cell wall stress agents such as Congo Red (CR), Calcofluor white (CFW), caspofungin and lytic enzymes. Lytic enzymes did not have enough effect on the strains to show difference in drug

sensitivity (data not shown). The *Δwsc-1* mutant struggled to grow in CR, CFW and caspofungin, while the *Δham-7* mutant had WT growth phenotype (Figure 5-1). The *Δwsc-1* sensitivity to these agents and the *Δham-7* resistance are consistent with the previous study [100]. Additionally, in *E. festucae,* the *ΔsymB* (*ham-7* ortholog) has WT growth under cell wall stress conditions [168]. Thus, *ham-7* is not likely to be involved in the maintenance of the cell wall structure and integrity, like *wsc-1*.

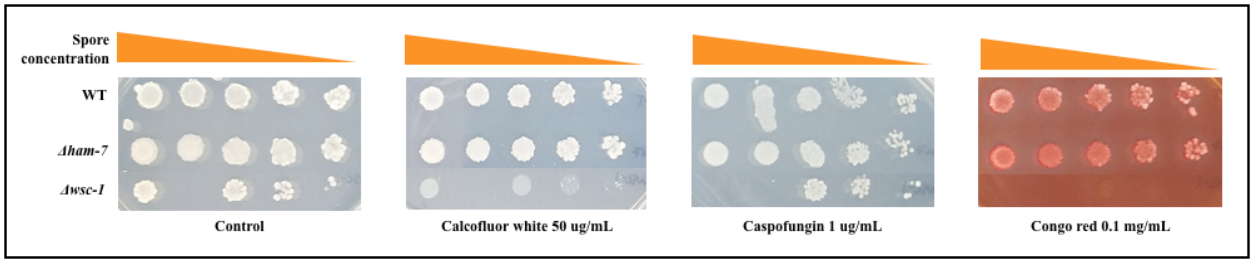

Figure 5-1. Cell wall drug sensitivity in *Δham-7*. We tested for *Δham-7* sensitivity to CR, CFW and caspofungin. Orange triangles indicate the concentration of conidia spotted on each plates. *Δham-7* has WT-like resistance to cell wall stress agents.

5.3.3. RNA-seq analysis

Expression pattern of genes down- and up-regulated in both *Δmak-1* and *Δmak-2* strains

The Venn diagram shows 139 and 106 genes that were significantly down- and up-regulated in *Δmak-1* and *Δmak-2* strains, respectively (Figure 5-2). We utilized reduce and visualize gene ontology (REVIGO) to reduce redundancy within the lists of GO terms in the differentially regulated genes [166]. The GO enrichments analysis was used to create treemaps to visualize the GO terms in two-level hierarchical graph [166]. Each rectangle represents a single cluster, which is then joined into superclusters of generally related GO terms. Superclusters and individual cluster representatives are displayed in different colors, and the sizes of the rectangles were adjusted to reflect the frequency of the GO term in the given list. One caveat to note in using REVIGO is that hypothetical proteins are not included in the treemap analysis.

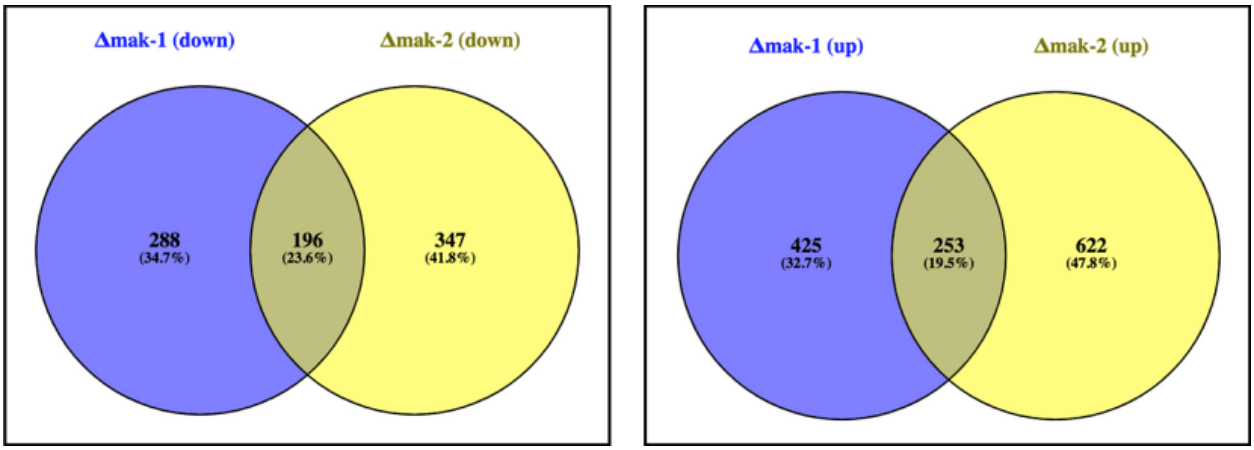

Figure 5-2.Venn diagram of genes down-regulated (left) and up-regulated (right) in *Δmak-1* and *Δmak-2*.

The 196 genes in the down-regulated list that overlapped between *Δmak-1* and *Δmak-2* strains formed four superclusters (syncytium formation by plasma membrane fusion, cellular response to chemical stimulus, positive regulation of macromolecule metabolism and membrane fusion) and single clusters for growth, signaling, cell communication, developmental process, reproduction and other cellular processes (Figure 5-3A). As expected, the biological processes that are down-regulated in *Δmak-1* and *Δmak-2* corroborate the functions that they are known to regulate; MAK-1/ADV-1 and MAK-2/PP-1 regulate cell communication, fusion, signaling, development, growth, response to stress and reproduction [129].

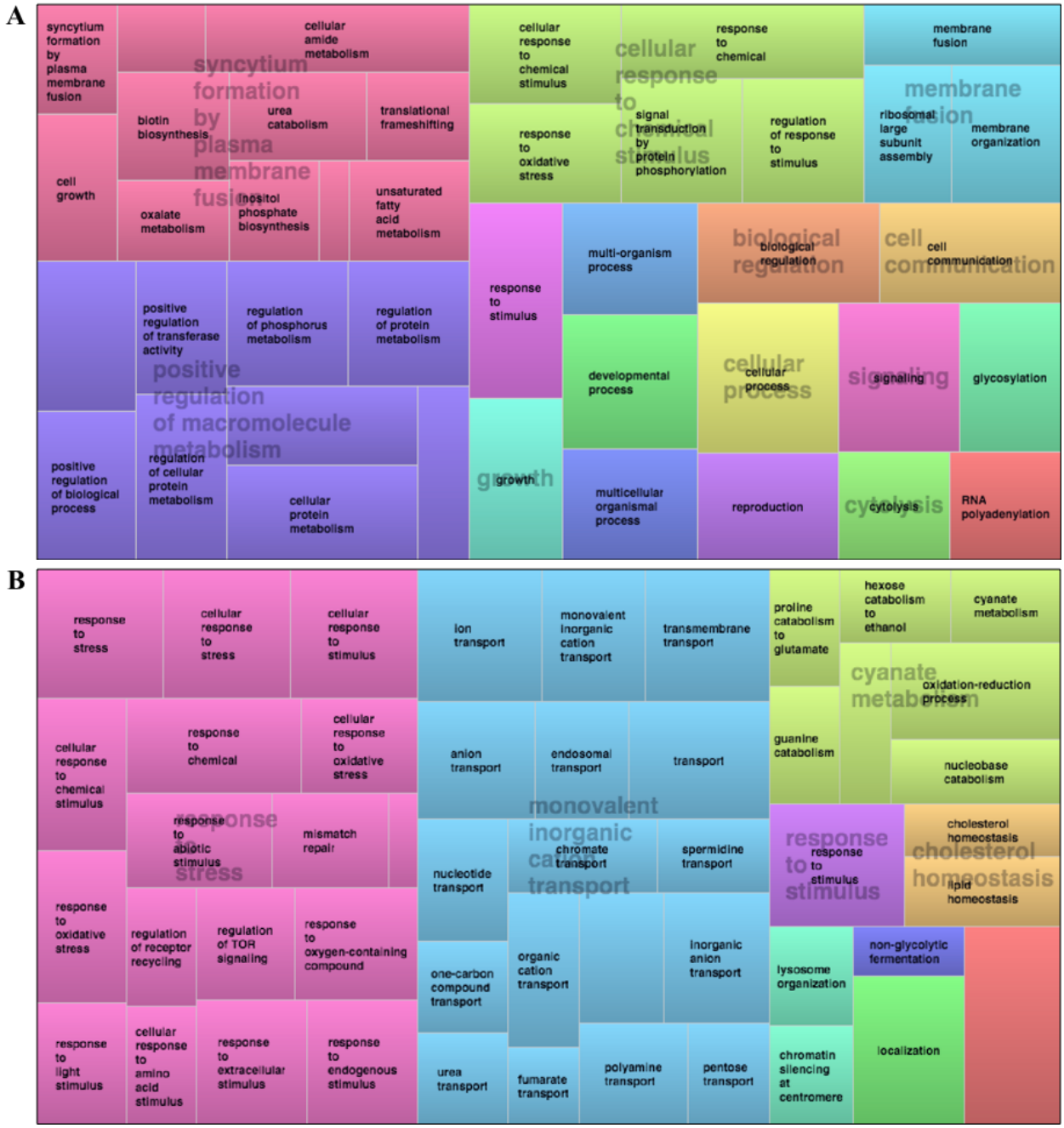

Figure 5-3. Treemaps of genes down- and up- regulated in both *Δmak-1* and *Δmak-2.* a) Superclusters in the down-regulated genes are syncytium formation by plasma membrane fusion (**rose pink**), cellular response to chemical stimulus (**green**), positive regulation of macromolecule metabolism (**purple**) and membrane fusion (**cyan**). b) Superclusters in the up-regulated genes are response to stress/stimulus (**rose pink & light purple**), monovalent inorganic cation transport (**teal**), cyanate metabolism (**olive green**) and cholesterol homeostasis (**orange**).

Up-regulated biological processes in *Δmak-1* and *Δmak-2* mutants are response to stress/stimulus, monovalent inorganic cation transport, cyanate metabolism and cholesterol homeostasis (Figure 5-3B). The up-regulation of cyanate metabolism in *Δmak-1* and *Δmak-2* indicates that *N. crassa* is metabolizing cyanate to provide a nitrogen and carbon source in fruiting bodies, and under damage or stress conditions [167-170]. NCU01258 (cyanate lyase) is also up-regulated in all *Δham-7, Δmak-1*, and *Δmak-2* mutants. As seen by the supercluster in Figure 5-3B, *mak-1* and *mak-2* only regulates some stress responses. OS-2, homologous to *S. cerevisiae* HOG1 pathway, is critical for regulating responses to various stresses (oxidative, heat stress, adaptation to changing osmotic pressure, etc) [171-172]. The OS pathway modules are not differentially regulated in *Δmak-1* and *Δmak-2* (except for *os-2* is slightly down in *Δmak-1*), however, suggesting that the OS-2 pathway ability to trigger stress response may not be affected.

5.3.4. The expression pattern in down-regulated genes in either *Δadv-1* or *Δpp-1*

Chromatin-immunoprecipation (ChIP)-sequencing and DNA affinity purification (DAP)-sequencing studies indicated communication and cell fusion genes are direct targets of ADV-1, including *ham-7* [129]. RNA-seq analysis also corroborated that *adv-1* and *pp-1* are positive regulators of communication and cell fusion; *Δadv-1* and *Δpp-1* strains are unable to undergo chemotropic interactions and cell fusion [129]. Additionally, it has been shown that *symB* is a direct downstream target of ProA, the homolog of *adv-1* in *E. festuca*e [168]. Previously, it has been shown that *mak-1* and *mak-2* function upstream of *adv-1* and *pp-1*, respectively [129]. Thus, we looked at the expression levels in *Δham-7, Δmak-1* and *Δmak-2* mutants of the 155 genes that were positively regulated by *adv-1* and/or *pp-1* [Monika], and found that 73 of the 155 (47%) genes were significantly down-regulated in all three deletion strains. The GO term enrichment for the 73 genes can be visualized with a treemap in Figure 5-4A, and the composition of GO term categories are response to chemicals and stimulus (29%), membrane fusion (13%), structural development (24%), reproduction (7%), and other cellular processes (28%). The *Δham-7*, *Δmak-1* and *Δmak-2* mutants are characterized by their flat phenotype, female sterility and defective cell fusion, thus these cellular processes are expected to be down-regulated in these mutants.

Figure 5-4. Treemap of *adv-1* and *pp-1* regulated genes. a) 73 genes are down-regulated in all *Δham-7, Δmak-1* and *Δmak-2*. In parallel with *Δham-7* to *Δmak-1* and *Δmak-2* flat phenotype, female sterility and defective cell fusion, the treemap shows down-regulation in response to chemicals and stimulus (29%, **purple & light purple**), membrane fusion (13%, **olive green**), structural development (24%, **rose pink, olive green & yellow**), reproduction (7%, **navy**), and other cellular processes (28%). b) 25 genes are down-regulated in *Δmak-1* and *Δmak-2,* not in *Δham-7.* 45% of the GO terms are involved in the regulation of transferase activity (**purple**, including regulation of protein phosphorylation and signaling cascade).

Aside from the expected cellular processes that are associated with *Δham-7* to *Δmak-1* and *Δmak-2* phenotypic defects, we examined the genes that were differentially regulated in *Δham-7* verses *Δmak-1* and *Δmak-2*. Our analysis revealed 16% (25/155) of the genes were down-regulated in only *Δmak-1* and *Δmak-2*. Because *mak-1* and *mak-2* are part of the signaling cascade, it is appropriate that 45% of the treemap in Figure 5-4B is part of regulation of transferase activity supercluster (signaling, cell communication, protein phosphorylation, etc). Many of the genes included in the transferase activity supercluster have a role in chemotropic interactions and communication, which were not down-regulated in *Δham-7* (Table 5-1).

Table 5-1. Down-regulated genes in *Δmak-1* and *Δmak-2,* but not in *Δham-7* that are positively regulated by *adv-1* and/or *pp-1* (values in each column are log2 fold change).

Gene description	Cellular function	*Δmak-1*	*Δmak-2*
NCU01509_hypothetical protein	adhesion	-4.33	-1.53
NCU04732_ham-11	communication	-1.82	-1.59
NCU02767_ham-6	communication	-1.75	-1.45
NCU02811_ham-8	communication	-1.80	-1.30
NCU06419_mek-1	communication	-1.25	-1.62
NCU02110_nox-1	communication	-0.98	-0.89
NCU04645_Mitochondrial biogenesis AIM24	communication	-2.05	-1.51
NCU05916_alpha-1,3-mannosyltransferase CMT1	communication	-0.98	-0.81
NCU05836_glycosyl hydrolase family 47 protein	communication	-1.50	-0.81
NCU04847_cyclin	development	-0.91	-1.74
NCU06989_Senescence-associated protein	development	-2.12	-1.60
NCU04058_bZIP Transcription Factor	DNA	-0.55	-1.30
NCU02558_SRF-type Transcription Factor	DNA	-0.67	-0.73
NCU05137_non-anchored cell wall protein 1	fungal cell wall remodeling	-3.49	-3.26
NCU09244_plp-1	heterokaryon incompatibility	-1.40	-1.28
NCU05629_hypothetical protein	hypothetical	-6.55	-3.82
NCU10052_hypothetical protein	hypothetical	-0.69	-1.07

NCU02950_hypothetical protein	hypothetical	-0.81	-1.00
NCU08224_hypothetical protein	hypothetical	-0.83	-0.75
NCU06912_hypothetical protein	hypothetical with SP	-1.74	-1.90
NCU05917_hypothetical protein	hypothetical with SP	-1.23	-0.85
NCU01289_hypothetical protein	hypothetical with SP+TM	-1.84	-1.36
NCU05915_hypothetical protein	hypothetical with SP+TM	-3.92	-1.09
NCU04928_hypothetical protein	hypothetical with TM	-1.05	-1.04
NCU05835_hypothetical protein	metabolism	-2.17	-1.03
NCU00340_pp-1	transcription factor	-0.51	-0.63

Narrowing our focus to the 49 communication and fusion genes (Table 5-2), 31, 41 and 42 genes that were significantly down-regulated in *Δham-7, Δmak-1* and *Δmak-2* mutants, respectively. The heatmap in Figure 5-5A shows *Δham-7* is only partially similar to *Δmak-1* expression patterns. The genes that were differentially regulated in the *Δmak-1* and *Δmak-2* mutants and not in *Δham-7* were mostly communication genes. Exclusively examining the communication components showed 29.4% (5/17) of the genes were significantly down-regulated in *Δham-7,* while 88.9% (16/18) and 14/18 (77.8%) were down in *Δmak-1* and *Δmak-2* cells, respectively (Figure 5-5B). The five genes that were down in *Δham-7* have only partial reduction in expression, which does not eliminate the possibility of functional communication in *Δham-7*. Additionally, genes that have predicted adhesion domains are 88.9% (8/9), 88.9% and 100% down-regulated in *Δham-7, Δmak-1* and *Δmak-2* mutants, respectively (Figure 5-5C). The 31 genes down-regulated in *Δham-7* include all the other categories of the fusion process: signaling, adhesion, heterokaryon incompatibility, fusion and fungal cell wall remodeling. Table 5-3 summarizes the number of genes down-regulated in the communication and fusion subgroups.

A

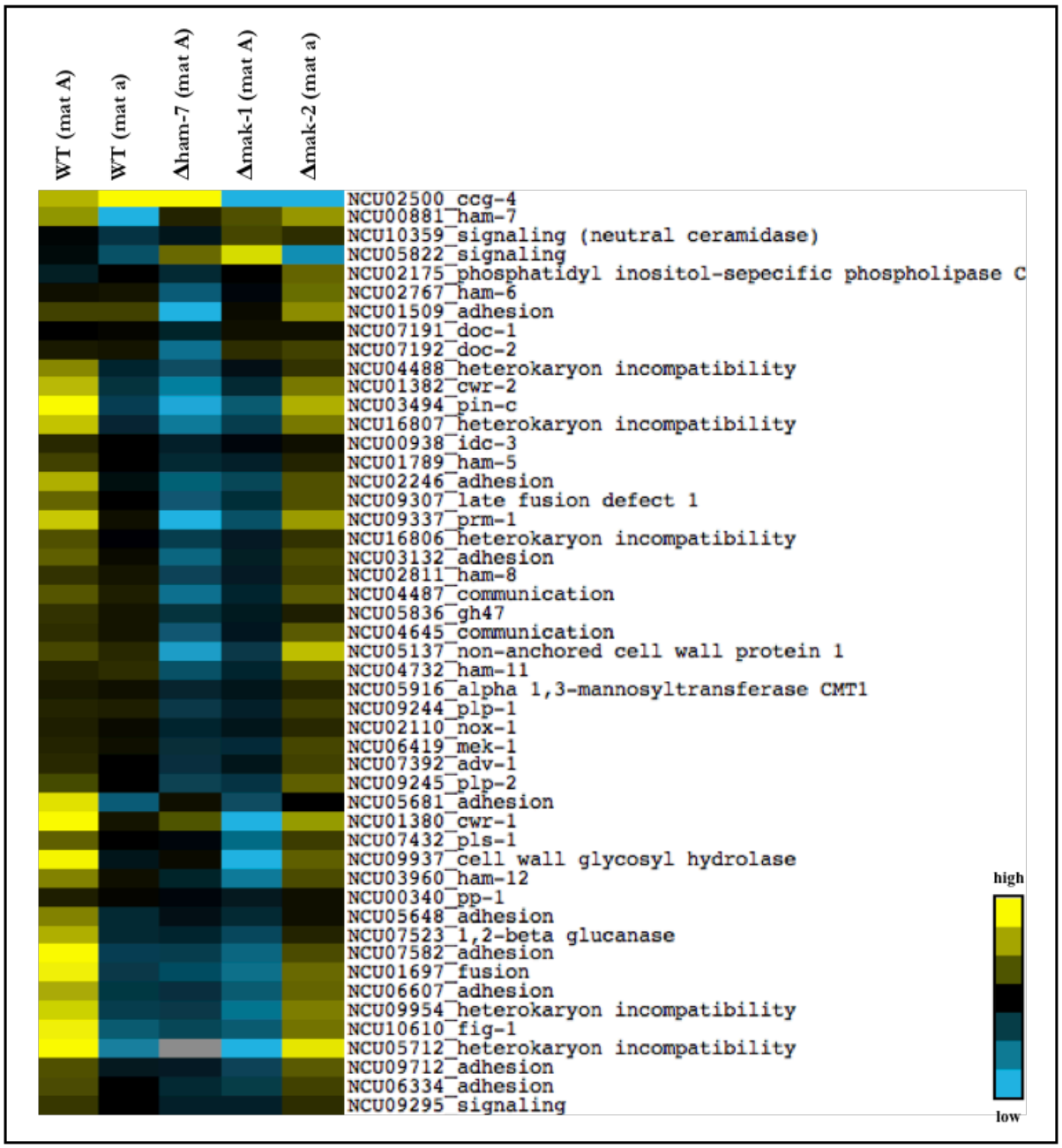
WT (mat A)
WT (mat a)
Δham-7 (mat A)
Δmak-1 (mat A)
Δmak-2 (mat a)
NCU02500 ccg-4
NCU00881 ham-7
NCU10359 signaling (neutral ceramidase)
NCU05822 signaling
NCU02175 phosphatidyl inositol-sepecific phospholipase C
NCU02767 ham-6
NCU01509 adhesion
NCU07191 doc-1
NCU07192 doc-2
NCU04488 heterokaryon incompatibility
NCU01382 cwr-2
NCU03494 pin-c
NCU16807 heterokaryon incompatibility
NCU00938 idc-3
NCU01789 ham-5
NCU02246 adhesion
NCU09307 late fusion defect 1
NCU09337 prm-1
NCU16806 heterokaryon incompatibility
NCU03132 adhesion
NCU02811 ham-8
NCU04487 communication
NCU05836 gh47
NCU04645 communication
NCU05137 non-anchored cell wall protein 1
NCU04732 ham-11
NCU05916 alpha 1,3-mannosyltransferase CMT1
NCU09244 plp-1
NCU02110 nox-1
NCU06419 mek-1
NCU07392 adv-1
NCU09245 plp-2
NCU05681 adhesion
NCU01380 cwr-1
NCU07432 pls-1
NCU09937 cell wall glycosyl hydrolase
NCU03960 ham-12
NCU00340 pp-1
NCU05648 adhesion
NCU07523 1,2-beta glucanase
NCU07582 adhesion
NCU01697 fusion
NCU06607 adhesion
NCU09954 heterokaryon incompatibility
NCU10610 fig-1
NCU05712 heterokaryon incompatibility
NCU09712 adhesion
NCU06334 adhesion
NCU09295 signaling
high
low

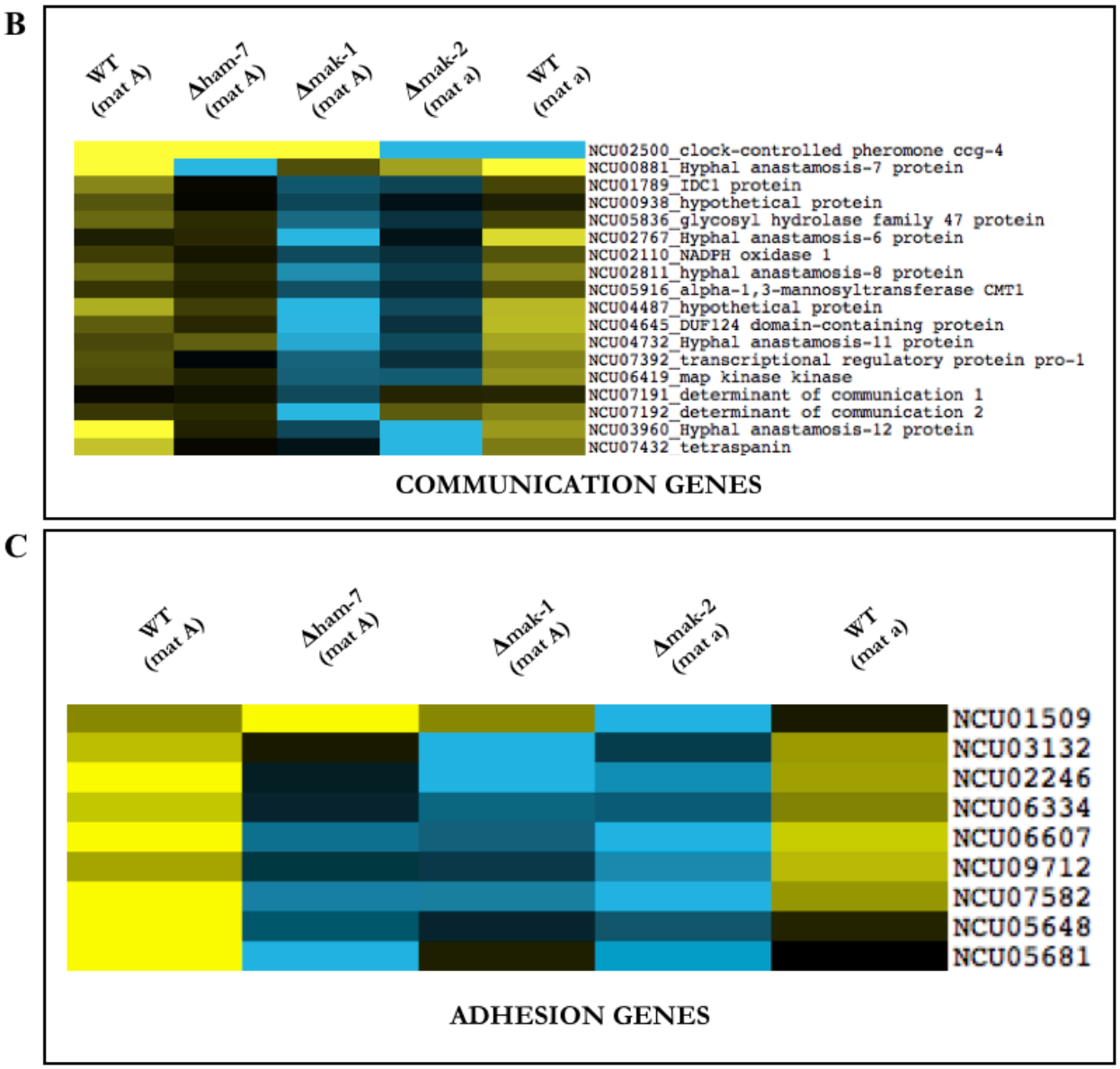

Figure 5-5. Differential expression of communication and fusion genes. a) Heatmap of 49 communication and fusion genes regulated by *adv-1* and *pp-1*, which show *Δham-7* only has partial similarity to *Δmak-1* expression. b) 29.4%, 88.9% and 77.8% of the communication genes were significantly down-regulated in *Δham-7, Δmak-1* and *Δmak-2*, respectively. c) 88.9%, 88.9% and 100% of the predicted adhesion genes were down-regulated in *Δham-7, Δmak-1* and *Δmak-2* germlings, respectively.

Table 5-2. Differential expression in communication and fusion genes in *Δham-7, Δmak-1* and *Δmak-2* (blank spaces indicate not significantly regulated; values in each column are log2 fold change)**.**

Gene description	Cellular function	*Δham-7*	*Δmak-1*	*Δmak-2*
NCU02246	adhesion	-2.35	-3.69	-2.14
NCU03132	adhesion	-0.96	-2.83	-1.43
NCU05648	adhesion	-2.26	-1.87	-0.95
NCU05681	adhesion	-4.23	-2.50	-1.33
NCU06334	adhesion	-1.51	-2.06	-1.57
NCU06607	adhesion	-3.01	-2.89	-2.73
NCU07582	adhesion	-4.09	-4.08	-2.64
NCU09712	adhesion	-1.45	-1.47	-2.27
NCU01509	adhesion		-4.33	-1.53
NCU00881_ham-7	communication	-6.80	-1.30	-0.86
NCU01789_ham-5	communication	-0.75	-1.52	-0.98
NCU03960_ham-12	communication	-1.34	-2.14	-2.98
NCU07392_adv-1	communication	-0.56	-1.32	-1.17
NCU07432_pls-1	communication	-1.12	-1.32	-2.53
NCU00938_idc-3	communication	-0.47	-1.09	
NCU02110_nox-1	communication		-0.98	-0.89
NCU02767_ham-6	communication		-1.75	-1.45
NCU02811_ham-8	communication		-1.80	-1.30
NCU04645	communication		-2.05	-1.51
NCU04732_ham-11	communication		-1.82	-1.59
NCU05836_gh47	communication		-1.50	-0.81
NCU05916_alpha 1,3-mannosyltransferase CMT1	communication		-0.98	-0.81
NCU06419_mek-1	communication		-1.25	-1.62
NCU07191_doc-1	communication		-0.66	
NCU07192_doc-2	communication		-2.23	

NCU04487	communication			-1.70
NCU02500_ccg-4	communication	1.84	5.78	
NCU01380_cwr-1	fungal cell wall remodeling	-2.98	-2.25	-8.20
NCU01382_cwr-2	fungal cell wall remodeling	-3.09	-4.33	-2.11
NCU07523_1,2-beta glucanase	fungal cell wall remodeling	-2.77	-2.68	-1.68
NCU09937_cell wall glycosyl hydrolase	fungal cell wall remodeling	-3.33	-2.77	-5.03
NCU05137_non-anchored cell wall protein 1	fungal cell wall remodeling		-3.49	-3.26
NCU01697	fusion	-3.87	-4.16	-3.12
NCU09307_late fusion defect 1	fusion	-1.16	-2.68	-1.73
NCU09337_prm-1	fusion	-2.22	-5.43	-3.24
NCU10610_fig-1	fusion	-4.40	-4.07	-2.91
NCU04488	heterokaryon incompatibility	-2.25	-2.95	-0.91
NCU09245_plp-2	heterokaryon incompatibility	-0.89	-2.03	-2.04
NCU09954	heterokaryon incompatibility	-3.57	-3.49	-3.48
NCU16807	heterokaryon incompatibility	-2.99	-4.36	-2.48
NCU03494_pin-c	heterokaryon incompatibility	-4.41		-3.64
NCU05712_heterokaryon incompatibility	heterokaryon incompatibility	-5.41		-6.62
NCU09244_plp-1	heterokaryon incompatibility		-1.40	-1.28
NCU16806_heterokaryon incompatibility	heterokaryon incompatibility			
NCU00340_pp-1	transcription factor		-0.51	-0.63
NCU09295	signaling	-0.74	-1.24	-1.12
NCU05822	signaling	-1.19	1.46	4.96

NCU10359_neutral ceramidase	signaling	-0.82		
NCU02175_phosphatidyl inositol-specific phospholipase C	signaling			-1.22

Table 5-3. Genes down-regulated in different fusion subcategories in *Δham-7, Δmak-1* and *Δmak-2*.

	Δham-7	***Δmak-1***	***Δmak-2***
adhesion	8/9	8/9	9/9
communication	5/17	16/18	14/18
fungal cell wall remodeling	4/5	5/5	5/5
fusion	4/4	4/4	4/4
heterokaryon incompatibility	6/8	5/8	7/8
signaling	3/4	2/4	3/4

Δmak-1 expression is not differentially expressed *Δham-7,* and transcription level is not indicative of MAK-1 activity. To determine the activity of MAK-1, we looked at a downstream target of MAK-1. Δ*mak-1* microarray data from a circadian rhythm study showed that MAK-1 is required for expression of some pathway target genes, such as NCU04352. NCU04352 is a putative chitin synthase, whose rhythmic accumulation is also dependent on P-MAK-1 [167]. In Δ*mak-1*, NCU04352 rhythmic expression was abolished and the expression levels remained low (relative to WT) at all times of day. This observation supported that P-MAK-1 positively regulated NCU04352 expression. However, there was no significant difference in NCU04352 expression in the *Δham-7* mutant. We can deduce that *Δham-7* has MAK-1 activity based on NCU04352 expression as a proxy, which further validates that *ham-7* is not upstream sensor of *mak-1*.

Figure 5-6 shows a summary of the mechanisms that are involved in communication and fusion in *N. crassa*. Individual deletion of these genes results in a non-WT fusion phenotype. The arrows between different complexes show the complex inner workings and the crosstalk between different pathways. The description of colors representing the different complexes can be found in the figure legend. The modification of this model is the outline of the proteins. All the genes down-regulated in *Δham-7* to *Δmak-1* and *Δmak-2* cells are outlined in red, and genes down in only *Δmak-1* and *Δmak-2* are outlined in blue. Many of the genes outlined in red and blue are membrane-bound, which show that *ham-7, mak-1* and *mak-2* influence many membrane-bound proteins.

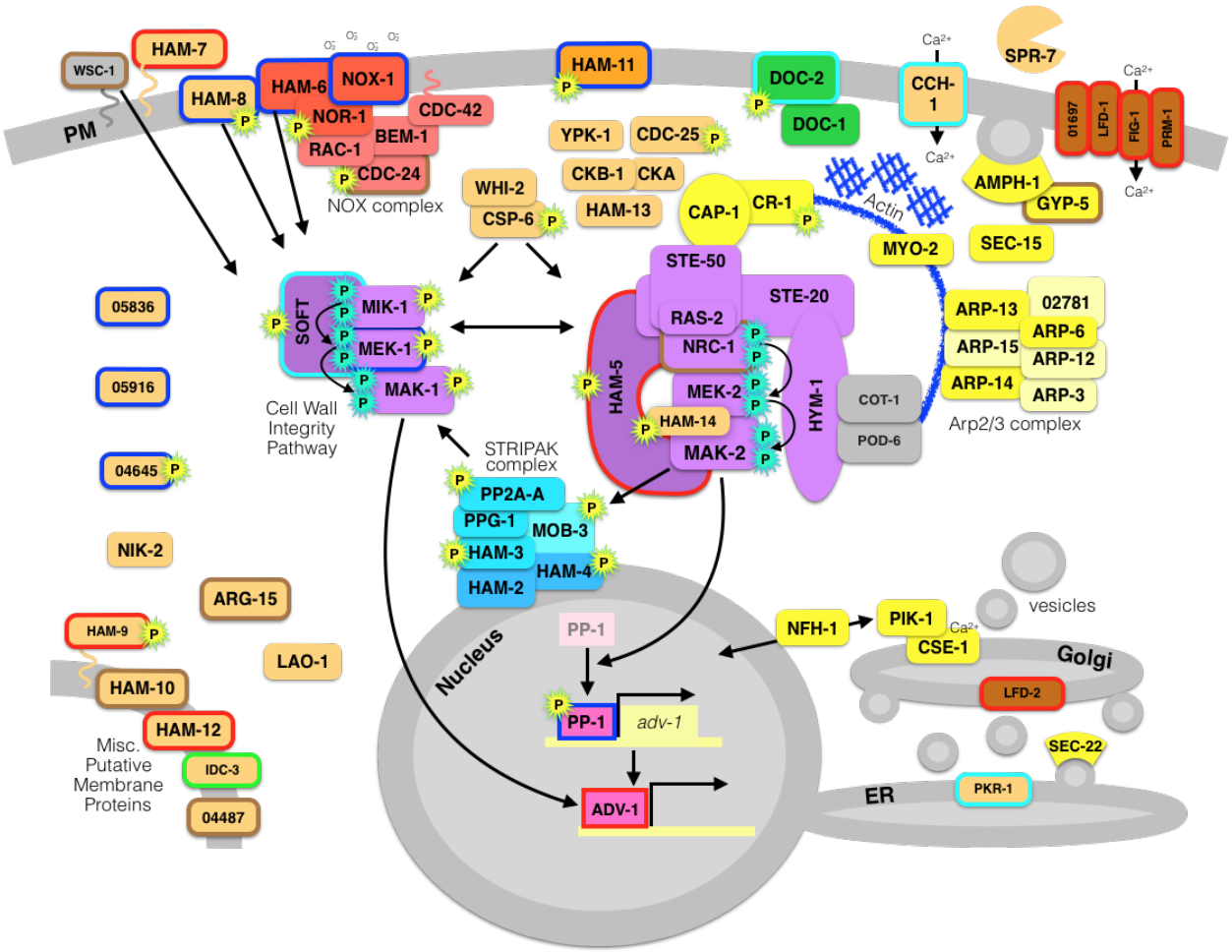

Figure 5-6. All currently known proteins required for germling communication and fusion in *N. crassa.* The original figure has been modified, where more detailed description can be found [129], to include the genes that are down-regulated in *Δham-7, Δmak-1* and *Δmak-2*. Border color: **red-** all *Δham-7, Δmak-1* and *Δmak-2;* **blue**- *Δmak-1* and *Δmak-2;* **green**- *Δham-7* and *Δmak-1;* **cyan**- *Δmak-1;* and **brown**- *Δmak-1*. Proteins are color-coded by function: **red**- NOX complex, **purple**- CWI pathway and MAK-2 signal response pathway, **yellow**- actin dynamics, vesicle trafficking, endocytosis/exocytosis, or secretion, **blue**- STRIPAK complex, **pink**- transcription factors, and **brown**- membrane fusion. *2*

5.3.5. PMO expression levels in the SREBP mutant *Δsah-2*

We have shown that *ham-7* is regulated by *adv-1*. But as a putative PMO, we looked to see if *ham-7* is regulated by cellulase activating transcription factors. The RNA-seq analysis on *Mclr-2, Δsah-2* and *Mclr-2Δsah-2* was conducted on samples grown in sucrose for 24 hours, not the same time-point as *Δham-7, Δmak-1* and *Δmak-2* germlings. Sterol regulatory element binding protein (SREBP) pathway negatively regulates PMOs, under lignocellulosic conditions in *N. crassa* [44]. *sah-2* is the SREBP transcription factor; *Δsah-2* and constitutive activation of *clr-2* (cellulase transcription factor, *Mclr-2*) result in cellulase hyperproduction [44,173]. The expression level of 12 of the 20 predicted PMO genes were significantly increased in the *Δsah-2* mutant as

compared to WT cells. The heatmap shows that most of the PMOs are affected by change in *clr-2* and *sah-2* (Figure 5-7). The majority of the PMO9 (cellulose) and PMO11 (starch) have a similar expression pattern, while PMO11 (chitin), PMO17 (unknown) and PMO18 (unknown) are regulated differently. NCU01380 belongs to PMO11 and is predicted to be a cell wall remodeling protein. With a role in cell fusion, it is not surprising that *ham-7* and NCU01380 are not regulated in the same manner as cellulose-acting PMOs.

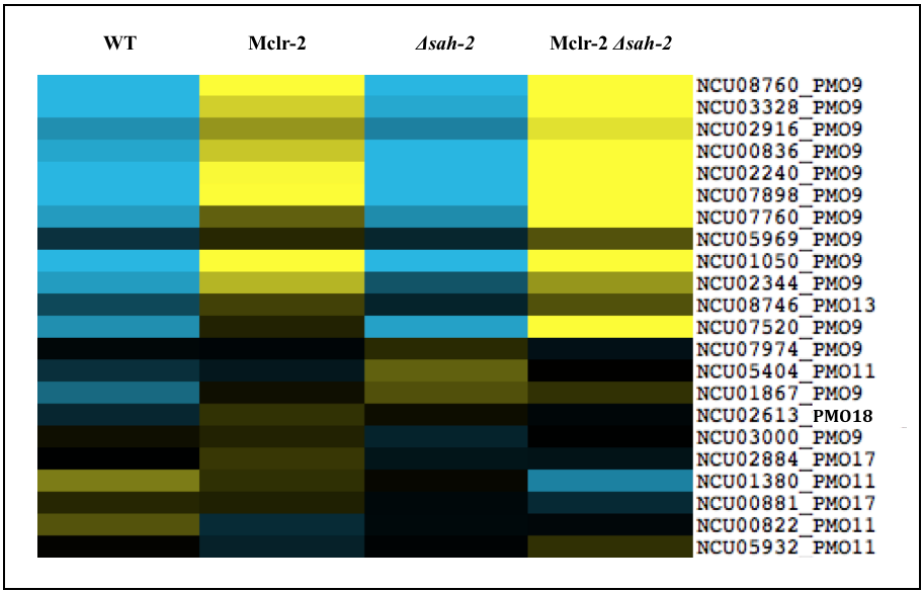

Figure 5-7. Differential expression of PMOs in *Mclr-2, Δsah-2* and *Mclr-2Δsah-2*. Majority of the PMO9 (cellulose) and PMO13 (starch) are regulated by *clr-2* and *sah-2,* however, PMO11 (chitin), PMO17 (unknown substrate) and PMO18 (unknown substrate) are regulated differently.

5.4. Discussion

While some GPI-anchored proteins function as the major structural components of the wall, others have important roles in cell wall biogenesis and remodeling [91]. *ham-7* does not serve as a structural component, as demonstrated by the WT-like resistance to cell wall drugs. The contrast in *Δwsc-1* and *Δham-7* phenotype also convey that these two genes are not working in the same cellular pathway; *wsc-1* is involved in cell wall stress and *ham-7* in cell fusion.

Additionally, *Δham-7* to *Δmak-1* and *Δmak-2* RNA-seq analysis challenges the hypothesis that *ham-7* is a cell wall sensor upstream of *mak-1*. If *ham-7* was disrupting cell fusion through the regulation of *mak-1*, we would expect same genes that are down-regulated in *mak-1* to be down in *Δham-7*. No significant change in the expression of downstream target of *mak-1* (NCU04352) suggest that MAK-1 activity is not affected. Consistent with the partial similarity in fusion gene expression (Figure 5-5A), 95, 121 and 106 (out of 155 genes that were regulated by *adv-1* and *pp-1*) were down-regulated in *Δham-7* to *Δmak-1* and *Δmak-2,* respectively. This partial overlap in differentially expressed genes between *Δham-7* and *Δmak-1,* suggesting that *ham-7* works downstream of *mak-1*.

The majority of the fusion genes in *Δham-7* are down-regulated, except the genes involved in communication (Table 5-3). This is unique to *Δham-7* because majority of the communication

genes are down-regulated in *Δmak-1* and *Δmak-2* mutants (mostly in *Δmak-1*). It is not surprising that 89% of the communication are down in *Δmak-1* since *mak-1* is required to initiate and maintain the chemotropic interactions of fusion cells [108]. These observations suggest that there is a possibility that communication complexes may still be functional in *Δham-7*.

In order to have a chemotropic growth, a signal has to be emitted and received by the potential fusion partner. An earlier study showed WT and *Δham-7* do not have chemotropic interactions, which is corroborated by absence of the oscillation of MAK-2-GFP in WT germlings near *Δham-7* germlings and visa versa [130]. This observation was followed by a later study that showed co-localization of HAM-5-GFP and MAK-2-mCherry, as puncta, at the hyphal tip in *Δham-7* mutants [127]. The MAK-2 complex assembles and disassembles at fusion tips every 8 minutes during WT germling communication [130]. After the formation of HAM-5/MAK-2 complexes at the hyphal tip, all the MAK-2 complex components undock and disassemble back to the cytoplasm. This cycle is repeated until the germlings fuse. The oscillation dynamics were absent in the *Δham-7* mutant and HAM-5/MAK-2 complexes were unable to disassemble (within the cell and at the cell cortex), which could be due to signaling defect in reception. Although the dogma is that no communication and fusion results in no oscillation, it would be constructive to carefully investigate the oscillation of SOFT and MAK-2 between *Δham-7* and WT germlings.

The PMO9 family behaves similarly and their secretion is regulated by *clr-2* and *sah-2,* while PMO11, PMO17 and PMO18 family members are not. NCU01380 is cell wall remodeling checkpoint gene-1 (*cwr-1*), predicted to be a putative chitin-acting PMO (PMO11). The conserved histidine brace and the axial tyrosine in *cwr-1* are required for catalytic activity to trigger the cell wall remodeling checkpoint (unpublished data from the lab). Interestingly, *ham-7* and *cwr-1* are both PMOs that are involved in cell fusion, and are not regulated by lignocellulosic secreting conditions [44]. Cell wall remodeling checkpoint occurs after cell fusion arrest post-contact between the germlings, thus it does not disrupt SOFT/MAK-2 oscillation or chemotropic growth (unpublished data from the lab). However, microscopy and RNA-seq data suggest that *Δham-7* do not have chemotropic growth or adhesion. Additionally, *cwr-1* expression is significantly reduced in *Δham-7, Δmak-1* and *Δmak-2* compared to WT, and significantly down-regulated in *Δham-7* compared to *Δmak-1*. Based off of these data, we deduce that *cwr-1* is working downstream of *ham-7, mak-1* and *mak-2*, with a shorter regulatory pathway from *ham-7* to *cwr-1*. The cells are likely able to recognize that the oscillation and chemotropic growth is absent, which down-regulates the expression of *cwr-1*. This also seen in *adv-1* and *pp-1* [129], suggesting that other fusion mutants would also down-regulate *cwr-1* expression.

The goal of performing RNA-seq analysis on *Δham-7, Δmak-1* and *Δmak-2* cells was to examine if *Δham-7* was upstream of *mak-1,* and to gain clues on its function. Our data indicates that *ham-7* is not working upstream, but rather downstream of *mak-1.* Next would be to answer how communication genes are differentially regulated in *Δmak-1* and *Δmak-2* in comparison to *Δham-7.* This can give an insight to where *ham-7* fits in the in the communication and fusion mechanism. We hope to unravel the function of *ham-7* during cell signaling, chemotropic interaction and cell remodeling during the cell fusion process through the concurrent biochemical work with the Marletta lab.

Chapter 6. Conclusions and future directions

6.1. The promiscuous and clingy partner: RanBPM

Initially starting as a project to study cellulase secretion, we have identified a mutant that is involved in the general secretory pathway. Utilizing the molecular tools available, we have created a NTG mutagenesis library to identify cellulase hyposecreting mutants that have a trafficking defect in EG-2-GFP. In our screen, we identified 10C2 mutant that mis-localizes EG-2-GFP to the nuclear envelope/ER with a growth defect and temperature sensitivity. With high-throughput sequencing of the genomic DNA, we mapped the locus of causal mutation on LGV. The 1 Mb region identified to have a 100% segregation between the Δ3βG-like progeny and 10C2-like progeny had 73 SNPs, but only nine were located inside an ORF with a missense mutation. The other 64 SNPs were located in intergenic regions and/or resulted in a silent (synonymous) mutation. From the nine genes, only six were available in the *N. crassa* knockout collection. We forced heterokaryons to identify the causal mutation in the nuclear export signal of NCU01409 (RanBPM).

Interestingly, ΔNCU01409 does not confer the same 10C2 phenotypic defects. Normally RanBPM is transported out of the nucleus by binding to an exportin (CRM1), and fails to exit the nucleus when one of the conserved leucine in the NES is mutated [83]. This is likely what is happening with the point mutation identified in NCU01409 in 10C2. Mutation in the NES alters its binding affinity to CRM1, impairing the dissociation of the CRM1-NES complexes from the nuclear pore complex. It is possible that a null mutation prevents the scaffolding protein from binding to any proteins, while NCU01409^{Leu177Phe} does not release the binding partners and interfere with their function. This is under the assumption that there are genetic redundancy of NCU01409, since it does not appear to be an essential gene (ΔNCU01409 has WT-like growth).

Following up on this project, the first priority is to confirm Leu177Phe as the causal mutation for the intracellular localization of EG-2-GFP; it will be interesting to see how this amino acid substitution in RanBPM is involved in targeting and secretion of cellulases and other cellular proteins. Even if RanBPM is not specific to cellulases, this study can enhance our knowledge of nucleocytoplasmic protein transport and regulation. It is typically thought that gain-of-function is favored in natural selection, as it increases the organism's fitness while loss-of-function is deleterious [174]. Subsequently, CRM1 binding assay can be used to compare the ability of WT NCU01409 and NCU01409^{Leu177Phe} to bind CRM1. Once the causal mutation is verified, next step is to examine NCU01409 interacting partners via co-IP and MS. These follow-up experiments will be helpful in revealing the involvement of RanBPM in *N. crassa* cellular processes.

6.2. PMO in disguise: HAM-7 functions in cell fusion not cellulose degradation

Filamentous fungal growth occurs through the formation of hyphal networks, where rapid exchange of water, nutrient, cellular constituents and genetic materials occur between fusing

cells [1]. Though there are advantages with hyphal fusion, cells are presented with increased risk of acquiring infectious cytoplasmic elements and exploitation by aggressive genotypes [139,175]. Thus, it is critical for germlings to be able to distinguish between self versus non-self before undergoing cell fusion. Although different forward and reverse genetics approaches identified genes involved in communication and cell fusion [6,27,29,94,121,130], functions of many remain unknown. The second part of this dissertation was dedicated to understanding the role of *ham-7* in germling fusion through genetic and biochemical study.

NCU02884 and HAM-7 have been categorized into a new family, PMO17, with an unknown binding substrate. Though different PMO families have low sequence homology, they maintain conservation of β-sandwich, disulfide bond(s) for stability, a type II Cu center, axial tyrosine and two histidine residues [151]. The histidine brace is indispensable for the function of PMOs. To confirm our hypothesis of HAM-7 as a putative PMO, we showed that point mutations (H18A and H76A) at the histidine residues incur *Δham-7*-like phenotypic defects. We focused on HAM-7 due to the inability of OE NCU02884 to compliment *Δham-7* defects. Deleting NCU02884 does not generate any fusion defective characteristics, indicating that only HAM-7 is involved in the cell fusion process.

Unlike the majority of the PMOs, HAM-7 is unique in that the deletion mutant confers fusion mutant characteristics and binds extracellularly to the cell membrane. To perform biochemical analyses of HAM-7, we attempted to secrete HAM-7 out of the cell by truncating the GPI-anchor site, however, that was not enough to release HAM-7 from the cell. Previous work suggest that cell wall proteins evolved to have functional redundancy by providing multiple crosslinking mechanisms to ensure the formation of a robust wall, as it is a critical structure for the survival of the fungi [125]. N-glycosylation is one method in which *N. crassa* crosslinks glycoproteins to the cell membrane/cell wall, thus we created HAM-7$^{N122Q\ N157Q\ N163Q}$ TR-GFP/V5 to remove these predicted crosslinkages. We were able to detect HAM-7$^{N122Q\ N157Q\ N163Q}$ TR-GFP in the cell lysate and the supernatant, while we only detected HAM-7$^{N122Q\ N157Q\ N163Q}$ TR-V5 in the cell lysate. A strain that secretes HAM-7 should have a consistent phenotype as *Δham-7* (reduced conidiation, flat growth and no germling fusion). Our collaborator will follow up by confirming HAM-7$^{N122Q\ N157Q\ N163Q}$ TR-GFP samples in the supernatant through MS and purifying the protein for substrate binding assays and catalytic activity.

We conducted RNA-sequencing to compare the expression levels of *Δham-7, Δmak-1* and *Δmak-2* to examine if *mak-1* was downstream of *ham-7*, and to gain clues on its function. When we looked at the expression levels of communication and fusion genes that are regulated by *adv-1* and *pp-1*, we saw that *Δham-7, Δmak-1* and *Δmak-2* have down-regulation in majority of genes involved in adhesion, fungal cell wall remodeling, fusion, heterokaryon incompatibility and signaling. However, most of the communication genes were only down-regulated in *Δmak-1* and *Δmak-2*, not in *Δham-7*. In addition to having a partial overlap in differentially expressed genes

between *Δham-7* and *Δmak-1*, *Δmak-1* and its downstream target gene was not down-regulated in the *Δham-7* mutant. In alignment with these observations, *Pprm1-luciferase* reporter assay showed that *ham-7* is involved in the cell fusion process subsequent to MAK-1/MAK-2 signaling networks. *Pprm1-luciferase* reporter system has been developed to determine whether communication genes function upstream or downstream of MAK-1/MAK-2 signaling complex, where they were able to show that these MAPK cascades were important for communication and fusion [140]. Communication mutants that had partial communication defect could express *Pprm1-luciferase*; those that had absolutely no communication, like *ham-7*, had very low expression of *Pprm1-luciferase*. MAK-1/MAK-2 downstream genes appear to be principally involved in coordinating the process of cell fusion, while upstream genes are involved in pre-fusion extracellular signaling [140]. *ham-7* has very low *Pprm1-luciferase* expression, which suggests that it is working downstream of MAK-1/MAK-2 to regulate the process of cell fusion rather than pre-fusion extracellular signaling.

Furthermore, the Marletta lab tested various substrates for PMO activity of NCU02884TR-HIS6X and only detected activity in the presence of laminarin [120]. Laminarin is one of the main cell wall components, which led us to hypothesize that HAM-7 breaking down its own cell wall. However, the substrate activity assay was contaminated by another hydrolase and have not been able to confirm the binding substrate. Although no confirmation has been made on the binding substrate of NCU02884, this does not eliminate the possibility of HAM-7 being involved in cell wall remodeling by breaking down its own cell wall.

HAM-7 could be binding to a substrate to turn it into a signal, but it does not seem unlikely due to the observation that *Δham-7* and WT cells do not have chemotropic growth; this observation also refutes its role in signal receiving. With the data presented, it appears that HAM-7 may be involved in the cell wall remodeling, such as breaking down of its own cell wall, rather than the communication aspect of cell fusion. This is why the biochemical analysis of binding substrate is critical in determining the role of HAM-7. We elucidated that *mak-1,* and likely for *mak-2* as well, are upstream of *ham-7* and we were able to secrete HAM-7 by mutating the N-glycosylation sites and truncating the GPI-anchor. A future direction is to follow up on the biochemical study by purifying the protein to identify the binding substrate and building the crystal structure. Evidence show the intricacy of the signaling network from the crosstalk, which contribute to the challenges in unraveling the functional relationships and roles in the cell-cell communication mechanisms. Figuring out the role of HAM-7 as a PMO will contribute to our understanding of cell fusion in filamentous fungi.

References

[1] Davis R.H. 2000. *Neurospora*: Contributions of a Model Organism. Oxford Univ Press.
[2] Perkins D. 2005. Why "Red bread mold" is an appropriate name for *Neurospora*. Fungal Genetics Newsletter 52:7-8.
[3] Beadle G.W. and Tatum E.L. 1945. *Neurospora*. Methods of producing and detecting mutations concerned with nutritional requirements. Amer. J. Bot. 32:678-686.
[4] Kuo H.C., Hui S., Choi J., Asiegbu F.O., Valkonen J.P.T. and Lee Y.H. 2014. Secret lifestyles of *Neurospora crassa*. Sci Rep. 4:5135.
[5] Queller D.C. 2011. Expanded social fitness and Hamilton's rule for kin, kith, and kind. PNAS. 108:10792–10799.
[6] Heller J., Zhao J., Rosenfield G., Kowbel D.K., Gladieus P. and Glass N.L. 2016. Characterization of Greenbeard Genes Involved in Long-Distance Kind Discrimination in a Microbial Eukaryote. PLoS Biol. 14(4):e1002431.
[7] Raju N. 1992. Genetic control of the sexual cycle in *Neurospora*. Mycol Res. 96(4):241-262.
[8] Hirsch H.M. 1954. Environmental factors influencing the differentiation of protoperithecia and their relation to tyrosinase and melanin formation in *Neurospora crassa*. Physiol. Plant. 7:m 72-92.
[9] Kubicek C.P., Mikus M., Schuster A., Schmoll M. and Seiboth B. 2009. Metabolic engineering strategies for the improvement of cellulase production by *Hypocrea jecorina.* Biotechnol. Biofuels 2:19.
[10] Shao S. and Hegde R.S. 2011. A calmodulin-dependent translocation pathway for small secretory proteins. Cell. 147:1576-1588.
[11] Xu C. and Ng D.T. 2015. O-mannosylation: The other glycan player of ER quality control. Semin Cell Dev Biol. 41:129-134.
[12] Bockers T.M., Kreutz M.R. and Pohl T. 1995. Glutaminyl-cyclase expression in the bovine/porcine hypothalamus and pituitary. J neuroendocrinol. 7(6):445-453.
[13] Van Coillie E., Proost P., Van Aelst I., Struyf S., Polfliet M., De Meester I., Harvey D.J., Van Damme J. and Opdenakker G. 1998. Functional comparison of two human monocyte chemotactic protein-2 isoforms, role of the amino-terminal pyroglutamic acid and processing by CD26/dipeptidyl peptidase IV. Biochemistry. 37(36):12672-12680.
[14] Gierz G. and Bartnicki-Garcia S. 2001. A three-dimensional model of fungal morphogenesis based on the vesicle supply center concept. J Theor Biol. 208:151– 164.
[15] Riquelme M. 2013. Tip growth in filamentous fungi:a road trip to the apex. Annu Rev Microbiol. 67:587– 609.
[16] Bowman B.J., Draskovic M., Freitag M. and Bowman E.J. 2009. Structure and distribution of organelles and cellular location of calcium transporters in *Neurospora crassa*. Eukaryot Cell. 8:1845– 1855.
[17] Devchand M. and Gwynne D.I. 1991. Expression of heterologous proteins in *Aspergillus*. J Biotechnol. 17:3-9.
[18] de Souza P.M. and de Oliveira Magalhães P. 2010. Application of microbial α-amylase in industry. Braz J Microbiol. 41(4):850–861.
[19] Reilly M.C., Magnuson J.K. and Baker S.E. 2016. Approaches to understanding protein hypersecretion in fungi. Fungal Biol Rev. 145-151.

[20] Verdoesa J.C., Punta P.J., Stouthamerb A.H. and van den Hondel C.A. 1994. The effect of multiple copies of the upstream region on expression of the *Aspergillus niger* glucoamylase-encoding gene. Sci Dir. 145(2):179-187.
[21] Verdoesa J.C., van Diepeningenb A.D., Punta P.J., Debets A.J., Stouthamer A.H. and van den Hondel C.A. 1994. Evaluation of molecular and genetic approaches to generate glucoamylase overproducing strains of *Aspergillus niger*. J Biotechnol. 36(2):165-175.
[22] Cherry J.R. and Fidantsef A.L. 2003. Directed evolution of industrial enzymes: an update. Curr Op Biotechnol. 14(4):438-443.
[23] Linke R., Thallinger G.G., Haarmann T., Eidner J., Schreiter M., Lorenz P., Seiboth B. and Kubicek C.P. 2015. Restoration of female fertility in *Trichoderma reesei* QM6a provides the basis for inbreeding in this industrial cellulase producing fungus. Biotechnol Biofuels. 8:155.
[24] Marsh P.B., Bollenbacher K., Butler M.L. and Raper K.B. 1949. The fungi concerned in fiber deterioration: II: their ability to decompose cellulose. Text Res J. 19:462–484.
[25] Tian C., Beeson W.T., Iavarone A.T., Sun J., Marletta M.A., Cate J.H. and Glass N.L. 2009. Systems analysis of plant cell wall degradation by the model filamentous fungus *Neurospora crassa*. PNAS. 106(52):22157-22162.
[26] Ellison C.E., Hall C., Kowbel D., Welch J., Brem R.B., Glass N.L. and Taylor J.W. 2011. Population genomics and local adaptation in wild isolates of a model microbial eukaryote. PNAS. 108:2831-2836.
[27] Palma-Guerrero J., Hall C.R., Kowbel D., Welch J., Taylor J.W., Brem R.B. and Glass N.L. 2013. Genome wide association identifies novel loci involved in fungal communication. PLOS Genet. 9(8).
[28] Galagan J.E., *et al*. 2003. The genome sequence of the filamentous fungus *Neurospora crassa.* Nature. 422(6934):859-868.
[29] Colot H.V., Park G., Turner G.E., Ringelberg C., Crew C.M., Litvinkova L., Weiss R.L., Borkovich K.A. and Dunlap J.C. 2006. A high-throughput gene knockout procedure for *Neurospora* reveals functions for multiple transcription factors. PNAS. 103(27):10352-10357.
[30] Kraut-Cohen, J. and Gerst J.E. 2010. Addressing mRNAs to the ER: *cis* sequences act up! Trends Biochem Sci. 35:459-469.
[31] Sidrauski C. and Walter P. 1997. The transmembrane kinase Ire1p is a site-specific endonuclease that initiates mRNA splicing in the unfolded protein response. Cell. 90(6):1031-1039.
[32] Kaufman R.J. 1999. Stress signaling from the lumen of the endoplasmic reticulum: coordination of gene transcriptional and translational controls. Genes Dev. 13(10):1211-33.
[33] Mori K., Kawahara T., Yoshida H., Yanagi H. and Yura T. 1996. Signalling from endoplasmic reticulum to nucleus: transcription factor with a basic-leucine zipper motif is required for the unfolded protein-response pathway. 1(9):803-817.
[34] Hollien J. 2013. Evolution of the unfolded protein response. Biochim Biophys Acta. 1833(11):2458-2463.
[35] Collén A., Saloheimo M., Bailey M., Penttilä M. and Pakula T.M. 2005. Protein production and induction of the unfolded protein response in *Trichoderma reesei* strain Rut-C30 and its transformant expressing endoglucanase I with a hydrophobic tag. Biotechnol Bioeng. 89:335–344.
[36] Brown N.A., de Gouvea P.F., Krohn N.G., Savoldi M. and Goldman G.H. 2013. Functional characterisation of the non-essential protein kinases and phosphatases regulating *Aspergillus nidulans* hydrolytic enzyme production. Biotechnol Biofuels. 6:91.

[37] Fan F., Ma G., Li J., Liu Q., Benz J.P., Tian C. and Ma Y. 2015. Genome-wide analysis of the endoplasmic reticulum stress response during lignocellulase production in *Neurospora crassa*. Biotechnol Biofuels. 8:66.
[38] Benz J.P., Chau B.H., Zheng D., Bauer S., Glass N.L. and Somerville C.R. 2014. A comparative systems analysis of polysaccharide-elicited responses in *Neurospora crassa* reveals carbon source-specific cellular adaptations. Mol Microbiol. 91:275–299.
[39] Montenegro-Montero A., Goity A. and Larrondo L.F. 2015. The bZIP Transcription Factor HAC-1 Is Involved in the Unfolded Protein Response and Is Necessary for Growth on Cellulose in *Neurospora crassa*. PLoS One. 10(7).
[40] Petranovic D., Tyo K., Vemuri G.N. and Nielsen J. 2010. Prospects of yeast systems biology for human health:integrating lipid, protein and energy metabolism. FEMS Yeast Res. 10(8):1046-1059.
[41] Colgan S.M., Hashimi A.A. and Austin R.C. 2011. Endoplasmic reticulum stress and lipid dysregulation. Expert Rev Mol Med. 13:e4.
[42] Rawson, R.B. 2003. The SREBP pathway--insights from Insigs and insects. Nat Rev Mol Cell Biol. 4(8):631-640.
[43] Reilly M.C., Qin L., Craig J.P., Starr T.L. and Glass N.L. 2015. Deletion of homologs of the SREBP pathway results in hyper-production of cellulases in *Neurospora crassa* and *Trichoderma reesei*. Biotechnol Biofuels. 8:121.
[44] Qin L., Wu V.W. and Glass N.L. 2017. Deciphering the Regulatory Network between the SREBP Pathway and Protein Secretion in *Neurospora crassa*. MBio. 8(2).
[45] Blobel G. 1977. International Cell Biology. Rockefeller Univ Press. 318-325.
[46] Wickner W. 1979. The assembly of proteins into biological membranes: The membrane trigger hypothesis. 48:23-45.
[47] Kreil G. 1981. Transfer of Proteins Across Membranes. Annu Rev Biochem. 50:715-31.
[48] Silhavy T.J., Benson S.A. and Emr S.D. 1983. Mechanisms of protein localization. 47(3):313-344.
[49] von Heijne G. 1985. Signal sequences. The limits of variation. J Mol Biol. 184(1):99-105.
[50] Hiller, K., Grote A., Scheer M., Münch R. and Jahn D. 2004. PrediSi: prediction of signal peptides and their cleavage positions. Nucleic Acids Res. 32:W375-379.
[51] Nielsen H., Engelbrecht J., Brunak S. and von Heijne G. 1997. Identification of prokaryotic and eukaryotic signal peptides and prediction of their cleavage sites. 10(1):1-6.
[52] Kraut-Cohen J., Afanasieva E., Haim-Vilmovsky L., Slobodin B., Yosef I., Bibi E. and Gerst J.E. 2013. Translation- and SRP-independent mRNA targeting to the endoplasmic reticulum in the yeast *Saccharomyces cerevisiae*. Mol Biol Cell. 24:3069-3084.
[53] Pyhtila, B., Zheng T., Lager P.J., Keene J.D., Reedy M.C. and Nicchitta C.V. 2008. Signal sequence- and translation -independent mRNA localization to the endoplasmic reticulum. RNA. 14(3):445-453.
[54] Schwartz, T.U. 2007. Origins and evolution of cotranslational transport to the ER. Adv. Exp. Med. Biol. 607:52-60.
[55] Ast R., Cohen. G. and Schuldiner M. 2013. A network of cytosolic factors targets SRP-independent proteins to the endoplasmic reticulum. Cell. 152(5):1134-1145.
[56] Rothblatt J.A., Deshaies R.J., Sanders S.L., Daum G. and Schekman R. 1989. Multiple genes are required for proper insertion of secretory proteins into the endoplasmic reticulum in yeast. J Cell Biol 109:2641– 2652.

[57] Jonikas M.C., Collins S.R., Denic V., Oh E., Quan E.M., Schmid V., Weibezahn J., Schwappach B., Walter P., Weissman J.S. and Schuldiner M. 2009. Comprehensive characterization of genes required for protein folding in the endoplasmic reticulum. Science 323:1693– 1697.
[58] Aridor M., Bannykh S.I., Rowe T. and Balch W.E., 1995. Sequential coupling between COPII and COPI vesicle coats in endoplasmic reticulum to Golgi transport. J Cell Biol. 131(4):875-893.
[59] Starr T.L., Gonçalves A.P., Meshgin N. and Glass N.L. 2018. The major cellulases CBH-1 and CBH-2 of *Neurospora crassa* rely on distinct ER cargo adaptors for efficient ER-exit. 107(2):229-248.
[60] Mayer M.P. and Bukau B. 2005. Hsp70 chaperones:cellular functions and molecular mechanism. Cell Mol Life Sci. 62(6):670.
[61] Wilkinson B. and Gilbert H.F. 2004. Protein disulfide isomerase. Biochim Biophys Acta 1699(1-2):35-44.
[62] Winterburn P.J. and Phelps C.F. 1972. The significance of glycosylated proteins. Nature. 236:147-151.
[63] Deshpande N., Wilkins M.R., Packer N. and Nevalainen H. 2008. Protein glycosylation pathways in filamentous fungi. 18(8):626-637.
[64] Lehle L., Strahl S. and Tanner W. 2006. Protein glycosylation, conserved from yeast to man:a model organism helps elucidate congenital human diseases. Angew Chem Int Ed Engl. 45(41):6802-6818.
[65] Ohneda M., Arioka M. and Kitamoto K. 2004. Isolation and Characterization of *Aspergillus oryzae* Vacuolar Protein Sorting Mutants. Appl Environ Microbiol. 71(8):4856-4861.
[66] Fajardo-Somera R.A., Bowman B. and Riquelme M. 2013. The plasma membrane proton pump PMA-1 is incorporated into distal parts of the hyphae independently of the Spitzenkörper in *Neurospora crassa*. 12(8):1097-1105.
[67] Free S.J. 2013. Fungal cell wall organization and biosynthesis. Adv Genet. 81:33–82.
[68] Liu J. 2017. Dissecting Cellulase Hypersecretion in *Neurospora crassa*. UC Berkeley, Open Access Publishing PLUS.
[69] Znameroski E.A., Coradetti S.T., Roche C.M., Tsai J.C., Iavarone A.T., Cate J.H. and Glass N.L. 2012. Induction of lignocellulose-degrading enzymes in *Neurospora crassa* by cellodextrins. PNAS. 109:6012-6017.
[70] McKenna A., Hanna M., Banks E., Sivachenko A., Cibulskis K., Kernytsky A., Garimella K., Altshuler D., Gabriel S., Daly M. and DePristo M.A. 2010. The Genome Analysis Toolkit: a Map Reduce framework for analyzing next-generation DNA sequencing data. Genome Res. 20(9):1297–303.
[71] Langmead B, Salzberg SL. 2012. Fast gapped-read alignment with Bowtie 2. Nat Methods. 9(4):357–359.
[72] Xiang Q., Rasmussen C. and Glass N.L. 2002. The *ham-2* Locus, Encoding a Putative Transmembrane Protein, Is Required for Hyphal Fusion in *Neurospora crassa*. Genetics. 160(1):169-180.
[73] Becker A, Chao D.Y., Zhang X., Salt D.E. and Baxter I. 2011. Bulk Segregant Analysis Using Single Nucleotide Polymorphism Microarrays. PLoS ONE. 6.
[74] Michelmore, RW, Para I. and Kesseli R.V. 1991. Identification of markers linked to disease-resistance genes by bulked segregant analysis: a rapid method to detect markers in specific genomic regions by using segregating populations. PNAS. 88:9828-32.

[75] Pomraning K.R., Smith K.M. and Freitag M. 2011. Bulk segregant analysis followed by high-throughput sequencing reveals the *Neurospora* cell cycle gene, *ndc-1*, to be allelic with the gene for ornithine decarboxylase, *spe-1*. Eukaryotic Cell. 10:724-733.
[76] Stefanov A.N. 2006. Bulked segregant analysis as a new tool for identification and cloning of genes in *Chlamydomonas reinhardtii.* Identification of TBC1. Concordia University.
[77] Wang, D., Li Z. Messing E.M and Wu G. 2002. Activation of Ras/Erk pathway by a novel MET-interacting. J Biol Chem. 277(39):36216-36222.
[78] Murrin L.C. and Talbot J.N. 2007. RanBPM, a Scaffolding Protein in the Immune and Nervous Systems. J Neuroimmune Pharmacol. 2(3):290-295.
[79] Suresh B., Ramakrishna S. and Baek K.H. 2012. Diverse roles of the scaffolding protein RanBPM. 17(7-8):379-387.
[80] Salemi L., Louireiro S.O. and Schild-Poulter C. 2015. Characterization of RanBPM molecular determinants that control its subcellular localization. PLoS One. 10(2).
[81] Kobayashi N., Yang J., Ueda A., Suzuki T., Tomaru K., Takeno M., Okuda K. and Ishigatsubo Y. 2009. RanBPM, Muskelin, p48EMLP, p44CTLH, and the armadillo-repeat proteins ARMC8α and ARMC8β are components of the CTLH complex. Gene. 396(2):236-247.
[82] Menon R.P., Gibson T.J. and Pastore A. 2004. The c terminus of fragile X mental retardation protein interacts with the multi-domain Ran-binding protein in the microtubule-organising centre. J Mol Biol. 343(1):43-53.
[83] Sorokin A.V., Kim E.R. and Ovchinnikov L.P. 2007. Nucleocytoplasmic transport of proteins. Biochemistry (Mosc). 72:1439–1457.
[84] D'Cruz A.A., Babon J.J., Norton R.S., Nicola N.A. and Nicholson S.E. 2013. Structure and function of the SPRY/B30.2 domain proteins involved in innate immunity. 22(1):1-10.
[85] Aldabbous M.G., Stout A., Huang I.C., Read, N.D. and Free, S.J. 2010. The *ham-5*, *rcm-1* and *rco-1* genes regulate hyphal fusion in *Neurospora crassa*. Microbiology 156:2621–2629.
[86] Buller, A. H. R. 1933. Researches on fungi, vol. 15. Longman, London, England.
[87] Fleissner, A., Simonin A.r., and Glass N.L. 2008. Cell fusion in the filamentous fungus, *Neurospora crassa*. Methods Mol. Biol. 475:21–38.
[88] Koehler, E. 1930. Zur Kenntnis der vegetativen anastomosen der Pilze (II. Mitteilung). Planta 10:495–522.
[89] Read N.D., Fleißner A., Roca M.G. and Glass, N.L., 2010. Cellular and molecular biology of filamentous fungi. ASM Press, Washington, DC. 260-273.
[90] Roca M. G., Read N.D. and Wheals A.E.. 2005. Conidial anastomosis tubes in filamentous fungi. FEMS Microbiol Lett. 249:191–198.
[91] Bowman S.M., Piwowar A., Al Dabbous M., Vierula J. and Free S.J. 2006. Mutational Analysis of the Glycosylphosphatidylinositol (GPI) Anchor Pathway Demonstrates that GPI-Anchored Proteins Are Required for Cell Wall Biogenesis and Normal Hyphal Growth in *Neurospora crassa*. Eukaryot Cell. 5(3):587-600.
[92] Glass, N.L., Jacobson D.J. and Shiu P.K.T. 2000. The genetics of hyphal fusion and vegetative incompatibility in filamentous ascomycete fungi. Annu. Rev Genet. 34:165–186.
[93] Gonçalves A.P., Heller J., Daskalov A., Videira A. and Glass N.L. 2017. Regulated Forms of Cell Death in Fungi. Front Microbiol. 8:1837.
[94] Fu C., Iyer P., Herkal A., Stout A. and Free S.J. 2011. Identification and Characterization of Genes Required for Cell-to-Cell Fusion in *Neurospora crassa*. 10(8):1100-1109.
[95] Aldabbous M.G., Stout A., Huang I.C., Read, N.D. and Free, S.J. 2010. The *ham-5, rcm-1* and *rco-1* genes regulate hyphal fusion in *Neurospora crassa*. Microbiol. 156:2621–2629.

[96] Baillat G., Moqrich A., Castets F., Baude A., Bailly Y., Benmerah A. and Monneron A. 2001. Molecular cloning and characterization of Phocein, a protein found from the Golgi complex to dendritic spines. Mol Biol Cell. 12:663–673.
[97] Read N.D., Fleißner A., Roca M.G. and Glass, N.L., 2010. Cellular and molecular biology of filamentous fungi. ASM Press, Washington, DC. 260-273.
[98] Fischer M.S. and Glass N.L. 2019. Communicate and Fuse: How Filamentous Fungi Establish and Maintain an Interconnected Mycelial Network. Front Microbiol.
[99] Rodicio R. and Heinisch J.J. Together we are strong—cell wall integrity sensors in yeasts. Yeast. (8):531-540.
[100] Maddi A., Dettman A., Fu C., Seiler S. and Free S. 2012. WSC-1 and HAM-7 Are MAK-1 MAP Kinase Pathway Sensors Required for Cell Wall Integrity and Hyphal Fusion in *Neurospora crassa*. PLoS ONE. 7(8).
[101] Levin D.E. 2005. Cell Wall Integrity Signaling in *Saccharomyces cerevisiae*. 69(2):262-291.
[102] Dettmann A., Heilig Y.,Ludwig S., Schmitt K., Illgen J., Fleißner A., Valerius O. and Seiler S. 2013. HAM-2 and HAM-3 are central for the assembly of the Neurospora STRIPAK complex at the nuclear envelope and regulate nuclear accumulation of the MAP kinase MAK-1 in a MAK-2-dependent manner. Mol Microbiol. 90(4):796-812.
[103] Pandey A., Roca M.G., Read N.D. and Glass N.L. 2004. Role of a MAP kinase during conidial germination and hyphal fusion in *Neurospora crassa*. Eukaryot Cell. 3, 348–358.
[104] Kothe G.O. and Free S.J. 1998. The isolation and characterization of *nrc-1* and *nrc-2*, two genes encoding protein kinases that control growth and development in *Neurospora crassa*. Genetics. 149, 117–130.
[105] Li D., Bobrowicz P., Wilkinson H.H., and Ebbole D.J. 2005. A mitogen-activated protein kinase pathway essential for mating and contributing to vegetative growth in *Neurospora crassa.* Genetics. 170:1091–1104.
[106] Widmann C., Gibson S., Jarpe M.B. and Johnson G.L. 1999. Mitogen-activated protein kinase:conservation of a three-kinase module from yeast to human. Physiol Rev. 79:143–180.
[107] Teichert I., Steffens E.K., Schnaß N., Fränzel B., Krisp C., *et al.*, 2014 PRO40 Is a Scaffold Protein of the Cell Wall Integrity Pathway, Linking the MAP Kinase Module to the Upstream Activator Protein Kinase C. PLoS Genet. 10.
[108] Weichert M., Lichius A., Priegnitz B.-E., Brandt U., Gottschalk J., Nawrath T., Groenhagen U., Read N.D., Schulz S. and Fleißner A. 2016 Accumulation of specific sterol precursors targets a MAP kinase cascade mediating cell–cell recognition and fusion. PNAS. 113:11877–11882.
[109] van Drogen F. and Peter M. 2002. Spa2p functions as a scaffold-like protein to recruit the Mpk1p MAP kinase module to sites of polarized growth. Curr Biol. 12(19):1698-1703.
[110] Fleißner A., Leeder A.C., Roca M.G., Read N.D. and Glass N.L. 2009. Oscillatory recruitment of signaling proteins to cell tips promotes coordinated behavior during cell fusion. PNAS. 106(46):19387-19392.
[111] Masloff S., Pöggeler S. and Kück U.. 1999. The pro1(+) gene from *Sordaria macrospora* encodes a C6 zinc finger transcription factor required for fruiting body development. Genetics 152(1):191–199.
[112] Roca M.G., Arlt J., Jeffree C.E. and Read N.D. 2005. Cell biology of conidial anastomosis tubes in *Neurospora crassa*. Eukaryot Cell. 4, 911–919.

[113] Pandey A., Roca M.G., Read N.D. and Glass N.L. 2004. Role of a MAP kinase during conidial germination and hyphal fusion in *Neurospora crassa*. Eukaryot Cell. 3:348–358.
[114] Shaul Y.D. and Seger R. 2007. The MEK/ERK cascade:from signaling specificity to diverse functions. Biochim Biophys Acta. 1773:1213–1226.
[115] Mendoza M.C., Vilela M., Juarez J.E., Blenis J. and Danuser G. 2015. ERK reinforces actin polymerization to power persistent edge protrusion during motility. Sci. Signal. 8.
[116] Bonner T.I., Oppermann N.H., Seeburg P., Kerby S.B., Gunnell M.A., Young A.C., Rapp U.R. 1986. The complete coding sequence of the human raf oncogene and the corresponding structure of the c-raf-1 gene. Nucleic Acids Res.14(2):1009-1015.
[117] Bonny C., Nicod P. and Waeber G. 1998. IB1, a JIP-1-related nuclear protein present in insulin-secreting cells. J Biol Chem. 273(4):1843-1846.
[118] Borden K.L., Boddy M.N., Lally J., O'Reilly N.J., Martin S., Howe K., Solomon E. and Freemont P.S. 1995. The solution structure of the RING finger domain from the acute promyelocytic leukaemia proto-oncoprotein. EMBO J.14(7):1532-1541.
[119] Bornfeldt K.E., Campbell J.S., Koyama H., Argast G.M., Leslie C.C., Raines E.W., Krebs E.G. and Ross R. 1997. The mitogen-activated protein kinase pathway can mediate growth inhibition and proliferation in smooth muscle cells. Dependence on the availability of downstream targets. J Clin Invest. 100(4):875-885.
[120] Span E.A. 2018. Structure and Mechanism of Fungal Polysaccharide Monooxygenases. UC Berkeley, Open Access Publishing PLUS.
[121] Dettmann A., Heilig Y., Valerius O., Ludwig S. and Seiler S. 2014. Fungal communication requires the MAK-2 pathway elements STE-20 and RAS-2, the NRC-1 adapter STE-50 and the MAP kinase scaffold HAM-5. PLoS Genet. 10(11).
[122] Rispail N., *et al.* 2009. Comparative genomics of MAP kinase and calcium–calcineurin signalling components in plant and human pathogenic fungi. Fungal Genet Biol. 46(4):287-298.
[123] Witzel F., Maddison L. and Blüthgen N. 2012. How scaffolds shape MAPK signaling:what we know and opportunities for systems approaches. Front Physiol. 3:475.
[124] Côte P., Sulea T., Dignard D., Wu C. and Whiteway M. 2011. Evolutionary reshaping of fungal mating pathway scaffold proteins. MBio. 2(1).
[125] Maddi A., Fu C. and Free S.J. 2012. The *Neurospora crassa* dfg5 and dcw1 genes encode alpha-1,6-mannanases that function in the incorporation of glycoproteins into the cell wall. PLoS One. 7(6).
[126] Fu C., Ao J., Dettmann A., Seiler S. and Free S.J. 2014. Characterization of the Neurospora crassa cell fusion proteins, HAM-6, HAM-7, HAM-8, HAM-9, HAM-10, AMPH-1 and WHI-2. PLoS One. 9(10).
[127] Jonkers W., Leeder A.C., Ansong C., Wang Y., Yang F., Starr T.L., Camp D.G. 2nd, Smith R.D. and Glass N.L. 2014. HAM-5 functions as a MAP kinase scaffold during cell fusion in *Neurospora crassa*. PLoS Genet. 10(11).
[128] Merlini L., Dudin O., Martin S. G., 2013 Mate and fuse: how yeast cells do it. Open Biol. 3:130008–130008.
[129] Fischer M.S., Wu V.W., Lee J.E., O'Malley R.C. and Glass N.L. 2018. Regulation of Cell-to-Cell Communication and Cell Wall Integrity by a Network of MAP Kinase Pathways and Transcription Factors in Neurospora crassa. Genetics. 209:489-506.
[130] Leeder A.C., Jonkers W., Li J. and Glass N.L. 2013. Early Colony Establishment in Neurospora crassa Requires a MAP Kinase Regulatory Network. Genetics. 195(3):883-898.

[131] Bloemendal S., Bernhards Y., Bartho K., Dettmann A., Voigt O., Teichert I., Seiler S., Wolters D.A., Pöggeler S. and Kück U. 2012. A homologue of the human STRIPAK complex controls sexual development in fungi. Mol Microbiol. 84:310-323.
[132] Maerz S., Ziv C., Vogt N., Helmstaedt K., Cohen N., Gorovits R., Yarden O. and Seiler S. 2008. The nuclear Dbf2-related kinase COT1 and the mitogen-activated protein kinases MAK1 and MAK2 genetically interact to regulate filamentous growth, hyphal fusion and sexual development in *Neurospora crassa*. Genetics 179:1313–1325.
[133] Goudreault M., D'Ambrosio L.M., Kean M.J., Mullin M.J., Larsen B.G., Sanchez A., Chaudhry S., Chen G.I., Sicheri F., Nesvizhskii A.I., Aebersold R., Raught B. and Gingras A.C. 2009. A PP2A phosphatase high density interaction network identifies a novel striatin-interacting phosphatase and kinase complex linked to the cerebral cavernous malformation 3 (CCM3) protein. Mol Cell Proteomics. 8(1):157-171.
[134] Kück U., Beier A.M. and Teichert I. 2016. The composition and function of the striatin-interacting phosphatases and kinases (STRIPAK) complex in fungi. Fungal Genet Biol. 90:31-38.
[135] Simonin A.R., Rasmussen C.G., Yang M. and Glass N.L. Genes encoding a striatin-like protein (*ham-3*) and a forkhead associated protein (*ham-4*) are required for hyphal fusion in *Neurospora crassa*. Fungal Genet Biol. 47(10):855-868.
[136] Bernhards Y. and Pöggeler S. 2011. The phocein homologue SmMOB3 is essential for vegetative cell fusion and sexual development in the filamentous ascomycete *Sordaria macrospora*. Curr Genet. 57(2):133-149.
[137] Nordzieke S., Zobel T., Fränzel B., Wolters D.A., Kück U. and Teichert I. 2015. A fungal SLMAP homolog plays a fundamental role in development and localizes to the nuclear envelope, ER, and mitochondria. Eukaryot Cell. 14(4):345-358.
[138] Gautier V., Tong L.C.H., Nguyen T.S., Debuchy R. and Silar P. 2018. PaPro1 and IDC4, Two Genes Controlling Stationary Phase, Sexual Development and Cell Degeneration in *Podospora anserina*. J Fungi (Basel). 4(3).
[139] Debets A.J.M. and Griffiths A.J.F. 1998. Polymorphism of *het*-genes prevents resource plundering in *Neurospora crassa.* Mycol. Res. 102:1343-1349.
[140] Fischer M.S., Jonkers W. and Glass N.L. 2019. Integration of Self and Non-self Recognition Modulates Asexual Cell-to-Cell Communication in *Neurospora crassa*. Genetics. 211(4):1255-1267.
[141] Lalucque H., Malagnac F., Green K., Gautier V., Grognet P., Chan Ho Tong L., Scott B. and Silar P. 2017. IDC2 and IDC3, two genes involved in cell non-autonomous signaling of fruiting body development in the model fungus *Podospora anserina*. Dev Biol. 421(2):126-138.
[142] Hemsworth G.R., Henrissat B., Davies G.J. and Walton P.H. 2014. Discovery and characterization of a new family of lytic polysaccharide monooxygenases. Nat Chem Biol 10(2):122–126.
[143] Harris P.V., *et al*. 2010. Stimulation of lignocellulosic biomass hydrolysis by proteins of glycoside hydrolase family 61: Structure and function of a large, enigmatic family. Biochemistry 49(15):3305–3316.
[144] Quinlan R.J., *et al.* 2011. Insights into the oxidative degradation of cellulose by a copper metalloenzyme that exploits biomass components. PNAS. 108(37):15079–15084.
[145] Phillips C.M., Beeson W.T., Cate J.H.D. and Marletta M.A. 2011. Cellobiose dehydrogenase and a copper-dependent polysaccharide monooxygenase potentiate cellulose degradation by *Neurospora crassa.* ACS Chem Biol 6(12):1399–1406.

[146] Beeson W.T., Phillips C.M., Cate J.H.D., Marletta M.A. 2012. Oxidative cleavage of cellulose by fungal copper-dependent polysaccharide monooxygenases. J Am Chem Soc 134(2):890–892
[147] Vaaje-Kolstad G., Westereng B., Horn S.J., Liu Z., Zhai H., Sørlie M., Eijsink V.G. 2010. An oxidative enzyme boosting the enzymatic conversion of recalcitrant polysaccharides. Science 330(6001):219–222.
[148] Forsberg Z., Røhr A.K., Mekasha S., Andersson K.K., Eijsink V.G., Vaaje-Kolstad G. and Sørlie M. 2014. Comparative study of two chitin-active and two cellulose-active AA10-type lytic polysaccharide monooxygenases. Biochemistry. 53(10):1647–1656.
[149] Forsberg Z., Vaaje-Kolstad G., Westereng B., Bunæs A.C., Stenstrøm Y., MacKenzie A., Sørlie M., Horn S.J. and Eijsink V.G. 2011. Cleavage of cellulose by a CBM33 protein. Protein Sci 20(9):1479–1483.
[150] Vu V.V. and Marletta M.A. 2016. Starch-degrading polysaccharide monooxygenases. Cell Mol Life Sci. 73(14):2809-2819.
[151] Hemsworth G.R., Davies G.J. and Walton P.H. 2013. Recent insights into copper-containing lytic polysaccharide monooxygenases. Curr Opin Struct Biol. 23(5):660-668.
[152] Field M.C., Moran P., Li W., Keller G.A. and Caras I.W. 1994. Retention and Degradation of Proteins Containing an Uncleaved Glycosylphosphatidylinositol Signal. J Biol Chem. 269(14):10830-10837.
[153] Richard F., Glass N. L. and Pringle A., 2012. Cooperation among germinating spores facilitates the growth of the fungus, *Neurospora crassa*. Biol Lett. 8:419–422.
[154] Simonin A., Palma-Guerrero J., Fricker M. and and Glass N.L. 2012. Physiological Significance of Network Organization in Fungi. Eukaryot Cell. 11(11):1345-1352.
[155] Maddi A. and Free S. 2010. α-1,6-Mannosylation of N-Linked Oligosaccharide Present on Cell Wall Proteins Is Required for Their Incorporation into the Cell Wall in the Filamentous Fungus *Neurospora crassa*. Eukaryot Cell. 9(11):1766-1775.
[156] Han D.P., Lohani M. and Cho M.W. 2007. Specific Asparagine-Linked Glycosylation Sites Are Critical for DC-SIGN- and L-SIGN-Mediated Severe Acute Respiratory Syndrome Coronavirus Entry. J Virol. 81(21):12029-12039.
[157] Cereghino J.L. and Cregg J.M. 2000. Heterologous protein expression in the methylotrophic yeast *Pichia pastoris*. FEMS Microbiol Rev. 24(1): 45-66.
[158] Park G., Pan S. and Borkovich K.A. 2008. Mitogen-activated protein kinase cascade required for regulation of development and secondary metabolism in *Neurospora crassa*. Eukaryot Cell 7:2113–2122.
[159] Read ND, Gorychev AB, Lichius A (2012) The mechanistic basis of self-fusion between conidial anastomosis tubes during fungal colony initiation. Fungal Biol Rev 26:1–11.
[160] Stevens D.A., Espiritu M. and Parmar R. 2004. Paradoxical Effect of Caspofungin:Reduced Activity against Candida albicans at High Drug Concentrations. Antimicrob Agents Chemother. 48(9):3407-3411.
[161] Livak K.J. and Schmittgen T.D. 2001 Analysis of Relative Gene Expression Data Using Real-Time Quantitative PCR and the 2−ΔΔCT Method. Methods. 25:402–408.
[162] Kim D., Langmead B. and Salzberg S.L. HISAT: A fast spliced aligner with low memory requirements. Nat Methods. 2015;12:357–360.
[163] Galagan J.E., et al. The genome sequence of the filamentous fungus *Neurospora crassa*. Nature. 2003;422:859–868.

[164] Trapnell C., Roberts A., Goff L,. Pertea G., Kim D., Kelley D.R., Pimentel H., Salzberg S.L., Rinn J.L. and Pachter L. 2012. Differential gene and transcript expression analysis of RNA-seq experiments with TopHat and Cufflinks. Nat Protoc. 7:562–578.
[165] Mi H., Huang X., Muruganujan A., Tang H., Mills C., Kang D. and Thomas P.D. 2017. PANTHER version 11: expanded annotation data from Gene Ontology and Reactome pathways, and data analysis tool enhancements. Nucleic Acids Res. 45(D1):D183-D189.
[166] Supek F., Bošnjak M., Škunca N. and Šmuc T. 2011. REVIGO Summarizes and Visualizes Long Lists of Gene Ontology Terms. PLoS One. 6(7).
[167] Bennett L.D., Beremand P., Thomas T.L. and Bell-Pedersen D. 2013. Circadian Activation of the Mitogen-Activated Protein Kinase MAK-1 Facilitates Rhythms in Clock-Controlled Genes in *Neurospora crassa*. Eukaryot Cell. 12(1):59-69.
[168] Green K.A., Becker Y., Tanaka A., Takemoto D., Fitzsimons H.L., Seiler S., Lalucque H., Silar P. and Scott B. 2017. SymB and SymC, two membrane associated proteins, are required for *Epichloë festucae* hyphal cell–cell fusion and maintenance of a mutualistic interaction with *Lolium perenne*. Mol Microbiol. 104(4):657-677.
[169] Ezzi M.I. and Lynch J.M. 2005. Biodegradation of cyanide by *Trichoderma* spp. and *Fusarium* spp. Enzyme and Microbial Technology. 37:849–854.
[170] Wang Z., Miguel-Rojas C., Lopez-Giraldez F., Yarden O., Trail F. and Townsend J.P. 2019. Metabolism and Development during Conidial Germination in Response to a Carbon-Nitrogen-Rich Synthetic or a Natural Source of Nutrition in *Neurospora crassa*. MBio. 10(2).
[171] Hohmann S. 2002 Osmotic stress signaling and osmoadaptation in yeasts. Microbiol Mol Biol Rev. 66:300–372.
[172] Sheikh-Hamad D. and Gustin M.C. 2004. MAP kinases and the adaptive response to hypertonicity: functional preservation from yeast to mammals. Am J Physiol Renal Physiol. 287:F1102–1110.
[173] Coradetti S.T., Craig J.P., Xiong Y., Shock T., Tian C. and Glass N.L. 2012. Conserved and essential transcription factors for cellulase gene expression in ascomycete fungi. PNAS. 109(19):7397-7402.
[174] Gross L. 2006. When Less Is More:Losing Genes on the Path to Becoming Human. 4(3).
[175] Cortesi, P., McCulloch C.E., Song H., Lin H. and Milgroom M.G. 2001. Genetic control of horizontal virus transmission in the chestnut blight fungus, *Cryphonectria parasitica*. Genetics 159:107-118
[176] Debets A.J.M. and Griffiths A.J.F. 1998. Polymorphism of *het*-genes prevents resource plundering in *Neurospora crassa.* Mycol. Res. 102:1343-1349
[177] Fischer M.S., Jonkers W. and Glass N.L. 2019. Integration of Self and Non-self Recognition Modulates Asexual Cell-to-Cell Communication in *Neurospora crassa*. Genetics. 211(4):1255-1267.